NACA-TR-685

NATIONAL ADVISORY COMMITTEE FOR AERONAUTICS

REPORT No. 685

MECHANISM OF FLUTTER

A THEORETICAL AND EXPERIMENTAL INVESTIGATION OF THE FLUTTER PROBLEM

By THEODORE THEODORSEN and I. E. GARRICK



1940

REPRODUCED BY
NATIONAL TECHNICAL
INFORMATION SERVICE
U.S. DEPARTMENT OF COMMERCE
SPRINGFIELD, VA. 22161

AERONAUTIC SYMBOLS

1. FUNDAMENTAL AND DERIVED UNITS

	Symbol	Metric		English	
		Unit	Abbreviation	Unit	Abbreviation
Length	l	meter	m	foot (or mile)	ft. (or mi.)
Time	t	second	s	second (or hour)	sec. (or hr.)
Force	F	weight of 1 kilogram	kg	weight of 1 pound	lb.
Power	P	horsepower (metric)		horsepower	hp.
Speed	V	kilometers per hour	k.p.h.	miles per hour	m.p.h.
		meters per second	m.p.s.	feet per second	f.p.s.

2. GENERAL SYMBOLS

W, Weight$=mg$

g, Standard acceleration of gravity$=9.80665$ m/s^2 or 32.1740 ft./sec.^{2}

m, Mass$=\frac{W}{g}$

I, Moment of inertia$=mk^2$. (Indicate axis of radius of gyration k by proper subscript.)

μ, Coefficient of viscosity

ν, Kinematic viscosity

ρ, Density (mass per unit volume)

Standard density of dry air, 0.12497 kg-m^{-4}-s^2 at 15° C. and 760 mm; or 0.002378 lb.-ft.$^{-4}$ sec.^{2}

Specific weight of "standard" air, 1.2255 kg/m^3 or 0.07651 lb./cu. ft.

3. AERODYNAMIC SYMBOLS

S, Area

S_w, Area of wing

G, Gap

b, Span

c, Chord

$\frac{b^2}{S}$, Aspect ratio

V, True air speed

q, Dynamic pressure$=\frac{1}{2}\rho V^2$

L, Lift, absolute coefficient $C_L=\frac{L}{qS}$

D, Drag, absolute coefficient $C_D=\frac{D}{qS}$

D_0, Profile drag, absolute coefficient $C_{D_0}=\frac{D_0}{qS}$

D_i, Induced drag, absolute coefficient $C_{D_i}=\frac{D_i}{qS}$

D_p, Parasite drag, absolute coefficient $C_{D_p}=\frac{D_p}{qS}$

C, Cross-wind force, absolute coefficient $C_C=\frac{C}{qS}$

R, Resultant force

i_w, Angle of setting of wings (relative to thrust line)

i_t, Angle of stabilizer setting (relative to thrust line)

Q, Resultant moment

Ω, Resultant angular velocity

$\rho\frac{Vl}{\mu}$, Reynolds Number, where l is a linear dimension (e.g., for a model airfoil 3 in. chord, 100 m.p.h. normal pressure at 15° C., the corresponding number is 234,000; or for a model of 10 cm chord, 40 m.p.s., the corresponding number is 274,000)

C_p, Center-of-pressure coefficient (ratio of distance of c.p. from leading edge to chord length)

α, Angle of attack

ϵ, Angle of downwash

α_0, Angle of attack, infinite aspect ratio

α_i, Angle of attack, induced

α_a, Angle of attack, absolute (measured from zero-lift position)

γ, Flight-path angle

REPORT No. 685

MECHANISM OF FLUTTER
A THEORETICAL AND EXPERIMENTAL INVESTIGATION OF THE FLUTTER PROBLEM

By THEODORE THEODORSEN and I. E. GARRICK

Langley Memorial Aeronautical Laboratory

207726—40——1

NATIONAL ADVISORY COMMITTEE FOR AERONAUTICS

HEADQUARTERS, NAVY BUILDING, WASHINGTON, D. C.

Created by act of Congress approved March 3, 1915, for the supervision and direction of the scientific study of the problems o flight (U. S. Code, Title 50, Sec. 151). Its membership was increased to 15 by act approved March 2, 1929. The members ar appointed by the President, and serve as such without compensation.

VANNEVAR BUSH, Sc. D., *Chairman*,
Washington, D. C.
GEORGE J. MEAD, Sc. D., *Vice Chairman*,
West Hartford, Conn.
CHARLES G. ABBOT, Sc. D.,
Secretary, Smithsonian Institution.
HENRY H. ARNOLD, Major General, United States Army,
Chief of Air Corps, War Department.
GEORGE H. BRETT, Brigadier General, United States Army,
Chief Matériel Division, Air Corps, Wright Field,
Dayton, Ohio.
LYMAN J. BRIGGS, Ph. D.,
Director, National Bureau of Standards.
DONALD H. CONNOLLY, B. S.,
Administrator of Civil Aeronautics.
ROBERT E. DOHERTY, M. S.,
Pittsburgh, Pa.
ROBERT H. HINCKLEY, A. B.,
Assistant Secretary of Commerce.
JEROME C. HUNSAKER, Sc. D.,
Cambridge, Mass.
SYDNEY M. KRAUS, Captain, United States Navy,
Bureau of Aeronautics, Navy Department.
FRANCIS W. REICHELDERFER, Sc. D.,
Chief, United States Weather Bureau.
JOHN H. TOWERS, Rear Admiral, United States Navy,
Chief, Bureau of Aeronautics, Navy Department.
EDWARD WARNER, Sc. D.,
Washington, D. C.
ORVILLE WRIGHT, Sc. D.,
Dayton, Ohio.

GEORGE W. LEWIS, *Director of Aeronautical Research*
S. PAUL JOHNSTON, *Coordinator of Research*

JOHN F. VICTORY, *Secretary*

HENRY J. E. REID, *Engineer in Charge, Langley Memorial Aeronautical Laboratory, Langley Field, Va.*

SMITH J. DEFRANCE, *Engineer in Charge, Ames Aeronautical Laboratory, Moffett Field, Calif.*

TECHNICAL COMMITTEES

AERODYNAMICS
POWER PLANTS FOR AIRCRAFT
AIRCRAFT MATERIALS

AIRCRAFT STRUCTURES
AIRCRAFT ACCIDENTS
INVENTIONS AND DESIGNS

Coordination of Research Needs of Military and Civil Aviation

Preparation of Research Programs

Allocation of Problems

Prevention of Duplication

Consideration of Inventions

LANGLEY MEMORIAL AERONAUTICAL LABORATORY

LANGLEY FIELD, VA.

AMES AERONAUTICAL LABORATORY

MOFFETT FIELD, CALIF.

Conduct, under unified control, for all agencies, of scientific research on the fundamental problems of flight.

OFFICE OF AERONAUTICAL INTELLIGENCE

WASHINGTON, D. C.

Collection, classification, compilation, and dissemination of scientific and technical information on aeronautics

9-20-40

REPORT No. 685

MECHANISM OF FLUTTER
A THEORETICAL AND EXPERIMENTAL INVESTIGATION OF THE FLUTTER PROBLEM

By Theodore Theodorsen and I. E. Garrick

SUMMARY

The results of the basic flutter theory originally devised in 1934 and published as N. A. C. A. Technical Report No. 496 are presented in a simpler and more complete form convenient for further studies. The paper attempts to facilitate the judgment of flutter problems by a systematic survey of the theoretical effects of the various parameters. A large number of experiments were conducted on cantilever wings, with and without ailerons, in the N. A. C. A. high-speed wind tunnel for the purpose of verifying the theory and to study its adaptability to three-dimensional problems. The experiments included studies on wing taper ratios, nacelles, attached floats, and external bracings. The essential effects in the transition to the three-dimensional problem have been established. Of particular interest is the existence of specific flutter modes as distinguished from ordinary vibration modes. On the basis of the concepts introduced, results that are apparently paradoxical could logically be brought into conformity with the theory. In fact, it is shown that there exists a rather remarkable agreement between theoretical and experimental results. A simple method is presented for numerical calculations of the flutter speed by routine operations, requiring no reference to the theory. Application is made to a complete numerical example. The matter of identifying possible types of flutter in an airplane and of determining the parameters is briefly discussed. A section treating the subject of forced vibrations of a wing in an air stream and the question of air damping in its relation to flutter is included.

INTRODUCTION

The theory of flutter.—The problem of flutter is passing through a period of rapid development. Full cognizance is taken of the value of the theory; a simple or an empirical understanding of this problem is not available and could, at best, be of value only to the investigator. An exact treatment of the basic flutter problem in two-dimensional flow, involving the important functions F and G relating to the air forces, was given by Theodorsen in 1934. (See reference 1.) These functions are simple combinations of Bessel functions; they have been rederived in related form by Cicala (reference 2) in 1935, by Kassner and Fingado (reference 3) in 1936, and also by Küssner (reference 4) in 1936, who pointed out the identity of the functions. At about this time, Garrick (reference 5) also established a check on the general functions F and G by comparing them with expressions by Wagner, Glauert, and von Kármán and Burgers for special cases.

The system of equations as given in the original paper is

$$(A)\quad \ddot{\alpha}A+\dot{\alpha}\frac{v}{b}B+\alpha C+\ddot{\beta}D+\dot{\beta}\frac{v}{b}E+\beta\frac{v^2}{b^2}F+\ddot{h}G$$
$$-2\left(a+\frac{1}{2}\right)\frac{v}{b}C(k)Z=0$$

$$(B)\quad \ddot{\alpha}H+\dot{\alpha}\frac{v}{b}I+\ddot{\beta}J+\dot{\beta}\frac{v}{b}K+\beta L+\ddot{h}M+\frac{T_{12}}{\pi}\kappa\frac{v}{b}C(k)Z=0$$

$$(C)\quad \ddot{\alpha}N+\dot{\alpha}\frac{v}{b}O+\ddot{\beta}P+\dot{\beta}\frac{v}{b}Q+\ddot{h}R+hS+2\kappa\frac{v}{b}C(k)Z=0$$

where A, B, C, etc., are given on page 10 of reference 1.

$$Z=\frac{v}{b}\alpha+\frac{\dot{h}}{b}+\left(\frac{1}{2}-a\right)\dot{\alpha}+\frac{T_{10}v}{\pi\ b}\beta+\frac{T_{11}}{2\pi}\dot{\beta}$$

and (table 1)

$$C(k)=F(k)+iG(k)$$

Putting

$$\alpha=\alpha_0 e^{i(\omega t+\varphi_0)}$$

$$\beta=\beta_0 e^{i(\omega t+\varphi_1)}$$

$$h=h_0 e^{i(\omega t+\varphi_2)}$$

where

$$\omega=\frac{kv}{b}$$

the determinant of the coefficients of α_0, β_0, and h_0 becomes

$$\kappa\omega^2\begin{vmatrix}\overline{R}_{a\alpha}+i\overline{I}_{a\alpha} & R_{a\beta}+iI_{a\beta} & R_{ah}+iI_{ah}\\ R_{b\alpha}+iI_{b\alpha} & \overline{R}_{b\beta}+i\overline{I}_{b\beta} & R_{bh}+iI_{bh}\\ R_{c\alpha}+iI_{c\alpha} & R_{c\beta}+iI_{c\beta} & \overline{R}_{ch}+i\overline{I}_{ch}\end{vmatrix}$$

where the R's and I's are listed in the appendix.

This determinant put equal to zero contains two simultaneous equations, the solution of which determines X and $1/k$ from which the (unknowns) flutter velocity and flutter frequency are obtained. Only the diagonal terms with bars contain the quantity X. All terms contain or are functions of $1/k$.

The work of numerous investigators, notably Becker and Föppl, has shown that the structural friction is mainly a function of amplitude, not of frequency. The structural friction can be described by a force in phase with the velocity but of a magnitude proportional to the restoring force. With each restoring-force term, say αC_α, there will be a friction term $i\alpha\ g_\alpha\ C_\alpha$, in which g_α is the damping coefficient. The net result is very simply that the restoring-force terms αC_α, βC_β, and hC_h have been replaced by terms of the form $\alpha C_\alpha (1+ig_\alpha)$, $\beta C_\beta(1+ig_\beta)$, $hC_h(1+ig_h)$. These friction coefficients occur only in the diagonal $\bar{I}$ terms of the determinant.

Technical flutter problems and the flutter parameters.—Experimental evidence, some of which is presented later, has been accumulated which indicates that, in the two-dimensional problem, the flutter speed can be closely predicted from the theory if the parameters are given with accuracy. (In fact, it seems that in some cases the flutter speed can be used to determine some parameters more precisely than by a direct method.) In the two-dimensional problem of flexure-torsion-aileron flutter, about a dozen different quantities are required to calculate the flutter speed. The determination of these parameters requires technical skill and experience and is perhaps the most difficult step in the solution of the flutter problem. A knowledge of the functional dependency of the flutter speed on each parameter is essential in order to obtain sufficient accuracy in the determination of the important ones and to prevent waste of time on those of less influence. This need is partly the purpose of the material given in this paper.

One of the problems in connection with an actual airplane is the identification of the combination of vibration modes that may cause flutter. In regard to wing flutter, in the case of flexure-torsion, the situation is fairly clear. It will be shown that normally the most important parameter is the center-of-gravity location. This constant can be obtained with considerable accuracy in the design stage. An accurate value of this parameter can also be experimentally obtained as the "dynamic" torsion axis, that is, the axis around which the wing, owing to the low bending frequency, oscillates when put into torsional resonance. The location of the (static) torsional stiffness axis is much more difficult to calculate or to determine experimentally but fortunately, as will be observed, its effect on the flutter velocity is small.

The internal damping coefficients are, moreover, of fairly small influence in flexure-torsion flutter; these parameters are also fairly difficult to obtain. On the whole, however, it may be said that this case of flutter can be fairly well handled.

Another important case, that of the combination flexure-aileron, was shown by the original study (reference 1) to be an essentially different type of flutter from flexure-torsion. Its primary characteristic is that, normally, the flutter is limited to a *range* of speeds. Below and above the extremes of this speed range there is aerodynamic stability. A reduction of the static moment of the aileron with respect to the hinge (balancing) reduces the range; that is, the lower limit is raised and the upper limit is lowered. Damping in the structure is found to have the same general effect. Sufficient internal friction will, in fact, completely eliminate the danger of flutter, as will also complete mass balance or the proper combination of both. The structural friction of a wing system, although not readily predictable, can be obtained by a ground test.

In regard to the tail assembly, the difficulty is somewhat greater since it may not be easy to identify the most dangerous combination or to predict or even to measure the necessary parameters, including the structural damping. It therefore seems that certain empirical or semiempirical aids will be required and that it will be necessary, for a time at least, to resort to flight-test methods as a final assurance against tail flutter.

The transition to the three-dimensional case of actual flutter is quite complex. It is necessary to consider an aerodynamic span effect (which fortunately is very small, see reference 6); the variation of the parameters along the span; the possibility of higher-order deflection modes; and, in certain cases, fractional span effects, as for partial ailerons. The most promising manner of attack on such problems is by means of the two-dimensional treatment with the introduction of certain weight functions and average parameters in conjunction with a study of representative models of reasonable simplicity, followed by a crystallization of the collected experience into generally applicable semiempirical correction factors. The present paper makes initial studies with this purpose in mind.

It is realized that, for high values of the flutter speed, a correction must be made for the effect of compressibility. In the first order, this effect is due to a change in the slope of the lift curve. The air forces in the steady case are known to be increased approximately in the ratio $1/\sqrt{1-M^2}$, where M is the Mach number. Consequently, a decrease in the flutter speed, roughly as $(1-M^2)^{1/4}$, is expected. This correction, although small through the usual flight range, becomes appreciable for speeds near sound speed. Until experimental verification is available, such correction is preferable to none and should be applied for high-speed airplanes. (See footnote 2, p. 9, for details.)

Content of paper.—A straightforward scheme is presented in the first section for routine calculation of the flutter speeds in the two-dimensional types; case 1, flexure-torsion; case 2, flexure-aileron; and case 3, torsion-aileron; and in the three-degrees-of-freedom type, flexure-torsion-aileron. A numerical example, referring to a modern large airplane, is included.

The second section deals with a survey of the effect of the flutter parameters on the critical velocity. The effect of changing the parameters within certain practical limits in cases 1, 2, and 3 is shown by a number of charts.

The discussion in the third section deals with the transition to a three-dimensional case, showing how a "representative" two-dimensional wing may be used to give the essential results. Both uniform and tapered cantilever wings are included. The question of the probable occurrence of higher-order bending modes in flutter is also discussed. The effects of "friction" and "coupling" are especially pronounced in higher-order flutter.

It is pointed out that the deflection mode occurring in flutter is quite different from that of the static condition and that the lowest bending frequency involved in flutter is greater than that of the lowest ordinary vibration mode. A new concept of flutter, that the mode arising in flutter is such that the flutter speed is a minimum, is then introduced. In other words, if *all* primary variables including friction could be included in the analysis, the actual mode would be determined from all possible modes as the one giving the minimum critical speed. This concept is useful in explaining certain otherwise paradoxical, experimental facts. The extreme difficulty of a direct analytic attack on the general case, even if all the physical parameters were specified, justifies the adapting of the two-dimensional treatment supplemented by empirical information obtained on actual wings. In fact, as will later be shown, the corrections are small.

Almost 100 separate experiments were conducted in the 8-foot high-speed tunnel. The fourth section deals with the experimental tests and results. About one-half of these tests pertain to flutter of wings in flexure-torsion; the rest pertain to aileron flutter. Cantilever wings of aluminum and of built-up wood construction were used. The tests were performed on a conveniently large scale, most of the wings having a chord of 1 foot and a span of about 7 feet. The air speeds ranged from 50 to about 300 miles per hour. A number of safety devices had to be employed to prevent the ruin of the tunnel equipment.

A section is included showing the theoretical effects of the air damping on the forced vibrations of a two-dimensional wing system. This study leads to a more comprehensive understanding of the flutter condition, since it studies not only the critical speed but also the approach to this speed. A number of figures are presented that show the nature of the response curves in both one and two degrees of freedom. It is perhaps worth mentioning that von Schlippe (reference 7) has employed an experimental flight method for determining the critical flutter speed, which is based upon the use of an impressed alternating exciting force. The practical value of experiments of this nature is yet somewhat doubtful since the flutter usually comes on rather explosively. In any case, the theoretical results are of interest because they indicate the critical frequency as well as the growth of the maximum response as the critical speed is approached.

METHOD FOR ROUTINE CALCULATION OF FLUTTER SPEED

The calculation of the flutter speed can be reduced to a routine procedure by the following scheme. Nothing more involved arises than the calculation of the numerical values of double and triple determinants.

Given are a maximum of seven original parameters κ, r_α^2, a, x_α, r_β^2, x_β, c, from which are formed the 18 constants $A_{\alpha 1}$, $A_{\alpha 2}$, $A_{\beta 1}$, $A_{\beta 2}$, etc., defined as follows:

$$A_{\alpha 1}=\frac{r_\alpha^2}{\kappa}+\left(\frac{1}{8}+a^2\right)$$

$$A_{\alpha 2}=\left(\frac{1}{2}-a\right)$$

$$A_{\beta 1}=\frac{r_\beta^2}{\kappa}-\frac{T_7}{\pi}+(c-a)\left(\frac{x_\beta}{\kappa}-\frac{T_1}{\pi}\right)$$

$$A_{\beta 2}=\frac{1}{\pi}\left[-2p-\left(\frac{1}{2}-a\right)T_4\right]$$

$$A_{\beta 3}=\frac{1}{\pi}(T_4+T_{10})$$

$$A_{h1}=\frac{x_\alpha}{\kappa}-a$$

$$B_{\alpha 1}=\frac{r_\beta^2}{\kappa}-\frac{T_7}{\pi}+(c-a)\left(\frac{x_\beta}{\kappa}-\frac{T_1}{\pi}\right)(=A_{\beta 1})$$

$$B_{\alpha 2}=\frac{1}{\pi}\left(p-T_1-\frac{1}{2}T_4\right)$$

$$B_{\beta 1}=\frac{r_\beta^2}{\kappa}-\frac{1}{\pi^2}T_3$$

$$B_{\beta 2}=-\frac{1}{2\pi^2}T_4T_{11}$$

$$B_{\beta 3}=\frac{1}{\pi^2}(T_5-T_4T_{10})$$

$$B_{h1}=\frac{x_\beta}{\kappa}-\frac{1}{\pi}T_1$$

$$C_{\alpha 1}=\frac{x_\alpha}{\kappa}-a(=A_{h1})$$

$$C_{\alpha 2}=1$$

$$C_{\beta 1}=\frac{x_\beta}{\kappa}-\frac{1}{\pi}T_1(=B_{h1})$$

$$C_{\beta 2}=-\frac{1}{\pi}T_4$$

$$C_{\beta 3}=0$$

$$C_{h1}=\frac{1}{\kappa}+1$$

These constants are obtained from the original variables and from the T table (table 2) given at the end of the report.

Another set of quantities $R_{a\alpha}$, $I_{a\alpha}$, etc., will be needed; their expressions are as follows:

$$R_{a\alpha}=-A_{\alpha 1}+\left(\frac{1}{4}-a^2\right)\frac{2G}{k}-\left(\frac{1}{2}+a\right)\frac{2F}{k^2}$$

$$I_{a\alpha}=\frac{1}{k}\left[A_{\alpha 2}-\left(\frac{1}{2}+a\right)\frac{2G}{k}-\left(\frac{1}{4}-a^2\right)2F\right]$$

$$R_{b\beta}=-B_{\beta 1}+\frac{1}{k^2}B_{\beta 3}-\frac{T_{12}}{2\pi}\frac{T_{11}}{2\pi}\frac{2G}{k}+\frac{T_{12}}{2\pi}\frac{T_{10}}{\pi}\frac{2F}{k^2}$$

$$I_{b\beta}=\frac{1}{k}\left(B_{\beta 2}+\frac{T_{12}}{2\pi}\frac{T_{10}}{\pi}\frac{2G}{k}+\frac{T_{12}}{2\pi}\frac{T_{11}}{2\pi}2F\right)$$

$$R_{ch}=-C_{h1}-\frac{2G}{k}$$

$$I_{ch}=\frac{1}{k}2F$$

These six quantities are derived from the constants already given and from two additional quantities F and G, which are functions of $1/k$. The quantity $1/k$ is, in reality, the independent variable in the problem. The quantities F and G occur in the forms $2F$, $2F/k^2$, and $2G/k$; their values are given in table 1 for different values of $1/k$. In order to facilitate the calculation of these quantities, the parts depending on $1/k$ are given in tables 3 and 4.

Additional constants involved are the frequencies Ω_α, Ω_β, and Ω_h, defined under the scheme for each case, and three damping constants g_α, g_β, and g_h. Generally all these constants are not simultaneously needed. The four cases will next be solved.

Case 1.—The problem is given by two quadratic equations, for convenience referred to as the "real" and the "imaginary" equations. The coefficients of each are given in the calculation scheme presented in the following section. The coefficient of the first term in each equation involves the constants g_α and g_h, the coefficients of internal friction or structural damping, which are given as original constants. The coefficient of the second term of each equation involves the g's and the R's and I's, just defined. The constant term in each of the equations is obtained by the schematic arrangement shown in the calculation scheme; it is made up from certain constants A_1, B_1, C_1, and D_1 together with the quantities $2F$, $2F/k^2$, and $2G/k$. The quantities A_1, B_1, C_1, and D_1 are simple determinants built up from the constants $A_{\alpha 1}$, etc.

The coefficients of the two equations must be calculated for a fixed value of $1/k$; these coefficients are then substituted into the equations and the solution, that is, the value of X, is found. The real equation usually has two solutions, and the imaginary equation usually has one. The values of X, or preferably of $\sqrt{X}$, are then plotted against $1/k$, and the procedure is repeated until continuous curves representing the two equations are obtained. (Attained judgment or the knowledge of the solution of similar cases may considerably reduce the labor involved because it is then possible to choose reasonable values of $1/k$ at the start. For wings and ailerons, $1/k$ is usually less than 5, very often around 1 or 2.) The point of intersection of the two curves represents the flutter point. Read off the values of X and $1/k$. The flutter speed is then given by the expression

$$v=\frac{r_\alpha\omega_\alpha b}{\sqrt{\kappa}}\frac{1}{k}\frac{1}{\sqrt{X}}$$

Case 2.—The coefficient of the first term in each of the two quadratic equations again involves the constants of internal friction g_β and g_h. The coefficient of the second terms is built up as in case 1. The constant term is built up likewise. Proceed as outlined for case 1. The critical speed is then

$$v=\frac{\omega_h b}{\sqrt{\kappa}}\frac{1}{k}\frac{1}{\sqrt{X}}$$

where $1/k$ and X are the values at the intersection point of the curves representing the real and the imaginary equations, respectively. There are usually two critical speeds.

Case 3.—Case 3 requires a more laborious calculation of the constant terms; otherwise, the procedure is the same as for cases 1 and 2. The flutter speed is given by

$$v=\frac{r_\alpha\omega_\alpha b}{\sqrt{\kappa}}\frac{1}{k}\frac{1}{\sqrt{X}}$$

Three degrees of freedom.—The case of three degrees of freedom requires the solution of two third-degree equations in X. The constants of the first, the second, and the third terms are readily recognized as containing only quantities already used under cases 1, 2, and 3. The expressions for the constant terms of the two equations, D^R and D^I, involve three-row determinants but can be obtained by straightforward calculations for each value of $1/k$. The point or points of intersection of the two curves representing the equations are again representative of the critical speed, which is given by

$$v=\frac{r_\alpha\omega_\alpha b}{\sqrt{\kappa}}\frac{1}{k}\frac{1}{\sqrt{X}}$$

CALCULATION SCHEME

Case 1 (h, α).—

Real equation:

Coefficient of X^2: $\Omega_h\Omega_\alpha(1-g_hg_\alpha)$

Coefficient of X: $\Omega_h(R_{a\alpha}-g_hI_{a\alpha})+\Omega_\alpha(R_{ch}-g_\alpha I_{ch})$

Constant: $M_1{}^R=A_1+B_1\frac{2G}{k}+C_1\frac{2F}{k^2}$

Imaginary equation: [1]

Coefficient of X^2: $\Omega_h\Omega_\alpha(g_h+g_\alpha)$

Coefficient of X: $\Omega_h(R_{a\alpha}g_h+I_{a\alpha})+\Omega_\alpha(R_{ch}g_\alpha+I_{ch})$

Constant: $M_1{}^I=\frac{1}{k}\left(D_1+C_1\frac{2G}{k}-B_12F\right)$

$$A_1=\begin{vmatrix}A_{\alpha1} & A_{h1}\\ C_{\alpha1} & C_{h1}\end{vmatrix}$$

$$B_1=\begin{vmatrix}A_{\alpha1} & -(\frac{1}{2}+a)\\ C_{\alpha1} & 1\end{vmatrix}+(\tfrac{1}{2}-a)\begin{vmatrix}-(\frac{1}{2}+a) & A_{h1}\\ 1 & C_{h1}\end{vmatrix}$$

$$C_1=-\begin{vmatrix}-(\frac{1}{2}+a) & A_{h1}\\ 1 & C_{h1}\end{vmatrix}-\begin{vmatrix}A_{\alpha2} & -(\frac{1}{2}+a)\\ C_{\alpha2} & 1\end{vmatrix}$$

$$=\begin{vmatrix}A_{h1}-A_{\alpha2} & -(\frac{1}{2}+a)\\ C_{h1}-C_{\alpha2} & 1\end{vmatrix}$$

$$D_1=-\begin{vmatrix}A_{\alpha2} & A_{h1}\\ C_{\alpha2} & C_{h1}\end{vmatrix}$$

$$\Omega_\alpha=1$$

$$\Omega_h=\left(\frac{\omega_h}{\omega_\alpha}\right)^2\frac{1}{r_\alpha{}^2}$$

$$X=\frac{r_\alpha{}^2}{\kappa}\left(\frac{\omega_\alpha}{\omega}\right)^2$$

$$v=\frac{r_\alpha\omega_\alpha b}{\sqrt{\kappa}}\frac{1}{k}\frac{1}{\sqrt{X}}$$

Case 2.—

Real equation:

Coefficient of X^2: $\Omega_\beta\Omega_h(1-g_\beta g_h)$

Coefficient of X: $\Omega_\beta(R_{ch}-g_\beta I_{ch})+\Omega_h(R_{b\beta}-g_hI_{b\beta})$

Constant: $M_2{}^R=A_2+\overline{A}_2\frac{1}{k^2}+\left(B_2+\overline{B}_2\frac{1}{k^2}\right)\frac{2G}{k}+C_2\frac{2F'}{k^2}$

Imaginary equation:

Coefficient of X^2: $\Omega_\beta\Omega_h(g_\beta+g_h)$

Coefficient of X: $\Omega_\beta(R_{ch}g_\beta+I_{ch})+\Omega_h(R_{b\beta}g_h+I_{b\beta})$

Constant: $M_2{}^I=\frac{1}{k}\left[D_2+C_2\frac{2G}{k}-\left(B_2+\overline{B}_2\frac{1}{k^2}\right)2F\right]$

$$A_2=\begin{vmatrix}B_{\beta1} & B_{h1}\\ C_{\beta1} & C_{h1}\end{vmatrix}$$

$$\overline{A}_2=-\begin{vmatrix}B_{\beta3} & B_{h1}\\ C_{\beta3} & C_{h1}\end{vmatrix}$$

$$B_2=\begin{vmatrix}B_{\beta1} & \frac{T_{12}}{2\pi}\\ C_{\beta1} & 1\end{vmatrix}+\frac{T_{11}}{2\pi}\begin{vmatrix}\frac{T_{12}}{2\pi} & B_{h1}\\ 1 & C_{h1}\end{vmatrix}$$

$$\overline{B}_2=-\begin{vmatrix}B_{\beta3} & \frac{T_{12}}{2\pi}\\ C_{\beta3} & 1\end{vmatrix}$$

$$C_2=-\begin{vmatrix}B_{\beta2}\frac{T_{12}}{2\pi}\\ C_{\beta2} & 1\end{vmatrix}-\frac{T_{10}}{\pi}\begin{vmatrix}\frac{T_{12}}{2\pi} & B_{h1}\\ 1 & C_{h1}\end{vmatrix}$$

$$D_2=-\begin{vmatrix}B_{\beta2} & B_{h1}\\ C_{\beta2} & C_{h1}\end{vmatrix}$$

$$\Omega_h=1$$

$$\Omega_\beta=\left(\frac{\omega_\beta}{\omega_h}\right)^2r_\beta{}^2$$

$$X=\frac{1}{\kappa}\left(\frac{\omega_h}{\omega}\right)^2$$

$$v=\frac{\omega_hb}{\sqrt{\kappa}}\frac{1}{k}\frac{1}{\sqrt{X}}$$

Case 3 (α, β).—

Real equation:

Coefficient of X^2: $\Omega_\alpha\Omega_\beta(1-g_\alpha g_\beta)$

Coefficient of X: $\Omega_\alpha(R_{b\beta}-g_\alpha I_{b\beta})+\Omega_\beta(R_{a\alpha}-g_\beta I_{a\alpha})$

Constant: $M_3{}^R=A_3+\overline{A}_3\frac{1}{k^2}+\left(B_3+\overline{B}_3\frac{1}{k^2}\right)\frac{2G}{k}$
$+\left(C_3+\overline{C}_3\frac{1}{k^2}\right)\frac{2F}{k^2}$

Imaginary equation:

Coefficient of X^2: $\Omega_\alpha\Omega_\beta(g_\alpha+g_\beta)$

Coefficient of X: $\Omega_\alpha(R_{b\beta}g_\alpha+I_{b\beta})+\Omega_\beta(R_{a\alpha}g_\beta+I_{a\alpha})$

Constant: $M_3{}^I=\frac{1}{k}\left[D_3+\overline{D}_3\frac{1}{k^2}+\left(C_3+\overline{C}_3\frac{1}{k^2}\right)\frac{2G}{k}\right.$
$\left.-\left(B_3+\overline{B}_3\frac{1}{k^2}\right)2F\right]$

$$A_3=\begin{vmatrix}A_{\alpha1} & A_{\beta_1}\\ B_{\alpha1} & B_{\beta1}\end{vmatrix}$$

$$\overline{A}_3=-\begin{vmatrix}A_{\alpha1} & A_{\beta3}\\ B_{\alpha1} & B_{\beta3}\end{vmatrix}-\begin{vmatrix}A_{\alpha2} & A_{\beta_2}\\ B_{\alpha2} & B_{\beta2}\end{vmatrix}$$

[1] Note that when the friction coefficients g are zero, a factor $1/k$ can be canceled out of all terms in all imaginary equations.

$$B_3=(\tfrac{1}{2}-a)\begin{vmatrix}-(\frac{1}{2}+a) & A_{\beta 1}\\ \frac{T_{12}}{2\pi} & B_{\beta 1}\end{vmatrix}+\frac{T_{11}}{2\pi}\begin{vmatrix}A_{\alpha 1} & -(\frac{1}{2}+a)\\ B_{\alpha 1} & \frac{T_{12}}{2\pi}\end{vmatrix}$$

$$\overline{B}_3=-(\tfrac{1}{2}-a)\begin{vmatrix}-(\frac{1}{2}+a) & A_{\beta 3}\\ \frac{T_{12}}{2\pi} & B_{\beta 3}\end{vmatrix}-\frac{T_{10}}{\pi}\begin{vmatrix}A_{\alpha 2} & -(\frac{1}{2}+a)\\ B_{\alpha 2} & \frac{T_{12}}{2\pi}\end{vmatrix}-\begin{vmatrix}-(\frac{1}{2}+a) & A_{\beta 2}\\ \frac{T_{12}}{2\pi} & B_{\beta 2}\end{vmatrix}$$

$$C_3=-(\tfrac{1}{2}-a)\begin{vmatrix}-(\frac{1}{2}+a) & A_{\beta 2}\\ \frac{T_{12}}{2\pi} & B_{\beta 2}\end{vmatrix}-\frac{T_{11}}{2\pi}\begin{vmatrix}A_{\alpha 2} & -(\frac{1}{2}+a)\\ B_{\alpha 2} & \frac{T_{12}}{2\pi}\end{vmatrix}-\frac{T_{10}}{\pi}\begin{vmatrix}A_{\alpha 1} & -(\frac{1}{2}+a)\\ B_{\alpha 1} & \frac{T_{12}}{2\pi}\end{vmatrix}-\begin{vmatrix}-(\frac{1}{2}+a) & A_{\beta 1}\\ \frac{T_{12}}{2\pi} & B_{\beta 1}\end{vmatrix}$$

$$\overline{C}_3=\begin{vmatrix}-(\frac{1}{2}+a) & A_{\beta 3}\\ \frac{T_{12}}{2\pi} & B_{\beta 3}\end{vmatrix}$$

$$D_3=-\begin{vmatrix}A_{\alpha 1} & A_{\beta 2}\\ B_{\alpha 1} & B_{\beta 2}\end{vmatrix}-\begin{vmatrix}A_{\alpha 2} & A_{\beta 1}\\ B_{\alpha 2} & B_{\beta 1}\end{vmatrix}$$

$$\overline{D}_3=\begin{vmatrix}A_{\alpha 2} & A_{\beta 3}\\ B_{\alpha 2} & B_{\beta 2}\end{vmatrix}$$

$$\Omega_\alpha=1$$

$$\Omega_\beta=\left(\frac{\omega_\beta}{\omega_\alpha}\right)^2\left(\frac{r_\beta}{r_\alpha}\right)^2$$

$$X=\frac{r_\alpha^2}{\kappa}\left(\frac{\omega_\alpha}{\omega}\right)^2$$

$$v=\frac{r_\alpha\omega_\alpha b}{\sqrt{\kappa}}\,\frac{1}{k}\,\frac{1}{\sqrt{X}}$$

Three degrees of freedom with friction.—

Real equation:

Coefficient of X^3: $\Omega_\alpha\Omega_\beta\Omega_h(1-g_\alpha g_\beta-g_\beta g_h-g_h g_\alpha)$

Coefficient of X^2: $\Omega_\alpha\Omega_\beta[(1-g_\alpha g_\beta)R_{ch}-(g_\alpha+g_\beta)I_{ch}]+\Omega_\beta\Omega_h[(1-g_\beta g_h)R_{a\alpha}-(g_\beta+g_h)I_{a\alpha}]$
$+\Omega_h\Omega_\alpha[(1-g_h g_\alpha)R_{b\beta}-(g_h+g_\alpha)I_{b\beta}]$

Coefficient of X: $\Omega_\alpha(M_2{}^R-g_\alpha M_2{}^I)+\Omega_\beta(M_1{}^R-g_\beta M_1{}^I)+\Omega_h(M_3{}^R-g_h M_3{}^I)$

Constant: $D^R=R+\overline{R}\frac{1}{k^2}+\left(S+\overline{S}\frac{1}{k^2}\right)\frac{2G}{k}+\left(T+\overline{T}\frac{1}{k^2}\right)\frac{2F}{k^2}$

Imaginary equation:

Coefficient of X^3: $\Omega_\alpha\Omega_\beta\Omega_h(g_\alpha+g_\beta+g_h+g_\alpha g_\beta g_h)$

Coefficient of X^2: $\Omega_\alpha\Omega_\beta[(1-g_\alpha g_\beta)I_{ch}+(g_\alpha+g_\beta)R_{ch}]+\Omega_\beta\Omega_h[(1-g_\beta g_h)I_{a\alpha}+(g_\beta+g_h)R_{a\alpha}]$
$+\Omega_h\Omega_\alpha[(1-g_h g_\alpha)I_{b\beta}+(g_h+g_\alpha)R_{b\beta}]$

Coefficient of X: $\Omega_\alpha(M_2{}^I+g_\alpha M_2{}^R)+\Omega_\beta(M_1{}^I+g_\beta M_1{}^R)+\Omega_h(M_3{}^I+g_h M_3{}^R)$

Constant: $D^I=\frac{1}{k}\left[U+\overline{U}\frac{1}{k^2}+\left(T+\overline{T}\frac{1}{k^2}\right)\frac{2G}{k}-\left(S+\overline{S}\frac{1}{k^2}\right)2F\right]$

$$R=-\begin{vmatrix} A_{\alpha 1} & A_{\beta 1} & A_{h1} \\ B_{\alpha 1} & B_{\beta 1} & B_{h1} \\ C_{\alpha 1} & C_{\beta 1} & C_{h1} \end{vmatrix}$$

$$\overline{R}=\begin{vmatrix} A_{\alpha 1} & A_{\beta 3} & A_{h1} \\ B_{\alpha 1} & B_{\beta 3} & B_{h1} \\ C_{\alpha 1} & C_{\beta 3} & C_{h1} \end{vmatrix}+\begin{vmatrix} A_{\alpha 2} & A_{\beta} & A_{h1} \\ B_{\alpha 2} & B_{\beta 2} & B_{h1} \\ C_{\alpha 2} & C_{\beta 2} & C_{h1} \end{vmatrix}$$

$$S=-\begin{vmatrix} A_{\alpha 1} & A_{\beta 1} & -(\frac{1}{2}+a) \\ B_{\alpha 1} & B_{\beta 1} & \frac{T_{12}}{2\pi} \\ C_{\alpha 1} & C_{\beta 1} & 1 \end{vmatrix}-(\tfrac{1}{2}-a)\begin{vmatrix} -(\frac{1}{2}+a) & A_{\beta 1} & A_{h1} \\ \frac{T_{12}}{2\pi} & B_{\beta 1} & B_{h1} \\ 1 & C_{\beta 1} & C_{h1} \end{vmatrix}-\frac{T_{11}}{2\pi}\begin{vmatrix} A_{\alpha 1} & -(\frac{1}{2}+a) & A_{h1} \\ B_{\alpha 1} & \frac{T_{12}}{2\pi} & B_{h1} \\ C_{\alpha 1} & 1 & C_{h1} \end{vmatrix}$$

$$\overline{S}=\begin{vmatrix} A_{\alpha 1} & A_{\beta 3} & -(\frac{1}{2}+a) \\ B_{\alpha 1} & B_{\beta 3} & \frac{T_{12}}{2\pi} \\ C_{\alpha 1} & C_{\beta 3} & 1 \end{vmatrix}+\begin{vmatrix} -(\frac{1}{2}+a) & A_{\beta 2} & A_{h1} \\ \frac{T_{12}}{2\pi} & B_{\beta 2} & B_{h1} \\ 1 & C_{\beta 2} & C_{h1} \end{vmatrix}+\begin{vmatrix} A_{\alpha 2} & A_{\beta 2} & -(\frac{1}{2}+a) \\ B_{\alpha 2} & B_{\beta 2} & -\frac{T_{12}}{2\pi} \\ C_{\alpha 2} & C_{\beta 2} & 1 \end{vmatrix}+\frac{T_{10}}{\pi}\begin{vmatrix} A_{\alpha 2} & -(\frac{1}{2}+a) & A_{h1} \\ B_{\alpha 2} & \frac{T_{12}}{2\pi} & B_{h1} \\ C_{\alpha 2} & 1 & C_{h1} \end{vmatrix}$$
$$+(\tfrac{1}{2}-a)\begin{vmatrix} -(\frac{1}{2}+a) & A_{\beta 3} & A_{h1} \\ \frac{T_{12}}{2\pi} & B_{\beta 3} & B_{h1} \\ 1 & C_{\beta 3} & C_{h1} \end{vmatrix}$$

$$T=\begin{vmatrix} A_{\alpha 1} & A_{\beta 2} & -(\frac{1}{2}+a) \\ B_{\alpha 1} & B_{\beta 2} & \frac{T_{12}}{2\pi} \\ C_{\alpha 1} & C_{\beta 2} & 1 \end{vmatrix}+\begin{vmatrix} A_{\alpha 2} & A_{\beta 1} & -(\frac{1}{2}+a) \\ B_{\alpha 2} & B_{\beta 1} & \frac{T_{12}}{2\pi} \\ C_{\alpha 2} & C_{\beta 1} & 1 \end{vmatrix}+\begin{vmatrix} -(\frac{1}{2}+a) & A_{\beta 1} & A_{h1} \\ \frac{T_{12}}{2\pi} & B_{\beta 1} & B_{h1} \\ 1 & C_{\beta 1} & C_{h1} \end{vmatrix}+(\tfrac{1}{2}-a)\begin{vmatrix} -(\frac{1}{2}+a) & A_{\beta 2} & A_{h1} \\ \frac{T_{12}}{2\pi} & B_{\beta 2} & B_{h1} \\ 1 & C_{\beta 2} & C_{h1} \end{vmatrix}$$
$$+\frac{T_{10}}{\pi}\begin{vmatrix} A_{\alpha 1} & -(\frac{1}{2}+a) & A_{h1} \\ B_{\alpha 1} & \frac{T_{12}}{2\pi} & B_{h1} \\ C_{\alpha 1} & 1 & C_{h1} \end{vmatrix}+\frac{T_{11}}{2\pi}\begin{vmatrix} A_{\alpha 2} & -(\frac{1}{2}+a) & A_{h1} \\ B_{\alpha 2} & \frac{T_{12}}{2\pi} & B_{h1} \\ C_{\alpha 2} & 1 & C_{h1} \end{vmatrix}$$

$$\overline{T}=-\begin{vmatrix} -(\frac{1}{2}+a) & A_{\beta 3} & A_{h1} \\ \frac{T_{12}}{2\pi} & B_{\beta 3} & B_{h1} \\ 1 & C_{\beta 3} & C_{h1} \end{vmatrix}-\begin{vmatrix} A_{\alpha 2} & A_{\beta 3} & -(\frac{1}{2}+a) \\ B_{\alpha 2} & B_{\beta 3} & \frac{T_{12}}{2\pi} \\ C_{\alpha 2} & C_{\beta 3} & 1 \end{vmatrix}$$

$$U=\begin{vmatrix} A_{\alpha 1} & A_{\beta 2} & A_{h1} \\ B_{\alpha 1} & B_{\beta 2} & B_{h1} \\ C_{\alpha 1} & C_{\beta 2} & C_{h1} \end{vmatrix}+\begin{vmatrix} A_{\alpha 2} & A_{\beta 1} & A_{h1} \\ B_{\alpha 2} & B_{\beta 1} & B_{h1} \\ C_{\alpha 2} & C_{\beta 1} & C_{h1} \end{vmatrix}$$

$$\overline{U}=-\begin{vmatrix} A_{\alpha 2} & A_{\beta 3} & A_{h1} \\ B_{\alpha 2} & B_{\beta 3} & B_{h1} \\ C_{\alpha 2} & C_{\beta 3} & C_{h1} \end{vmatrix}$$

Note that five of the determinants occurring in the expressions for T and $\overline{T}$ occur also in the expressions for S and $\overline{S}$.

$$\Omega_\alpha=1$$

$$\Omega_\beta=\left(\frac{\omega_\beta}{\omega_\alpha}\right)^2\left(\frac{r_\beta}{r_\alpha}\right)^2$$

$$\Omega_h=\left(\frac{\omega_h}{\omega_\alpha}\right)^2\frac{1}{r_\alpha{}^2}$$

$$X=\frac{r_\alpha{}^2}{\kappa}\left(\frac{\omega_\alpha}{\omega}\right)^2$$

$$v=\frac{r_\alpha\omega_\alpha b}{\sqrt{\kappa}}\frac{1}{k}\frac{1}{\sqrt{X}}$$

NUMERICAL EXAMPLE

The following example refers to a modern large airplane. The parameters, which were furnished by the manufacturer, are:

$\kappa=0.25$ $\qquad$ $r_\alpha{}^2=0.25$

$a=-0.4$ $\qquad$ $c=0.6$

$x_\alpha=0.2$ $\qquad$ $x_\beta=0$

$r_\beta{}^2=0.0012$

A verbal description of the representative parameters used in the example is: wing density, σ, about 2.5 pounds per square foot per chord length (in ft); stiffness-axis location, 30 percent of the chord from the leading edge; center-of-gravity location, 40 percent of the chord from the leading edge; aileron length, one-fifth of the total chord; balanced aileron (center of gravity of aileron at hinge axis, $x_\beta=0$). (The structural damping coefficients g_α, g_β, and g_h will be kept zero, corresponding to a safety factor.) It is not necessary to specify the chord length $2b$ and the torsional frequency ω_α until the final step. The following frequency ratios, however, are specified:

$$\left(\frac{\omega_h}{\omega_\alpha}\right)^2=1/16$$

$$\left(\frac{\omega_\beta}{\omega_h}\right)^2=3/2$$

That is, the torsional frequency is four times the bending frequency and the aileron frequency is 1.22 times the bending frequency. The constants from which are composed all the determinants in the calculation scheme are tabulated as follows:

$A_{\alpha 1}=1.285$ $A_{\alpha 2}=.9$ $A_{\beta 1}=.02374$ $A_{\beta 2}=.23679$ $A_{\beta 3}=.40744$ $A_{h1}=1.2$	$B_{\alpha 1}=0.02374$ $B_{\alpha 2}=.04009$ $B_{\beta 1}=.007028$ $B_{\beta 2}=.021177$ $B_{\beta 3}=.01651$ $B_{h1}=.02322$	$C_{\alpha 1}=1.2$ $C_{\alpha 2}=1$ $C_{\beta 1}=.02322$ $C_{\beta 2}=.14238$ $C_{\beta 3}=0$ $C_{h1}=5.0$
$-\left(\frac{1}{2}+a\right)=-0.1$	$\frac{T_{12}}{2\pi}=0.006357$	1

The equations are written explicitly for $1/k=1$, that is, $2G/k=-0.2006$, $2F=1.0788$, $2F/k^2=1.0788$.

Case 1 (flexure-torsion).—

Real equation:

The coefficient of X^2 is

$$\frac{1}{16}\times 4\times 1=\frac{1}{4}$$

The coefficient of X is

$$\frac{1}{4}(-1.285-0.12593)+1(-5.0+0.2006)=-5.15213$$

The constants

$$A_1=4.985$$
$$B_1=-0.125$$
$$C_1=0.7$$
$$D_1=-3.3$$

Hence the constant term is

$$M_1{}^R=4.985+(-0.125)\ (-0.2006)+0.7(1.0788)=5.76524$$

The real equation is then

$$\frac{1}{4}X^2-5.15213X+5.76524=0$$

Imaginary equation:

The coefficient of X is

$$\frac{1}{4}(0.9-0.07703)+1(1.0788)=1.28454$$

The constant term $M_1{}^I$ is

$$-3.3+0.7(-0.2006)-(-0.125)(1.0788)=-3.30557$$

The imaginary equation is then

$$1.28454X-3.30557=0$$

The roots of the real equation are $X=1.187$ and 19.421, and the root of the imaginary equation is $X=2.573$, or

$$\sqrt{X}=1.089,\ 4.407,\ \text{and}\ 1.604$$

These values of $\sqrt{X}$ are plotted against $1/k$ in figure 1. The curves traced by plotting the roots are shown in the figure. The intersection is at $\sqrt{X}=1.594$, $1/k=2.46$. The flutter speed is then

$$v=\frac{1}{2}\times 2\times\frac{2.46}{1.594}b\omega_\alpha=1.542b\omega_\alpha$$

In the present example, the chord $2b$ is 12 feet and ω_α is 90 (corresponding to a torsional frequency of 859 cyles per minute); $b\omega_\alpha$ is then 540 feet per second or

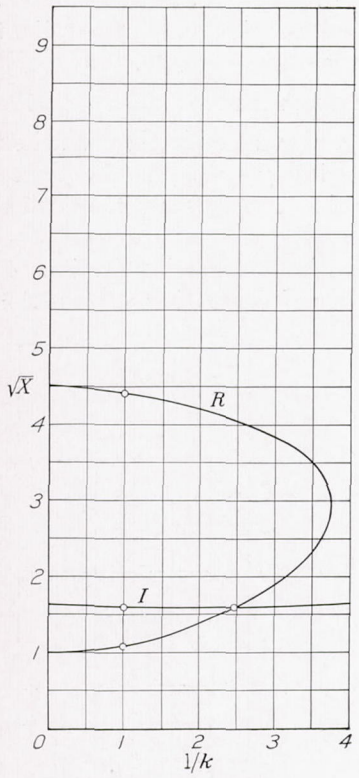


FIGURE 1.—Case 1. Numerical example. The roots $\sqrt{X}$ of the real and the imaginary equations against $1/k$.

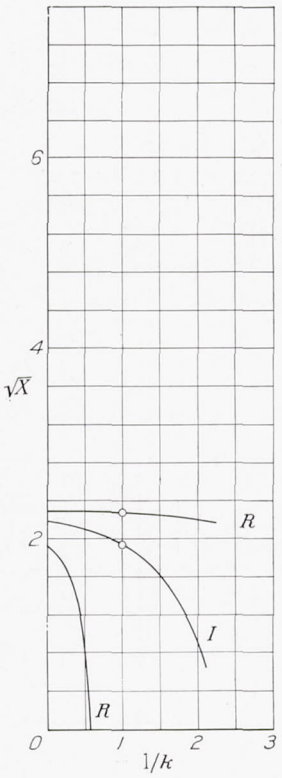


FIGURE 2.—Case 2. Numerical example. The roots $\sqrt{X}$ of the real and the imaginary equations against $1/k$.

about 368 miles per hour. Hence the flutter speed is, for this case, 567 miles per hour.[2]

Case 2 (flexure aileron).—

Real equation:

The coefficient of X^2 is

$$\frac{3}{2}\times 0.0012\times 1=0.0018$$

The coefficient of X is

$$0.0018(-5+0.2006)+1(-0.007028+0.020470)=0.004803$$

The constants

$$A_2=0.034601$$
$$\overline{A}_2=-0.08255$$
$$B_2=0.008154$$
$$\overline{B}_2=-0.016510$$
$$C_2=-0.024980$$
$$D_2=-0.10258$$

The constant term $M_2{}^R=-0.07322$.

The real equation is then

$$0.0018X^2+0.004803X-0.07322=0$$

Imaginary equation:

The coefficient of X is

$$0.0018\times 1.0788+1(0.021177+0.0003184)=0.023437$$

The constant term $M_2{}^I=-0.088554$

The imaginary equation is then

$$0.023437X-0.088554=0$$

The roots of the real equation are $X=5.182$ and -7.85 and the root of the imaginary equation is $X=3.778$ or (for the positive roots) $\sqrt{X}=2.276$ and 1.944. These values of $\sqrt{X}$ are plotted against $1/k$ in figure 2. The curves traced by the roots are shown in the figure. Since no intersection exists, this case is stable.

Case 3 (torsion-aileron).—

Real equation:

The coefficient of X^2 is

$$1\times\frac{3}{32}\times\frac{0.0012}{0.25}=0.00045$$

The coefficient of X is

$$1(-0.007028+0.020470)+0.00045(-1.285-0.12593)=0.012807$$

The constants

$$A_3=0.008468 \qquad C_3=-0.003129$$
$$\overline{A}_3=-0.021110 \qquad \overline{C}_3=-0.004241$$
$$B_3=0.000799 \qquad D_3=-0.026964$$
$$\overline{B}_3=0.002090 \qquad \overline{D}_3=-0.001474$$

The constant term $M_3{}^R=-0.021173$

The real equation is then

$$0.00045X^2+0.012807X-0.021173=0$$

Imaginary equation:

The coefficient of X is

$$(0.021177+0.0003184)+0.00045(0.9-0.07703)=0.021865$$

The constant term $M_3{}^I=-0.030076$

The imaginary equation is then

$$0.021865X-0.030076=0$$

The roots of the real equation are $X=1.567$ and -30.03 and the root of the imaginary equation is $X=1.375$ or (for the positive roots) $\sqrt{X}=1.252$ and 1.173. These values for the $\sqrt{X}$ are plotted against $1/k$ in figure 3. The curve traced by the roots is shown in the figure. Since no intersection exists, this case is also stable.

Three degrees of freedom (flexure-torsion-aileron).—

Real equation:

The coefficient of X^3 is

$$1\times 0.00045\times\tfrac{1}{4}=0.0001125$$

[2] The compressibility correction: Let the calculated flutter speed for the incompressible fluid be v_i and let the corresponding speed for the compressible fluid be v_c Denote v_i/c by M_i and v_c/c by M_c, where c is the velocity of sound. Then (see Introduction)

$$M_c{}^2\frac{1}{\sqrt{1-M_c{}^2}}=M_i{}^2$$

or, on solving for $M_c{}^2$,

$$M_c{}^2=M_i{}^2\left(\sqrt{1-\frac{M_i{}^4}{4}}-\frac{M_i{}^2}{2}\right)$$
$$\cong M_i{}^2\left(1-\frac{M_i{}^2}{2}+\frac{M_i{}^4}{8}-\ \ldots\right)$$

For example, with $v_i=567$ m. p. h., $M_i=567/760=0.746$, $M_c=0.650$, and $v_c=494$ m. p. h. Note that the example given refers to sea level; at altitude, the example should be based on another value of κ and an appropriate value of the velocity of sound.

The coefficient of X^2 is

$$0.00045(-4.7994)+0.0001125(-1.41093)+\tfrac{1}{4}(0.013442)=0.001042$$

The coefficient of X is

$$1(-0.07322)+0.00045(5.76524)+\tfrac{1}{4}(-0.021173)=-0.07592$$

The constants are

$R=-0.032848$	$T=0.017042$
$\overline{R}=0.077092$	$\overline{T}=0.028790$
$S=-0.004381$	$U=0.103485$
$\overline{S}=-0.000344$	$\overline{U}=0.017720$

The constant term $D^R=0.094635$

The real equation is then

$$0.0001125X^3+0.001042X^2-0.07592X+0.094635=0$$

Imaginary equation:

The coefficient of X^2 is

$$0.00045(1.0788)+0.0001125(0.82297)+\tfrac{1}{4}(0.021495)=0.005952$$

The coefficient of X is

$$1(-0.088554)+0.00045(-3.30557)+\tfrac{1}{4}(-0.030076)=-0.097561$$

The constant term $D^I=0.11711$

The imaginary equation is then

$$0.005952X^2-0.097561X+0.1171=0$$

The positive roots of the real equation are $X=1.270$ and 21.0 and the roots of the imaginary equation are 1.302 and 15.08, or $\sqrt{X}=1.126$ and 4.58, and 1.141 and 3.883. These values of $\sqrt{X}$ are plotted against $1/k$ in figure 4. The curves traced by the roots against $1/k$ are shown in the figure. The intersection is at $\sqrt{X}=1.06$, $1/k=0.875$. Hence

$$v=\tfrac{1}{2}\times 2\times\frac{0.875}{1.06}b\omega_\alpha=0.826b\omega_\alpha$$

For $2b=12$ feet and $\omega_\alpha=90$, the flutter speed is 304 miles per hour.

These examples have been selected from several listed under the last part of the following section, to which the reader may refer for other examples, including the case of an unbalanced aileron.

THEORETICAL SURVEY OF THE EFFECT OF THE FLUTTER PARAMETERS

The purpose of this section is the study of the effect on the critical speed of the various independent variables. Although the theory in itself permits the solution of any particular case without difficulty, it is somewhat difficult to obtain a perspective of the effects of the parameters. Because of the many variables, this survey has been limited to the magnitudes and the ranges of most practical interest. It is realized that the effect of increasing or decreasing a certain parameter is dependent on the values chosen for the others. As a mathematical experiment, it is possible to change one variable and to keep *all* the others constant. With reference to practical problems, however, the change of one parameter is usually accompanied by unavoidable changes in several of the others. This fact must be kept in mind when actual or proposed changes intended to increase the flutter speed of airplanes are considered. This discussion is intended to give only the salient facts; the charts contain the complete data.

CASE 1 (FLEXURE-TORSION)

The flutter speed for case 1 is plotted in the coefficient form $v/b\omega_\alpha$. In the following graphs, the frequency ratio ω_h/ω_α is generally used as abscissa and the critical flutter coefficient $v/b\omega_\alpha$, as ordinate.

The graphs under each of the following sections of case 1 are arranged in order of decreasing values of κ,

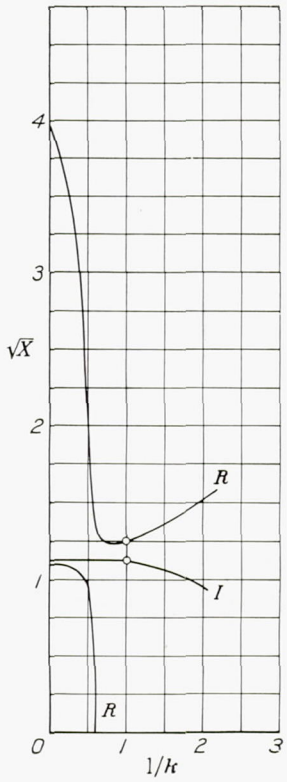


FIGURE 3.—Case 3. Numerical example. The roots $\sqrt{X}$ of the real and the imaginary equations against $1/k$.

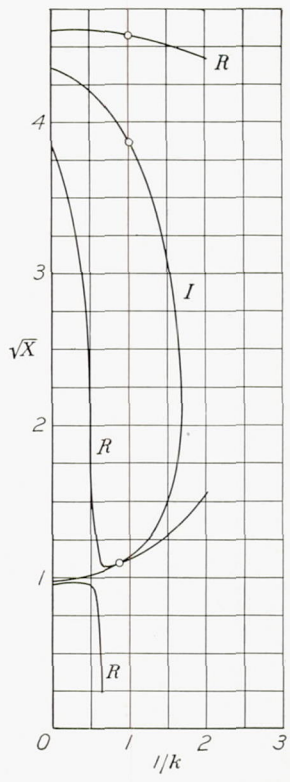
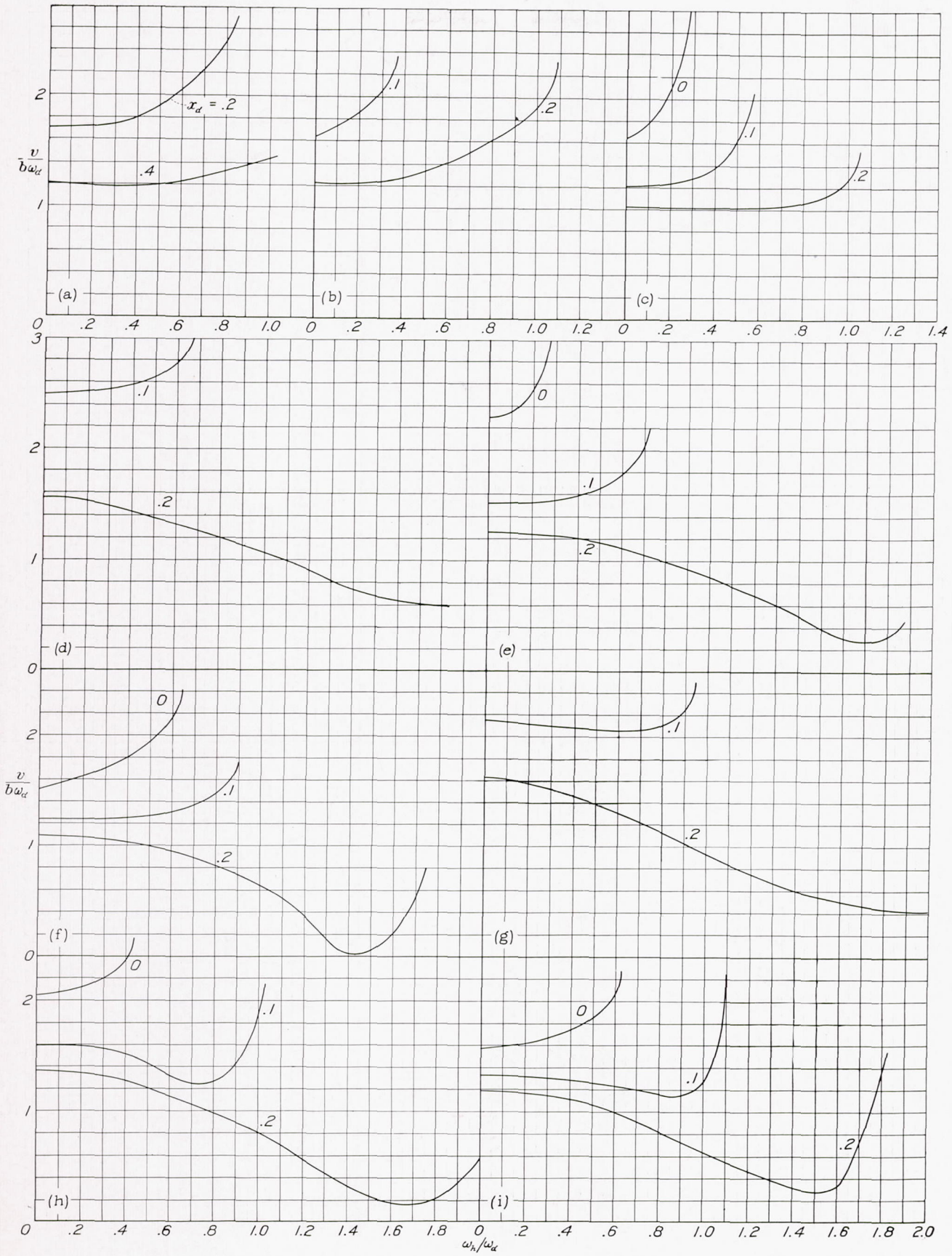


FIGURE 4.—Three degrees of freedom. Numerical example. The roots $\sqrt{X}$ of the real and the imaginary equations against $1/k$.

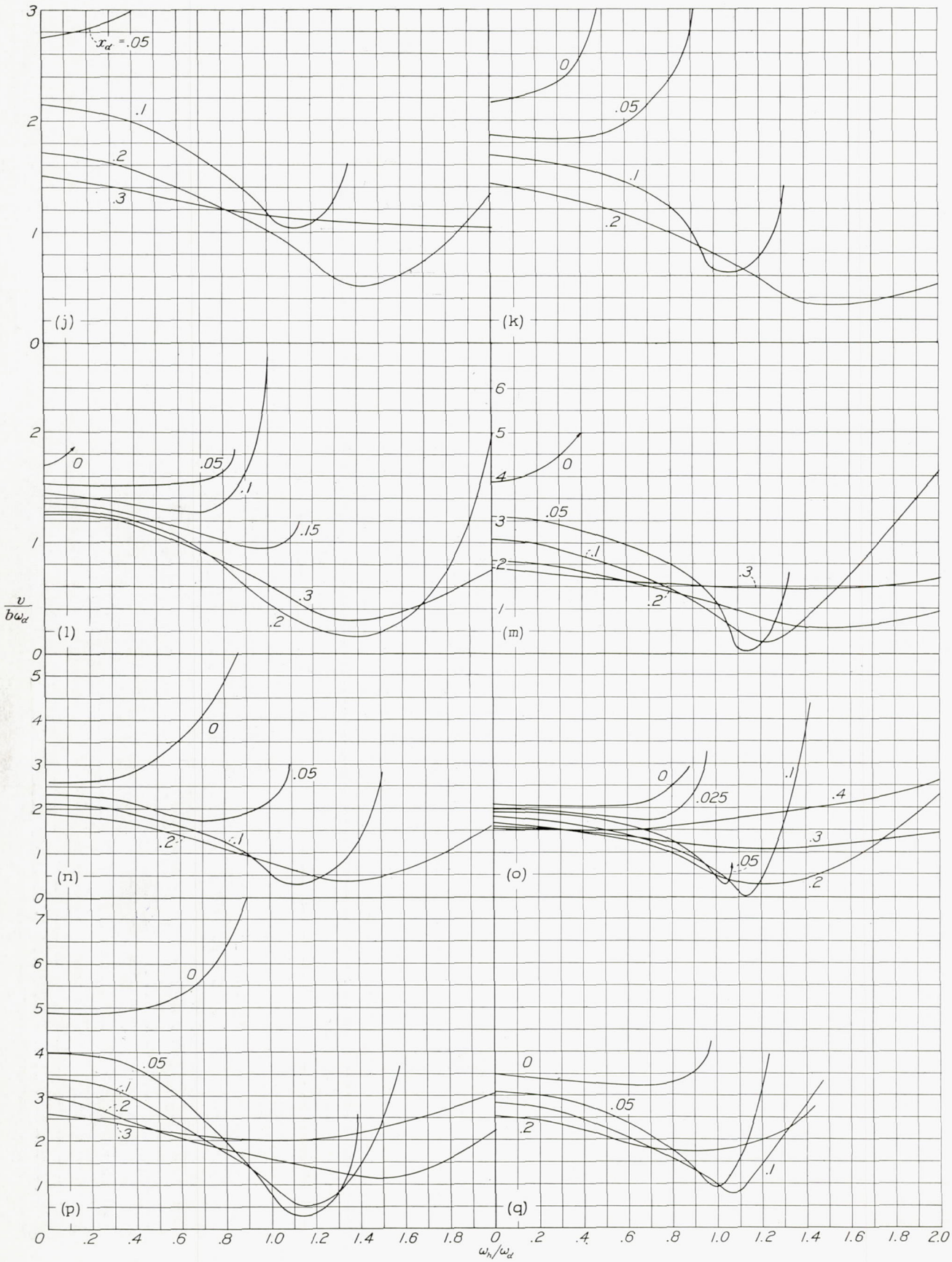
starting with $\kappa=1/2$ (lightest wings) and ending with $\kappa=1/20$ (heaviest). The range of κ for present-day airplanes is approximately $\kappa=1/3$ to $\kappa=1/15$. The graphs are further arranged in order of increasing values of a, starting with the smallest values of a (stiffness axis in the most forward location). In most cases, the radius of gyration is kept at a fixed value $r_\alpha^2=1/4$.

Effect of center of gravity x_α.—The effect of x_α on flutter speed is given in graph I–A. It may be observed that there is usually a decrease in the critical speed as the frequency ratio ω_h/ω_α is increased from zero and that the curves tend to a minimum near the frequency ratio $\omega_h/\omega_\alpha=1$. There are cases, however, in which the minimum critical speed lies at $\omega_h/\omega_\alpha=0$. The transition takes place for a certain small value of x_α.



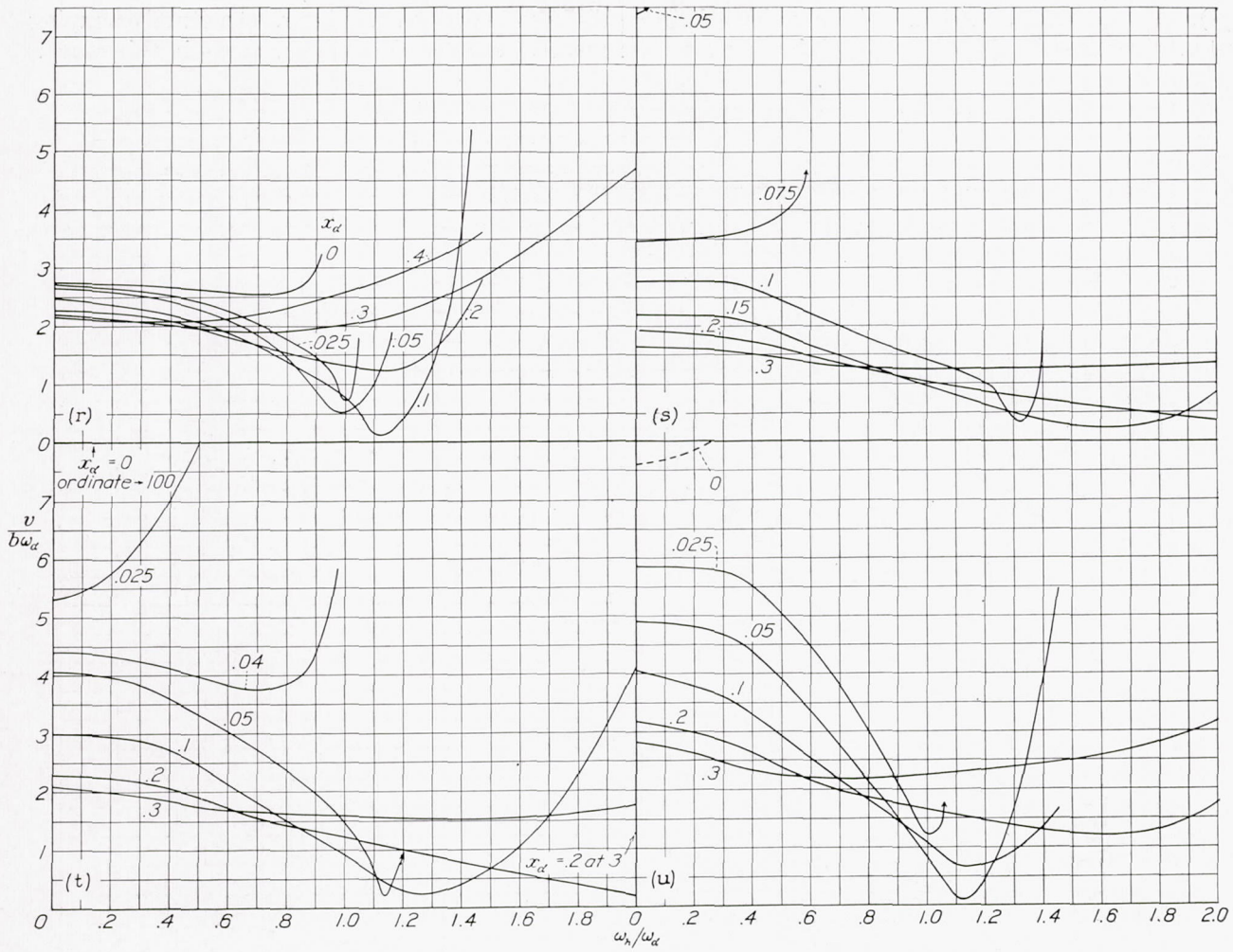
(a) $\kappa=\frac{1}{2}$; $a=-0.4$; $x_\alpha=0$ stable; $x_\alpha=0.1$ stable; $v_D/b\omega_\alpha=1.58$.
(b) $\kappa=\frac{1}{2}$; $a=-0.3$; $x_\alpha=0$ stable; $v_D/b\omega_\alpha=1.12$.
(c) $\kappa=\frac{1}{2}$; $a=-0.2$; $v_D/b\omega_\alpha=0.913$.
(d) $\kappa=\frac{1}{2}$; $a=-0.4$; $x_\alpha=0$ stable; $v_D/b\omega_\alpha=1.94$.
(e) $\kappa=\frac{1}{2}$; $a=-0.3$; $v_D/b\omega_\alpha=1.37$.
(f) $\kappa=\frac{1}{2}$; $a=-0.2$; $v_D/b\omega_\alpha=1.12$.
(g) $\kappa=\frac{1}{4}$; $a=-0.4$; $x_\alpha=0$ stable; $v_D/b\omega_\alpha=2.24$.
(h) $\kappa=\frac{1}{4}$; $a=-0.3$; $v_D/b\omega_\alpha=1.58$.
(i) $\kappa=\frac{1}{4}$; $a=-0.2$; $v_D/b\omega_\alpha=1.29$.

Graph I-A (a-i).—The effect of x_α; the flutter coefficient against the frequency ratio; $r_\alpha^2=1/4$. Case 1 (h, α).



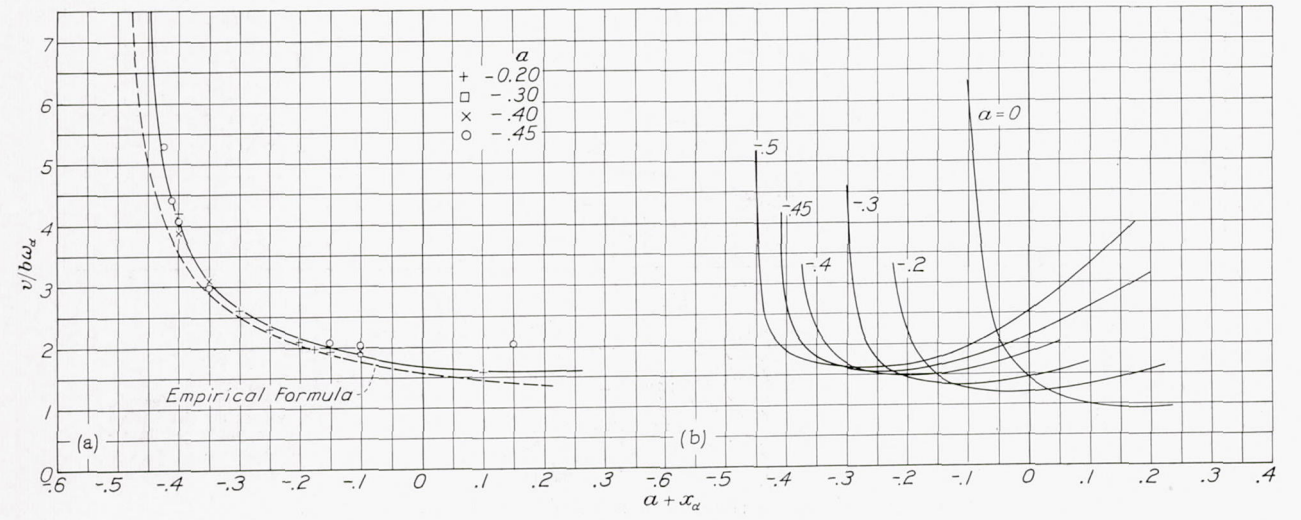
(j) $\kappa=\frac{1}{5}$; $a=-0.4$; $v_D/b\omega_\alpha=2.5$; $x_\alpha=0$, starts at ordinate 6.9.
(k) $\kappa=\frac{1}{5}$; $a=-0.3$; $v_D/b\omega_\alpha=1.77$.
(l) $\kappa=\frac{1}{5}$; $a=-0.2$; $v_D/b\omega_\alpha=1.45$.
(m) $\kappa=\frac{1}{10}$; $a=-0.4$; $v_D/b\omega_\alpha=3.54$.
(n) $\kappa=\frac{1}{10}$; $a=-0.3$; $v_D/b\omega_\alpha=2.5$.
(o) $\kappa=\frac{1}{10}$; $a=-0.2$; $v_D/b\omega_\alpha=2.05$.
(p) $\kappa=\frac{1}{20}$; $a=-0.4$; $v_D/b\omega_\alpha=5.0$.
(q) $\kappa=\frac{1}{20}$; $a=-0.3$; $v_D/b\omega_\alpha=3.54$.

Graph I-A (j-q).—The effect of x_α; the flutter coefficient against the frequency ratio; $r_\alpha{}^2=1/4$. Case 1 (h, α).



(r) $\kappa=\frac{1}{20}$; $a=-0.2$; $v_D/b\omega_\alpha=2.88$.
(s) $\kappa=\frac{1}{5}$; $a=-0.45$; $v_D/b\omega_\alpha=3.54$.
(t) $\kappa=\frac{1}{10}$; $a=-0.45$; $v_D/b\omega_\alpha=5.0$.
(u) $\kappa=\frac{1}{20}$; $a=-0.45$; $v_D/b\omega_\alpha=7.07$.

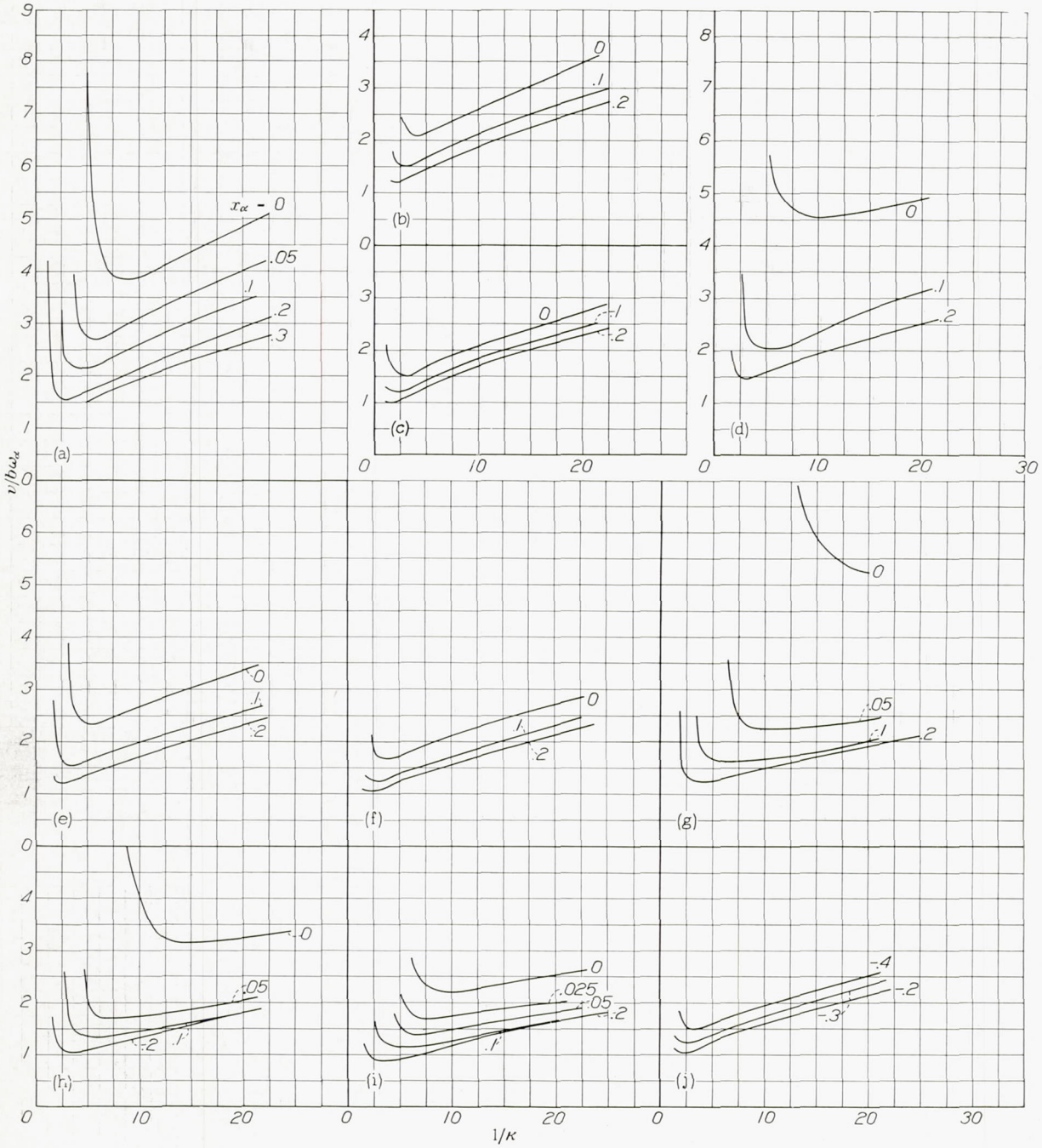
Graph I–A (r–u).—The effect of x_α; the flutter coefficient against the frequency ratio; $r_\alpha^2=1/4$. Case 1 (h, α).



(a) $\kappa=\frac{1}{10}$; $\left(\frac{\omega_h}{\omega_\alpha}\right)^2=0$. (b) $\kappa=\frac{1}{10}$; $\left(\frac{\omega_h}{\omega_\alpha}\right)^2=\frac{1}{2}$.

Graph I–B.—The effect of the stiffness axis; the flutter coefficient against the center-of-gravity location; $r_\alpha^2=1/4$. Case 1 (h, α).

This value is greater the larger the values of κ (light wings). For instance, when $\kappa=1/4$, a value of $x_\alpha=$ about 0.1 (graph I–A (g)) brings the minimum near the speed near unity frequency ratio from zero to infinity. As may be observed later, structural damping will greatly alter the shape of the curve in this range.



(a) $\left(\frac{\omega_h}{\omega_\alpha}\right)^2=0$; $a=-0.4$.

(b) $\left(\frac{\omega_h}{\omega_\alpha}\right)^2=0$; $a=-0.3$.

(c) $\left(\frac{\omega_h}{\omega_\alpha}\right)^2=0$; $a=-0.2$.

(d) $\left(\frac{\omega_h}{\omega_\alpha}\right)^2=1/10$; $a=-0.4$.

(e) $\left(\frac{\omega_h}{\omega_\alpha}\right)^2=1/10$; $a=-0.3$.

(f) $\left(\frac{\omega_h}{\omega_\alpha}\right)^2=1/10$; $a=-0.2$.

(g) $\left(\frac{\omega_h}{\omega_\alpha}\right)^2=1/2$; $a=-0.4$.

(h) $\left(\frac{\omega_h}{\omega_\alpha}\right)^2=1/2$; $a=-0.3$.

(i) $\left(\frac{\omega_h}{\omega_\alpha}\right)^2=1/2$; $a=-0.2$.

(j) $\left(\frac{\omega_h}{\omega_\alpha}\right)^2=1/10$; $x_\alpha=0.2$. In this section of the graph, the values on the curves refer to a, not to x_α as in sections (a) to (i).

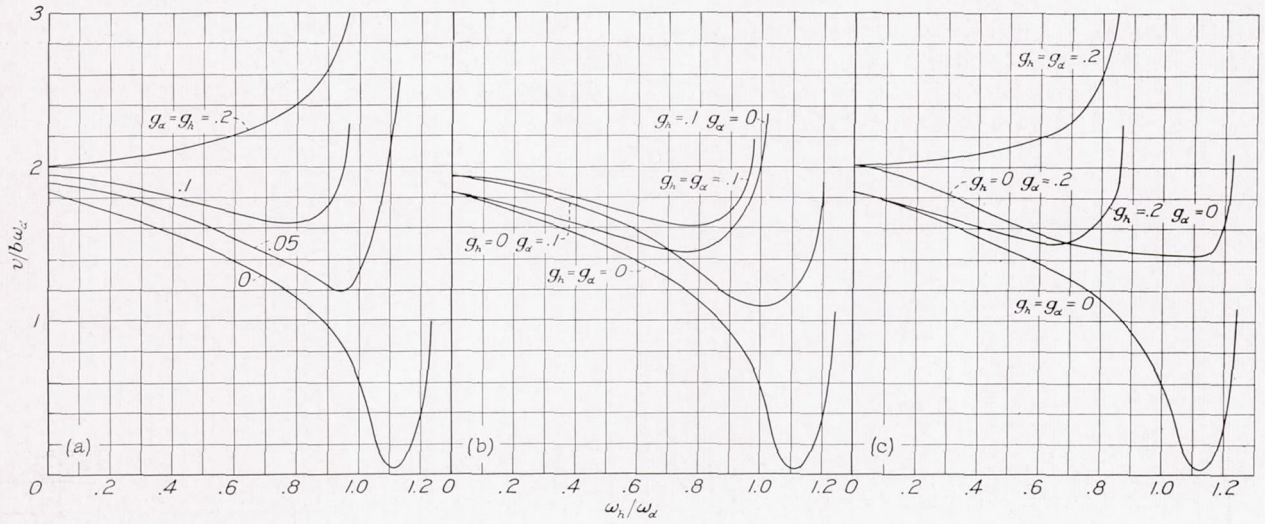
Graph I–C (a–j).—The effect of x_α; the flutter coefficient against $1/\kappa$; $r_\alpha^2=1/4$. Case 1 (h, α).

origin. For $\kappa=1/10$, x_α must be close to zero (graph I–A (m)) to cause transition. The transition is critical; graph I–A (m) shows that a 2.5-percent change in the position of the center of gravity changes the flutter

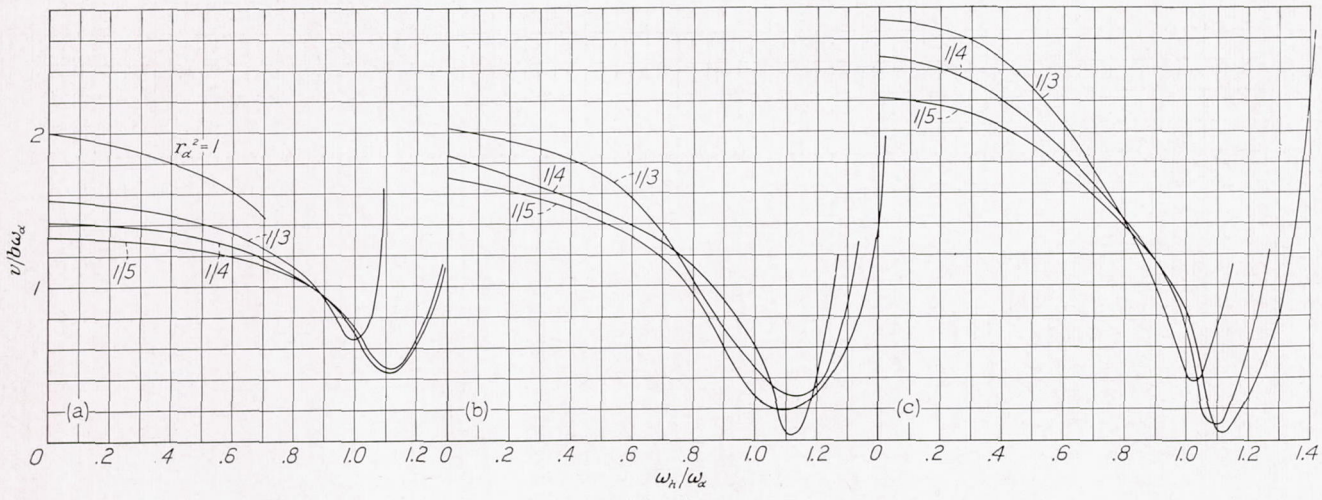
The range of most practical importance is, however, the neighborhood of the zero frequency ratio. (For wings, the ratio is approximately 1/4.) In this range, the parameter of greatest significance is really the com-

bination $\frac{1}{2}+a+x_\alpha$. In other words, the flutter speed is very nearly a function of the location of the center of gravity with respect to the forward quarter-chord position and not of the distance relative to the stiffness axis. Graph I–B (a) shows clearly that the value of a actually has no influence on the flutter speed. Outside of this range, that is, for larger values of ω_h/ω_α, the relationship is less simple. Graph I–B (b) shows the dependency on the center-of-gravity location for various positions of the stiffness axis a. For a constant x_α, that is, for a constant distance between the stiffness axis and the center of gravity, the flutter speed is increased as the stiffness axis (and center of gravity) is moved forward.

Graph I–C shows the flutter coefficient plotted against $1/\kappa$. The normal range of wings is included in the diagram (the heaviest wings to the right). The diagrams are arranged in order of increasing values of $(\omega_h/\omega_\alpha)^2$ and of a. An interesting result is the existence of a minimum critical speed that falls in the range of light wings ($\kappa=1/3$ to $1/5$). Graph I–C (d) gives very normal values of the parameters as used for most wings. These curves, for a *given* wing, may be taken to give the effect of altitude. Note that, for a given wing with $\kappa=1/5$ at sea level, κ becomes $1/10$ at approximately 15,000 feet, with a resulting increase in the flutter speed under normal circumstances. For the case with $x_\alpha=0.2$ given in graph I–C (d), the increase in the flutter coefficient is from 1.6 to 1.95, or about 20 percent. It is possible that, for very light wings, the flutter speed might decrease with altitude until a certain altitude is reached. For high values of $1/\kappa$ (heavy wings), the flutter speed increases nearly as the square root of the wing density, $1/\kappa$.



Graph I–D (a–c).—The effect of structural friction; the flutter coefficient against the frequency ratio; $\kappa=1/10$; $a=-0.2$; $x_\alpha=0.1$. Case 1 (h, α).



(a) $\kappa=1/5$. (b) $\kappa=1/10$. (c) $\kappa=1/20$.

Graph I–E (a–c).—The effect of radius of gyration; the flutter coefficient against the frequency ratio; $a=-0.2$, $x_\alpha=0.1$. Case 1 (h, α).

Effect of structural friction g_α, g_h.—Graph I–D is intended to show the effect of the structural friction on the critical speed. As the coefficients of friction are increased, there is a definite tendency for the often pronounced minimum flutter speed near $\omega_h/\omega_\alpha\cong 1.0$ to disappear and to produce response curves of the type

obtained for negative value of x_α. In the range of most practical interest ($\omega_h/\omega_\alpha \cong 0$), the torsional friction is the more important.

Effect of radius of gyration r_α.—Graph I–E is arranged in conventional order. Note that the flutter coefficient in the low ω_h/ω_α range increases with increase in the radius of gyration. This increase in the flutter coefficient does not necessarily correspond to an increase in the flutter speed; it *does* if the torsional frequency ω_α is kept constant. If the *stiffness* is kept constant, which means that ω_α is decreased as $1/r_\alpha$, the flutter speed is actually decreased, as is shown in the following table.

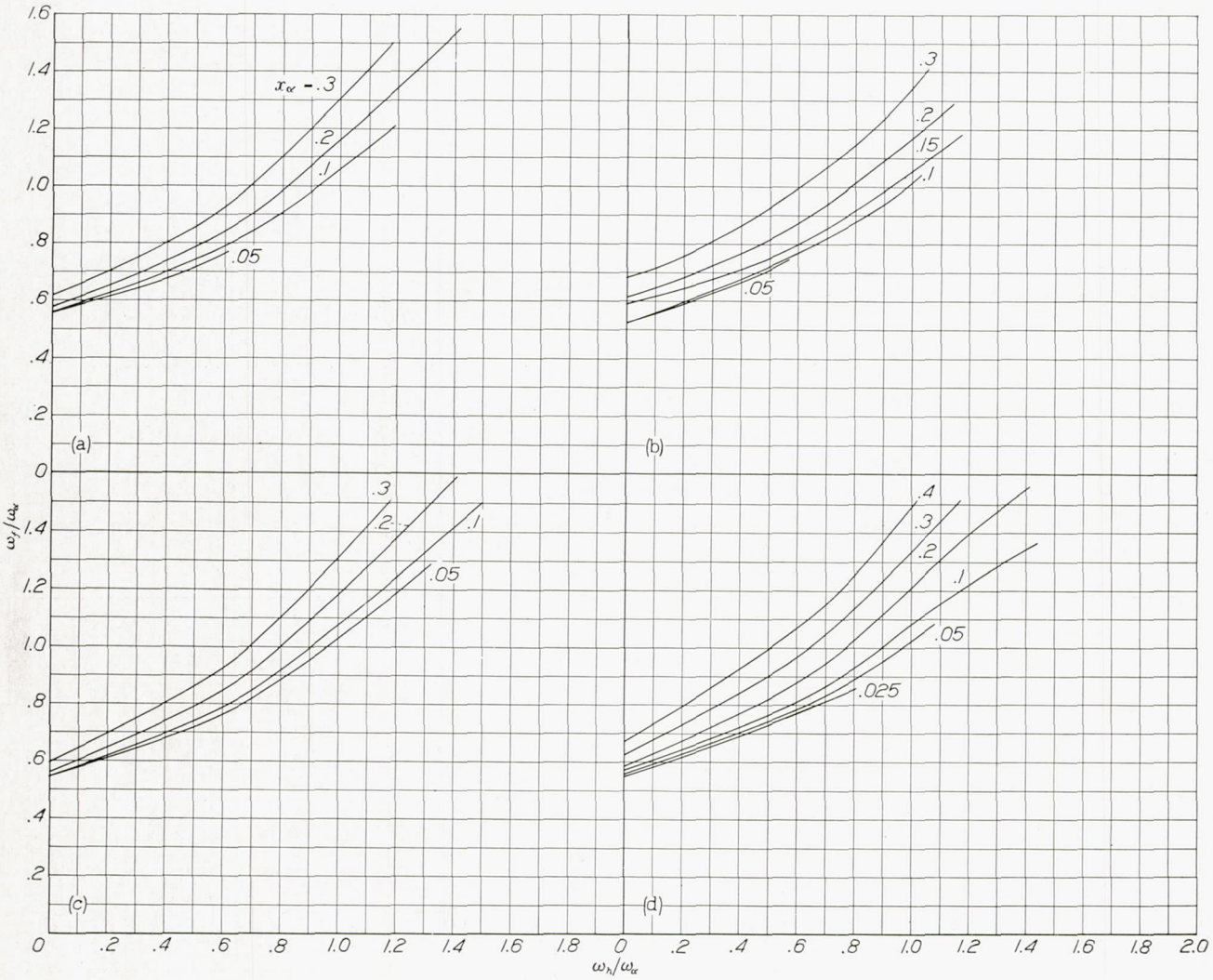
FLUTTER SPEED FOR CONSTANT TORSIONAL STIFFNESS

[$a=-0.2$, $x_\alpha=0.1$, $(\omega_h/\omega_\alpha)^2=0$]

κ \ r_α^2	1/5	1/4	1/3
1/5	100	97.6	92.4
1/10	91.2	88.6	84.8
1/20	84	83.2	80.2

(Values in the preceding table are given in relation to the value for $\kappa=1/5$, $r_\alpha^2=1/5$, which is the case of lowest wing density and smallest radius of gyration.) The speed corresponding to given stiffness drops if any mass is added so that r_α, the density $1/\kappa$, or both are increased. Hence, any mass added not for the purpose of increasing the stiffness or moving the center of gravity forward is detrimental.

Flutter frequency.—The flutter frequency is shown in graph I–F. It is seen, for instance, that for small values of ω_h/ω_α, the flutter frequency is around 60 percent of the torsional frequency ω_α; for higher values of the flexural frequency, the flutter frequency approaches or exceeds the torsional. This graph is primarily of interest in connection with experimental flutter research.



(a) $\kappa=1/5$; $a=-0.4$. (b) $\kappa=1/5$; $a=-0.2$.
(c) $\kappa=1/10$; $a=-0.4$. (d) $\kappa=1/10$; $a=-0.2$.

Graph I–F (a–d).—Flutter frequency ratio as dependent on x_α against frequency ratio; $r_\alpha^2=1/4$. Case 1 (h, α).

Coupling factor ξ.—Consider a two-dimensional case of flutter in which only a *part* of the total length of the (infinitely long) wing is given the second degree of freedom. This arrangement, because of the deficient

coupling, exhibits a higher critical speed. Call the fraction having *both* degrees of freedom, ξ. The results are shown for several values of ξ in graph I–G.

Divergence velocity and approximate flutter formula.—It can be shown that the divergence velocity may be expressed in nondimensional form as

$$\frac{v_D}{b\omega_\alpha}=\sqrt{\frac{r_\alpha^2}{\kappa}\quad\frac{\frac{1}{2}}{\frac{1}{2}+a}}$$

The divergence velocity $v_D/b\omega_\alpha$ is given in graphs I–A. This velocity is usually higher than the flutter velocity.

An empirical expression, which is useful in quickly obtaining the order of magnitude of the flutter speed for small values of ω_h/ω_α and which appears to hold very well for heavy wings (with $\kappa<1/10$) is given by

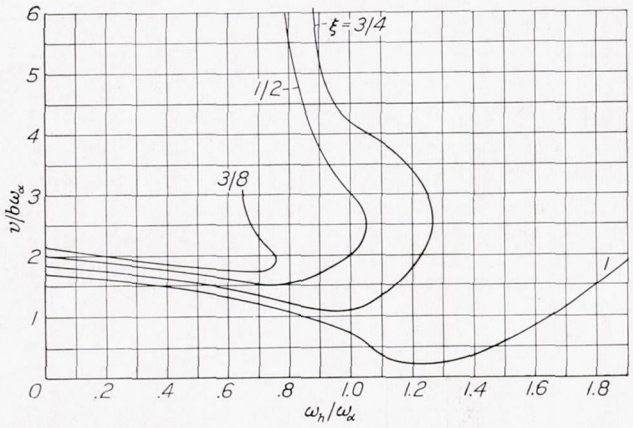
$$\frac{v_f}{b\omega_\alpha}\cong\sqrt{\frac{r_\alpha^2}{\kappa}\quad\frac{\frac{1}{2}}{\frac{1}{2}+a+x_\alpha}}$$

Graph I–B (a) shows the curve obtained from the empirical expression (dashed) and a curve based on the exact values (in full lines).

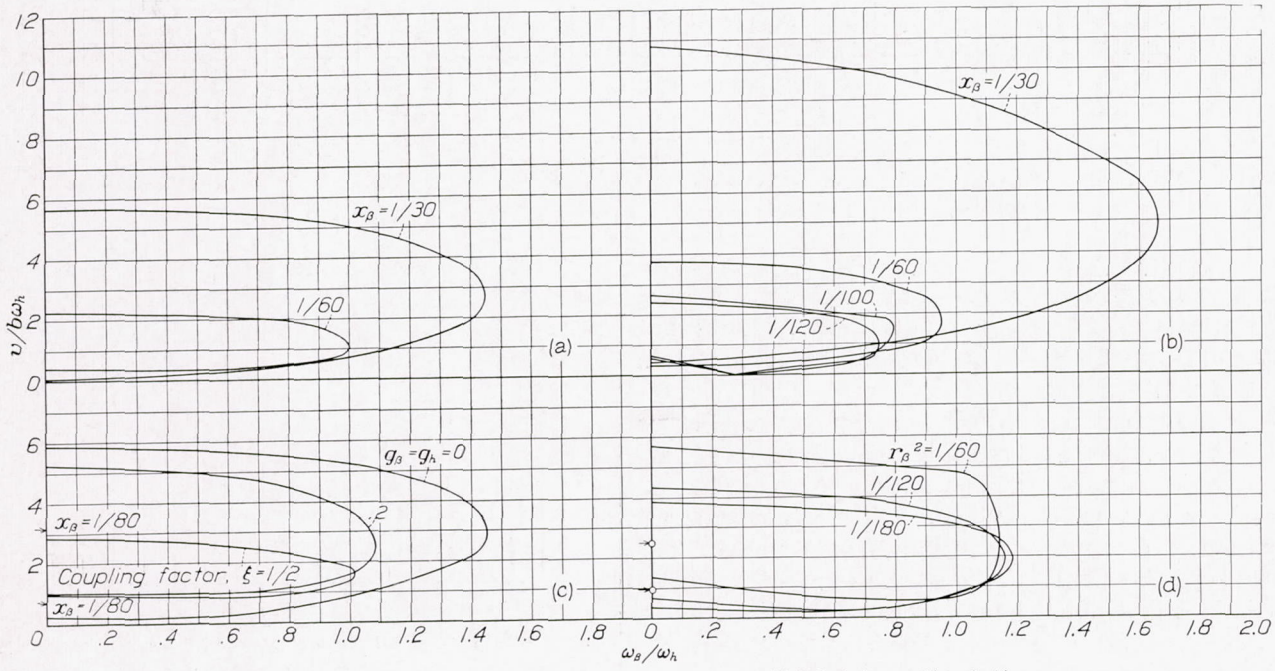
CASE 2 (FLEXURE-AILERON)

The flutter coefficient for case 2 is $v/b\omega_h$. The frequency ratio ω_β/ω_h is ordinarily used as abscissa. The graphs are again arranged in order of increasing wing density. Two values of the location of the aileron hinge axis c have been included. The first value, $c=\frac{1}{2}$, or the aileron chord equal to 25 percent of the total chord, is intended to represent a wing-aileron combination; the second value, $c=0$, or the aileron chord equal to 50 percent of the total chord represents a stabilizer-elevator or a fin-rudder combination. Several values of x_β and r_β^2 and of the damping coefficients g_β and g_h have been included.

It should be mentioned that ordinarily, as shown in reference 1, case 2 differs basically from case 1 by the existence of a *flutter range* extending between a lower and an upper flutter speed. This range of flutter can be reduced or eliminated by various means. It is important also to notice that, beyond a certain value of the frequency ratio ω_β/ω_h, in fact, for a value slightly greater than unity, no critical speed exists, since the critical area does not extend much beyond this point. The reduction of the center-of-gravity distance from the



Graph I–G.—The effect of the coupling factor ξ; the flutter coefficient against the frequency ratio; $\kappa=\frac{1}{10}$; $a=-0.2$; $x_\alpha=0.2$.



(a) Effect of x_β; $\kappa=\frac{1}{5}$; $r_\beta^2=\frac{1}{120}$.
(b) Effect of x_β; $\kappa=\frac{1}{10}$; $r_\beta^2=\frac{1}{120}$.
(c) Effect of g_β and g_h; $\kappa=\frac{1}{10}$; $r_\beta^2=\frac{1}{160}$; $x_\beta=\frac{1}{40}$.
(d) Effect of r_β^2; $\kappa=\frac{1}{10}$; $x_\beta=\frac{1}{60}$.

Graph II–A (a–d).—Flutter coefficient against frequency ratio; $c=\frac{1}{2}$. Case 2 (β, h).

hinge has the effect of reducing and finally eliminating the critical flutter area. Internal damping shows the same general effect. The fact that the aileron extends effectively over a shorter length is theoretically expressed by a "coupling factor" ξ, which is the length of the aileron divided by the total length of the wing executing deflection. The effect of ξ is shown in some of the graphs.

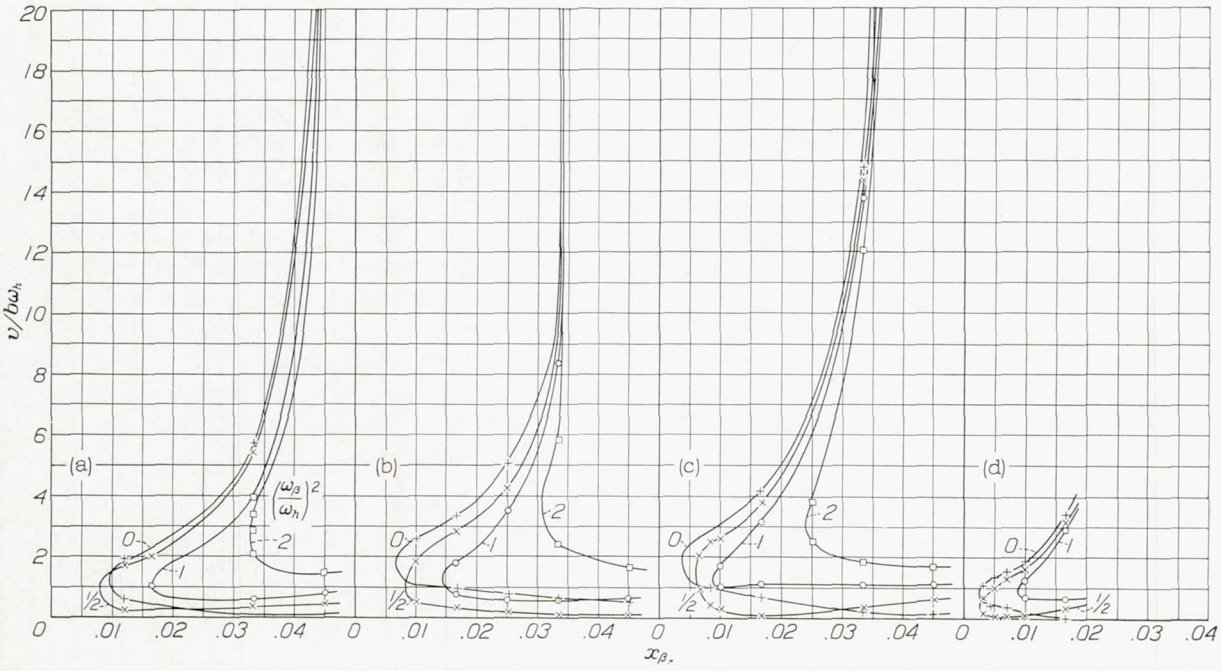
Effect of frequency ω_β/ω_h $(c=\frac{1}{2})$.—Graphs II–A (a) and (b) show the effect of varying x_β in reducing the critical area. The effect of damping is shown in graph II–A (c) and, finally, the effect of r_β^2 in graph II–A (d).

Effect of center of gravity x_β $(c=\frac{1}{2})$.—Graph II–B shows the flutter coefficient against the center-of-gravity distance x_β, giving, for two values of κ, the effect of varying the frequency ratio ω_β/ω_h at three values of r_β^2. Note that for large x_β (beyond normal range) the type of flutter reverts to that of case 1; that is, the upper flutter speed becomes infinite for a certain value of x_β.

It is important to notice, by considering each curve in this figure, that x_β must be decreased below a certain value, which is rather critical, in order to avoid flutter. If x_β is larger than this value, the lower flutter speed remains at a virtually constant, small value. The frequency ratio exhibits a similar effect; that is, flutter is eliminated beyond a certain frequency ratio often greater than unity, whereas for smaller ratios, the lower flutter speed remains at a low, nearly constant value. In other words, a critical frequency ratio can be defined for each value of the unbalance and, inversely, a definite critical value of the unbalance can be defined for each value of the frequency ratio. It is necessary then to choose the largest frequency ratio or the smallest unbalance, then to calculate the other value, and finally to choose the most practical combination, using a margin of safety.

Effect of radius of gyration r_β $(c=\frac{1}{2})$.—Graph II–C shows, for a typical wing-aileron case, the effect of changing the radius of gyration for various values of the frequency ratio.

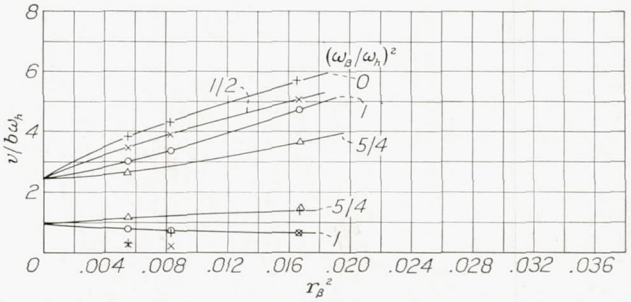
Effect of frequency ω_β/ω_h $(c=0)$.—In the preceding graphs, the hinge axis was at $c=\frac{1}{2}$. Graphs II–D, II–E, and II–F show the results for $c=0$. The curves are arranged in order and show the effect of x_β, r_β^2, g_h, and g_β for $\kappa=\frac{1}{5}$ and $\frac{1}{10}$. One curve is also included for $\kappa=\frac{1}{2}$ (graph II–D (d)).



(a) $c=\frac{1}{2}$; $\kappa=\frac{1}{5}$; $r_\beta^2=\frac{1}{120}$. (b) $c=\frac{1}{2}$; $\kappa=\frac{1}{5}$; $r_\beta^2=\frac{1}{60}$. (c) $c=\frac{1}{2}$; $\kappa=\frac{1}{10}$; $r_\beta^2=\frac{1}{120}$. (d) $c=\frac{2}{3}$; $\kappa=\frac{1}{5}$; $r_\beta^2=\frac{1}{300}$.

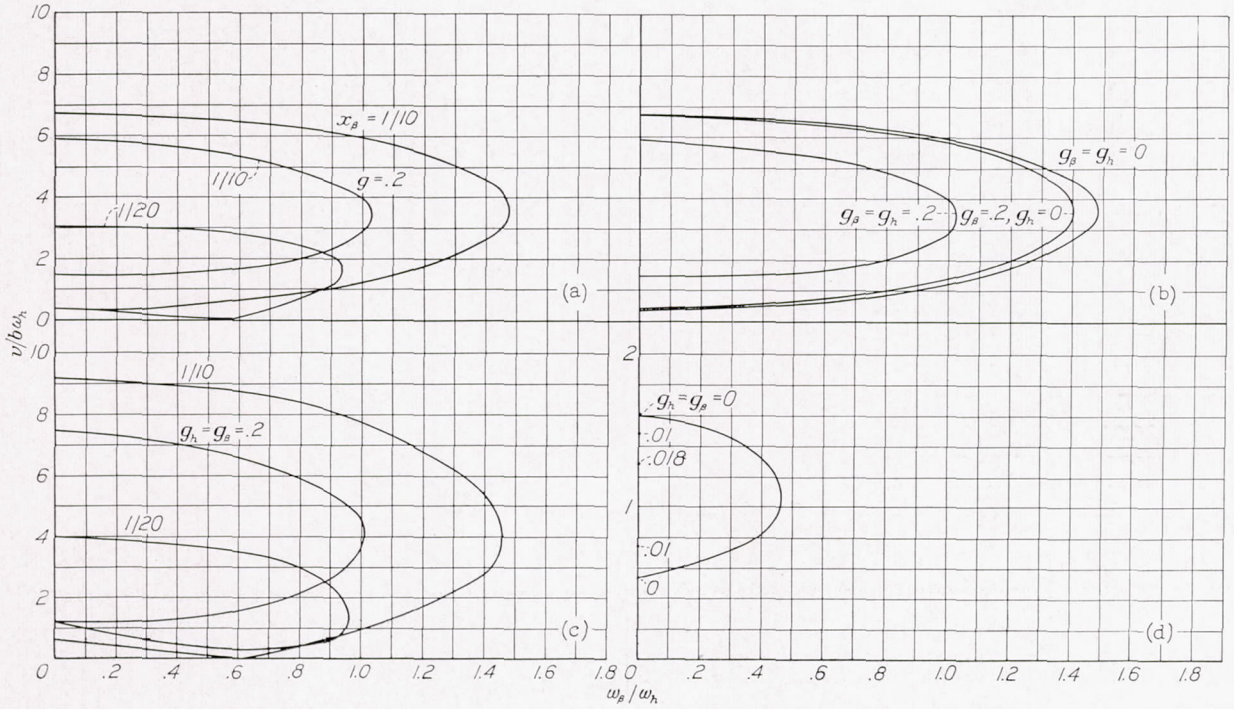
Graph II–B (a–d).—Flutter coefficient against x_β for various frequency ratios. Case 2 (β, h).

Effect of center of gravity x_β $(c=0)$.—The figures are given in graph II–E, arranged as usual.



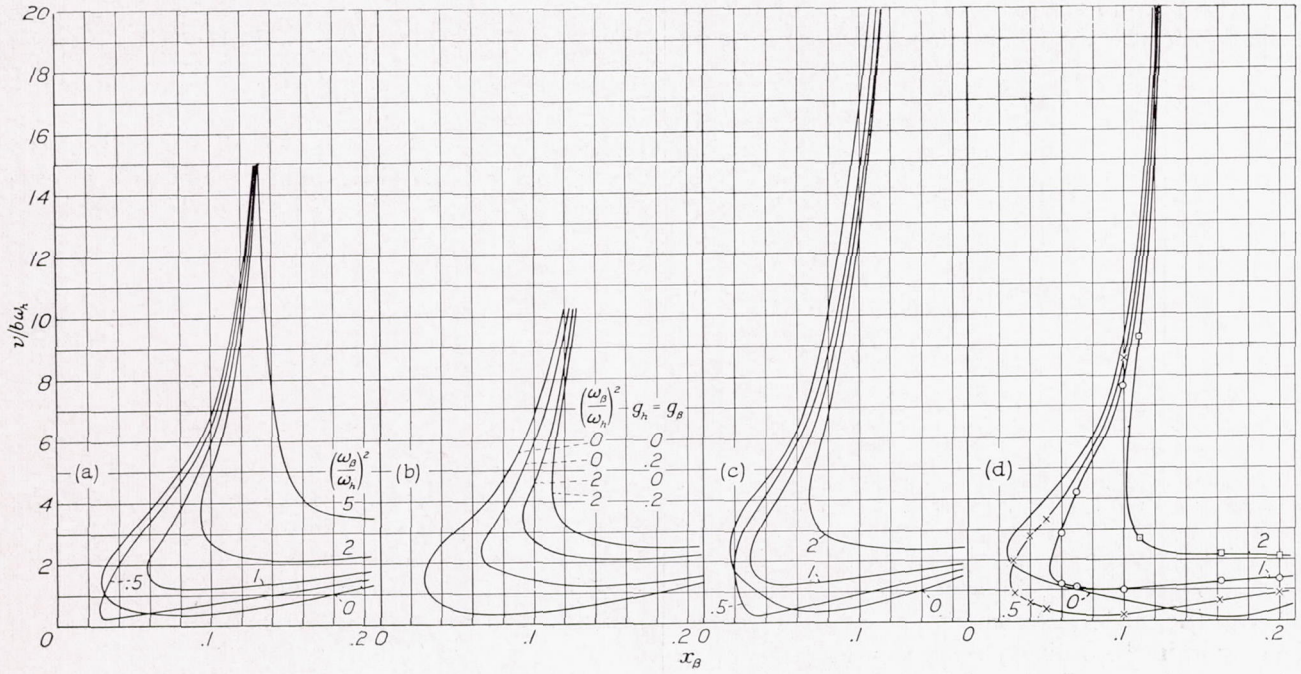
Graph II–C.—Flutter coefficient against r_β^2 for various frequency ratios; $c=\frac{1}{2}$; $\kappa=\frac{1}{10}$; $x_\beta=\frac{1}{60}$. Case 2 (β, h).

Effect of coupling factor $(c=0)$.—In graph II–F the effect of the coupling factor ξ is shown for an extreme case of unbalance (x_β large). The superimposed effect



(a) $\kappa = 1/5$; $r_\beta^2 = 1/20$; $x_\beta = 1/10$, $1/20$.
(b) $\kappa = 1/5$; $r_\beta^2 = 1/20$; $x_\beta = 1/10$.
(c) $\kappa = 1/5$; $r_\beta^2 = 1/10$; $x_\beta = 1/10$, $1/20$.
(d) $\kappa = 1/5$; $r_\beta^2 = 1/20$.

Graph II–D (a–d).—Flutter coefficient against frequency ratio, showing effect of x_β, g_β, and g_h; $c = 0$. Case 2 (β, h).



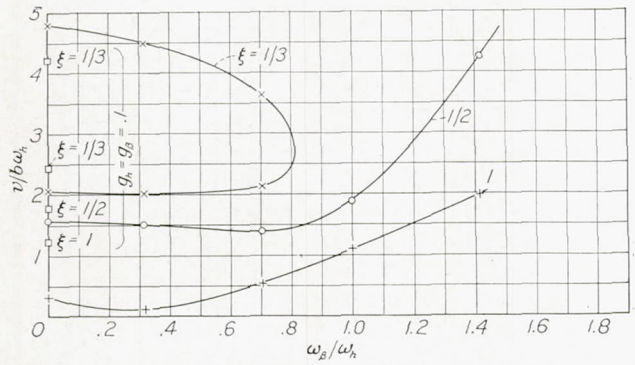
(a) $\kappa = 1/5$; $r_\beta^2 = 1/20$.
(b) $\kappa = 1/5$; $r_\beta^2 = 1/20$.
(c) $\kappa = 1/10$; $r_\beta^2 = 1/20$.
(d) $\kappa = 1/5$; $r_\beta^2 = 1/10$.

Graph II–E (a–d).—Flutter coefficient against x_β for various frequency ratios; $c = 0$. Case 2 (β, h).

of damping is shown for the zero frequency ratio. Notice how the coupling factor ($\xi \to 0$) gradually eliminates the flutter area.

CASE 3 (TORSION-AILERON)

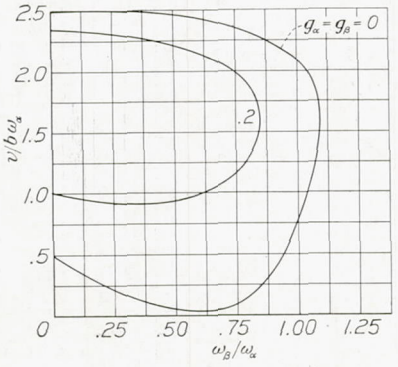
Three graphs, III–A, III–B, and III–C, are presented. There is a similarity to case 2. Graph III–A shows how the internal damping increases the lower flutter



Graph II–F.—Effect of coupling factor ξ; flutter coefficient against frequency ratio; $c=0$; $\kappa=1/5$; $r_\beta^2=1/6$; $x_\beta=1/4$ (an extreme case of unbalance). Also effect of friction for $\omega_\beta/\omega_h=0$.

speed. Graph III–B represents data taken from an actual case of a light wing with a smaller aileron. Note the striking similarity to case 2. For the value $x_\beta=0.0066$ (completely unbalanced aileron), $\omega_\beta/\omega_\alpha$ must be greater than 0.6 to avoid flutter; for the more normal value $x_\beta=0.002$, $\omega_\beta/\omega_\alpha$ need only be $\geqq 0.1$. The flutter area is eliminated by reducing x_β to a slightly smaller value.

Case 3 (torsion-aileron) is probably of less practical importance because the elimination of flutter for case

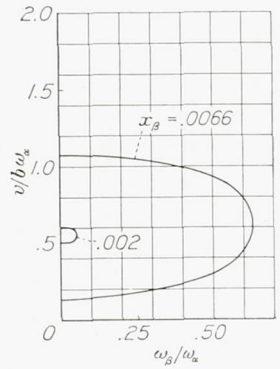


Graph III–A.—Effect of friction coefficients g_α, g_β; flutter coefficient against frequency ratio; $c=0.5$; $\kappa=1/10$; $a=-0.4$; $r_\alpha^2=1/4$; $x_\beta=1/80$; $r_\beta^2=1/160$. Case 3.

2 ordinarily excludes the possibility of flutter in case 3; but it is noted that, in order to eliminate mass coupling in the torsion-aileron case, a complete balance of the aileron in the ordinary sense ($x_\beta=0$) is not quite sufficient. It is actually found in the case of a heavy wing and no internal friction (with $x_\beta=0$) that the flutter speed is low, particularly near $\omega_\beta=\omega_\alpha$. Even a slight amount of friction, however, is sufficient to cancel the cause of this flutter. Graph III–C (fairly heavy wing) shows that, for no friction, a small overbalance ($x_\beta<0$) is necessary to eliminate flutter. For light wings, the effect is less pronounced and $x_\beta=0$ is usually sufficient. It may be observed from the original set of equations that true balance against rotation implies $r_\beta^2+(c-a)\,x_\beta=0$.

THREE DEGREES OF FREEDOM

In order to familiarize the reader with the complete case of three degrees of freedom and its relationship to the three subcases, a set of typical figures is shown. The constants used are the same as those in the numerical example (p. 8) with some additions. Case

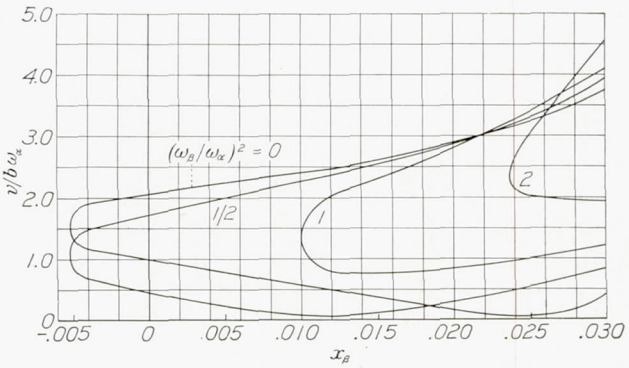


Graph III–B.—Effect of x_β; flutter coefficient against frequency ratio; $c=0.6$; $\kappa=1/4$; $a=-0.4$; $r_\alpha^2=1/4$; $r_\beta^2=0.0012$. Case 3(α, β).

1 is shown in figure 1 under the numerical example. The flutter coefficient $v/b\omega_\alpha=1.542$.

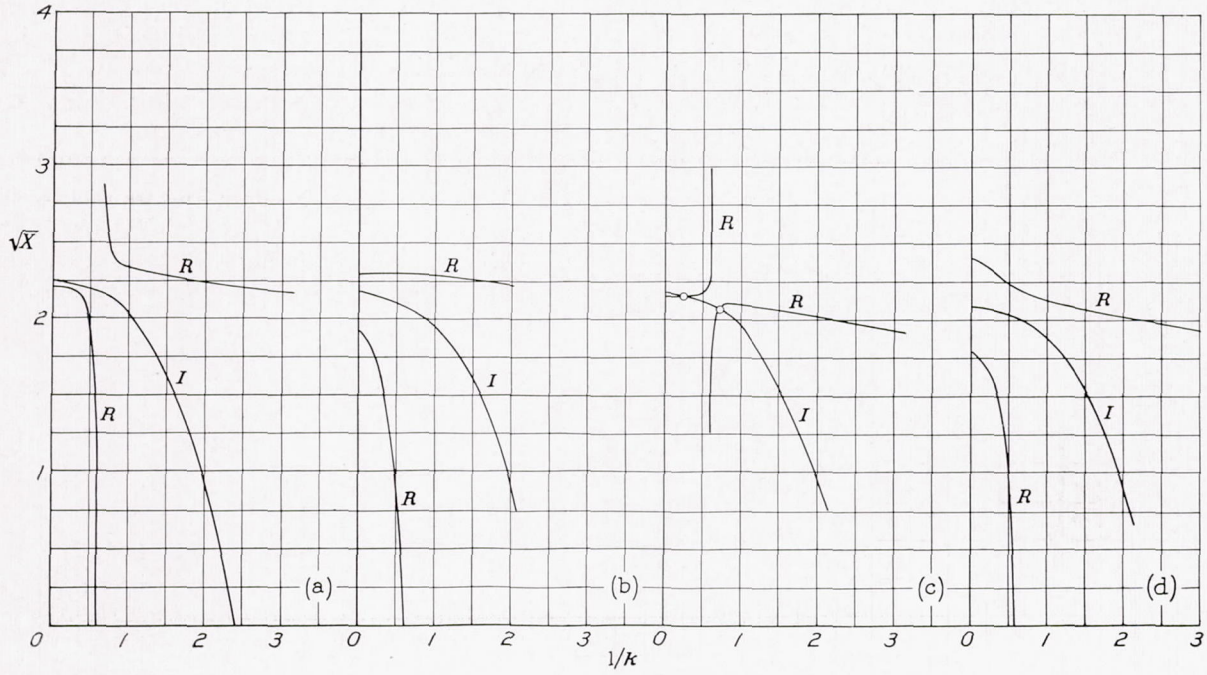
Case 2 is shown in figure 5; each part of the figure refers to different combinations of x_β and ω_β/ω_h. No flutter occurs for the combinations shown in figures 5 (a) and 5 (b) because of the balanced aileron and none in figure 5 (d) because of the large aileron frequency. For the combination shown in figure 5 (c), there is a normal range of flutter with two flutter points shown.

Case 3 is shown in figure 6; each part refers, respectively, to the same aileron parameters used in case 2. (Note that ω_h/ω_α is 1/4 in all cases.) The combinations



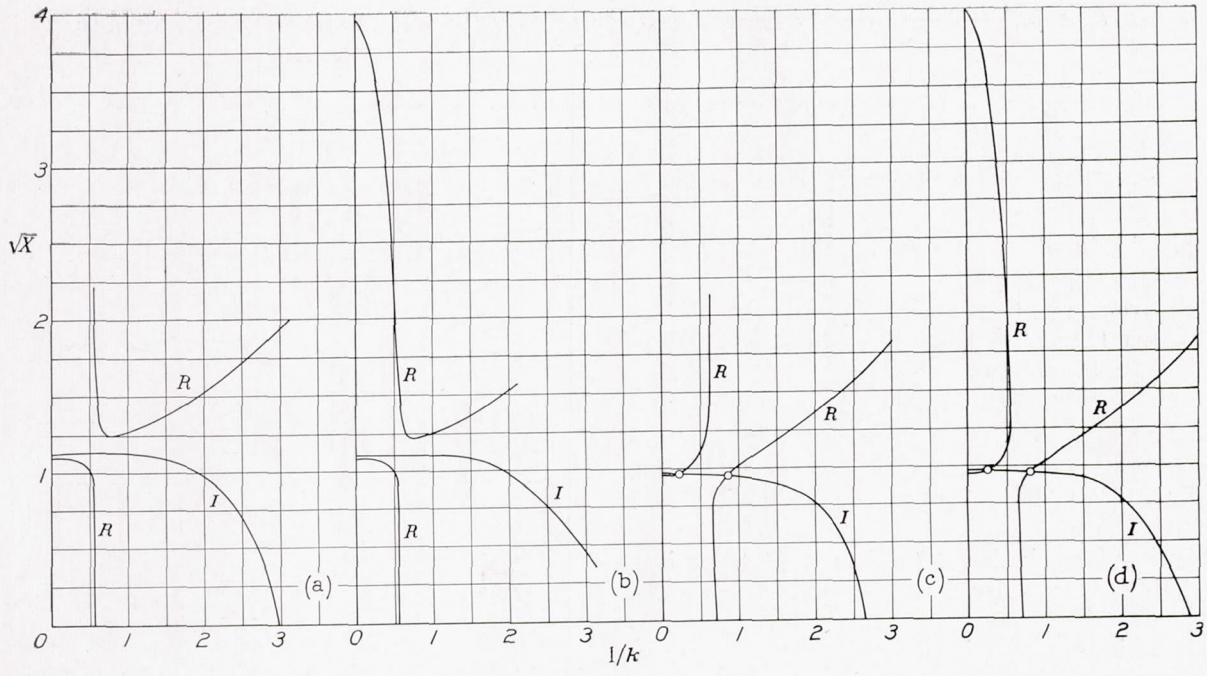
Graph III–C.—Flutter coefficient against x_β for various frequency ratios. $c=0.5$; $\kappa=1/10$; $r_\alpha^2=1/4$; $r_\beta^2=1/160$; $a=-0.4$. Case 3.

shown in figures 6 (a) and 6 (b) are again stable because of the aileron mass balance. For the arrangement shown in figure 6 (d), the aileron frequency is not high enough to prevent flutter as it did in case 2. Conditions are still worse for the combination shown in figure 6 (c).



(a) $\left(\frac{\omega_\beta}{\omega_h}\right)^2=0;\ x_\beta=0.$ (b) $\left(\frac{\omega_\beta}{\omega_h}\right)^2=3/2;\ x_\beta=0.$ (c) $\left(\frac{\omega_\beta}{\omega_h}\right)^2=0;\ x_\beta=0.0066.$ (d) $\left(\frac{\omega_\beta}{\omega_h}\right)^2=3/2;\ x_\beta=0.0066.$

FIGURE 5.—Case 2. The roots $\sqrt{X}$ of the real and the imaginary equations against $1/k$. Same parameters as in numerical example except as indicated.



(a) $\left(\frac{\omega_\beta}{\omega_\alpha}\right)^2=0;\ x_\beta=0.$ (b) $\left(\frac{\omega_\beta}{\omega_\alpha}\right)^2=3/32;\ x_\beta=0.$ (c) $\left(\frac{\omega_\beta}{\omega_\alpha}\right)^2=0;\ x_\beta=0.0066.$ (d) $\left(\frac{\omega_\beta}{\omega_\alpha}\right)^2=3/32;\ x_\beta=0.0066.$

FIGURE 6.—Case 3. The roots $\sqrt{X}$ of the real and the imaginary equations against $1/k$. Same parameters in numerical example except as indicated.

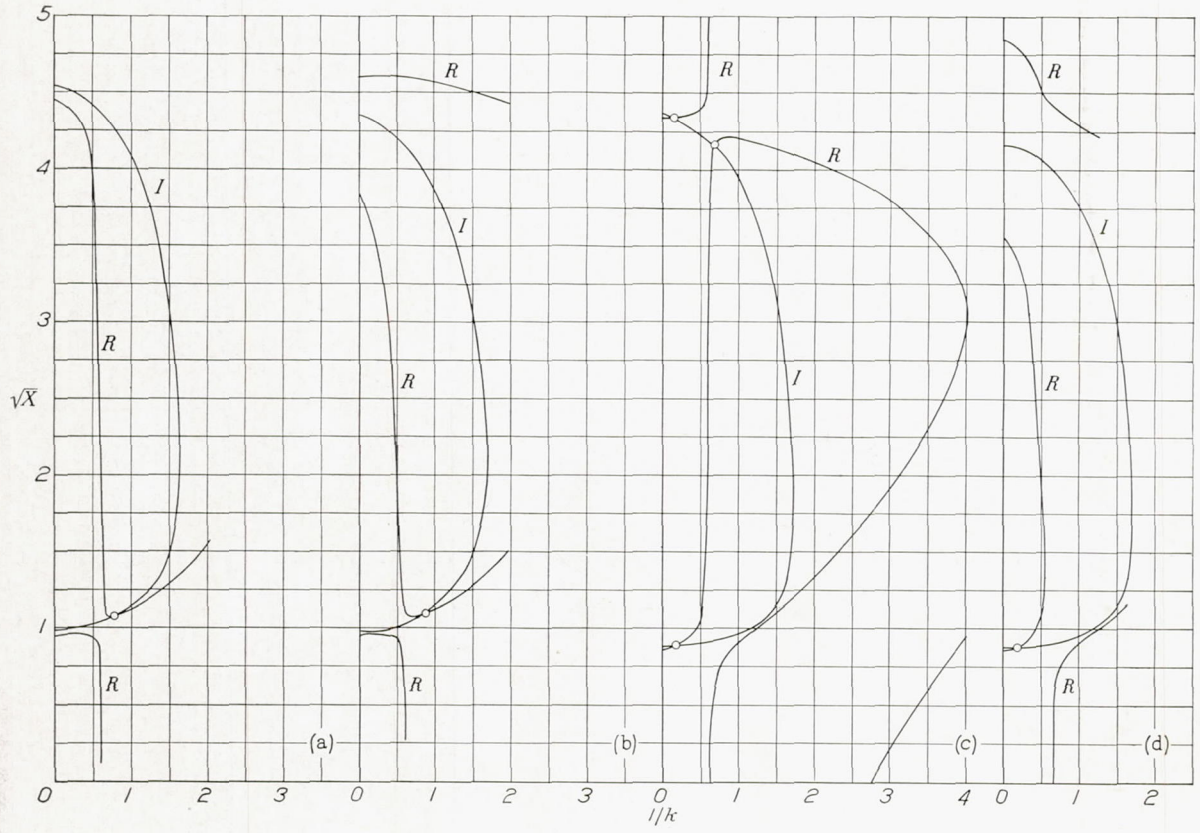
For the case of three degrees of freedom, figure 7 shows the results arranged in the same order as under cases 2 and 3. For the conditions given in figures 7 (a) and 7 (b), flutter existed only in case 1. The flutter point shown is therefore essentially case 1 flutter. The value of the flutter coefficient, however, has actually *decreased* from its case 1 value of 1.542 to 0.70 and 0.825, respectively.

For the arrangement shown in figure 7 (d), flutter exists in cases 1 and 3. Here the ranges completely merge, indicating stability at only very low speed. Flutter exists in all three cases for the combination shown in figure 7 (c). The case 2 flutter can be recognized, almost unchanged, while again the flutter ranges of case 1 and case 3 have merged, as in figure 7 (d).

Figure 8 has been included to show that there is a considerable lowering of the flutter speed for low values of the aileron frequency even though the aileron is balanced. This condition is probably not of primary concern because a small amount of friction, particularly g_α, will restore the flutter speed to its full (case 1) value. It is to be noted, however, that a slight overbalance ($x_\beta < 0$) may be desirable.

TRANSITION TO THREE-DIMENSIONAL FLUTTER PROBLEMS

The previous theory relates to two-dimensional flutter and, strictly, to a wing of infinite length. The second restriction is not very troublesome, the aspect-ratio, or span, effect being relatively unimportant and by no means as great as the aspect-ratio effect associated with stationary flows. It may be disregarded and tacitly considered as a safety factor, since an air speed of the order of a few percent more than that in two-dimensional flow is necessary to cause flutter.



(a) $\left(\frac{\omega_\beta}{\omega_h}\right)^2=0$; $x_\beta=0$. (b) $\left(\frac{\omega_\beta}{\omega_h}\right)^2=3/2$; $x_\beta=0$. (c) $\left(\frac{\omega_\beta}{\omega_h}\right)^2=0$; $x_\beta=0.0066$. (d) $\left(\frac{\omega_\beta}{\omega_h}\right)^2=3/2$; $x_\beta=0.0066$.

FIGURE 7.—Three degrees of freedom. The roots $\sqrt{X}$ of the real and the imaginary equations against $1/k$. Same parameters as in numerical example except as indicated.

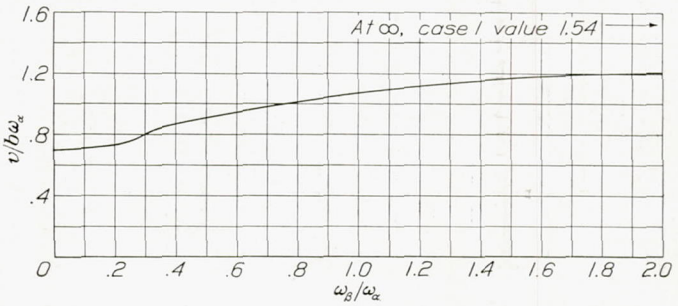


FIGURE 8.—Flutter coefficient against frequency ratio $\omega_\beta/\omega_\alpha$. Three degrees of freedom. $\kappa=0.25$; $a=-0.4$; $x_\alpha=0.2$; $r_\alpha^2=1/4$; $c=0.6$; $x_\beta=0$; $r_\beta^2=0.0012$; $g_\alpha=g_h=0$.

Consider the case of a rectangular cantilever wing. Some authors have attempted a solution on the assumption that the response curves in torsion and deflection under normal conditions (zero air speed) may be used in the flutter theory. It is contended that this assumption is false. Several rather interesting experimental results will be presented in the next section, which show directly and indirectly that the modes in flutter differ radically from the ordinary ones. The following questions arise: (1) Does the wing flutter in the first, second, or third, etc., bending "mode"? (2) Are these modes in any way related to the ordinary types of vibration modes?

Consider first the case of a very high bending mode. It is useful to consider the two-dimensional case as representing the "averages" of parameters and variables of the three-dimensional case. The variable h now appearing in the (two-dimensional) equations refers to the "average" h which approaches zero even though the local h in the loops is very large. It is, furthermore, evident that the average curvatures are greater, the greater the mode. Both these conditions are equivalent to a large coefficient of internal damping, since the work lost per cycle refers to a very small average h.

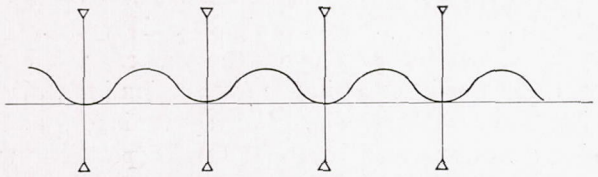


FIGURE 9.—Schematic figure for higher-order bending mode of cantilever wing restrained by wires and with deflections in phase.

The coefficient, in fact, rapidly approaches an infinite value as the number n of the mode is increased. It is probable that the second "flutter" mode involves a coefficient of damping 20 to 50 times larger than that of the first.

A study of the graphs with specific reference to the effect of damping shows that higher flutter modes can be expected only under very special circumstances. This fact does not mean that flutter occurs in the lowest (zero air speed) bending mode.

The bending frequency in flutter of a cantilever beam is determined by a certain minimum condition. The wing will, of course, flutter at the lowest speed possible. It will, therefore, not assume its lowest (stationary) bending mode but will tend to assume a mode of a higher frequency. Since this higher frequency tends to uncouple the h degree of freedom, the actual response ordinarily happens to be a cross between the first and the second modes. Large internal friction will tend to push the response closer to the first mode. The result is a flutter speed distinctly lower than that calculated on the basis of the frequency of the ordinary fundamental bending mode. The flutter speed calculated by using the lowest bending frequency is too favorable. In the case of wings of small internal friction (solid metal wings), the actual flutter speed is only about 0.9, the speed calculated on the basis of the lowest bending frequency. In the case of conventional wings, the error is apparently in the order of only 1 or 2 percent, a fortunate coincidence because it permits the use of a small experimental-empirical correction. This point of view is in harmony with the Rayleigh principle, which states that any response function whatsoever corresponds to a frequency higher than that of the fundamental.

To recapitulate: *The bending frequency involved in the flutter of a cantilever wing is greater than that observed at zero air speed; the more so, the lower the internal damping of the wing structure.*

This interesting phenomenon is demonstrated by the photograph of the flutter of a uniform cantilever beam (see fig. 18) presented in the experimental section, which shows that the maximum amplitude is not at the tip but is rather close to the middle of the span.

Another very convincing experimental proof of this phenomenon, given in the experimental section of this paper, is that a counterweight at the tip section in front of the center of gravity actually *lowers* the flutter speed of a uniform cantilever wing. For a relatively small counterweight, the tip section is beyond a node in the h curve. In this same connection, another rather remarkable experiment was made: A cantilever wing flutters at about 200 miles per hour. The point where the node of the second bending mode (at zero air speed) intersects the torsional stiffness axis was fixed by connecting this point by wires to the tunnel walls. The wing subsequently fluttered at 150 miles per hour. The flutter stopped when the wire broke! The explanation is that the bracing wires "couple" a bending mode that was previously entirely "uncoupled." It should be noted that the frequency actually involved in this flutter is again in excess of that of the second bending mode (at zero air speed); large forces are therefore transmitted through the wire supports from the walls.

In order to illustrate more convincingly how the support wires lower the flutter speed, reference is made to figure 9, which shows a high-order bending mode of a wing. If this bending frequency is about equal to the torsional frequency, the lowest flutter speed is obtained. When the support wires are removed, the wing will tend to vibrate about a fixed mass center line, with the result that the average h deflection becomes zero and all h couplings disappear. The α moments and the h forces transmitted to the support are good measures of what may be called the effective values of α and h when the two-dimensional theory is applied to three-dimensional cases. For instance, the transmittal of a small h force to the support indicates that the positive and the negative h values very nearly cancel. The h effect, although locally large, may very nearly cancel itself. This fact does not prevent the use of a certain (small) average or effective h in the calculations. With no internal friction, the flutter speed is not changed. As was pointed out before, the use of the small effective h for higher modes is, in reality, equivalent to employing a greatly increased coefficient of internal friction.

This discussion and associated experiments lead to the important conclusion: A bracing wire *may* lower the critical speed of a cantilever wing or fin. It usually does lower the critical speed when the internal damping in the structure is low.

For a rectangular cantilever wing, there is no difficulty in regard to the other parameters. With the bending modes considered known, the variables α, β, and h were given simply as average values and used in the two-dimensional solution. Inspection shows that the flutter speed of a uniform cantilever wing is essentially that of the two-dimensional case involving the same parameters and the proper frequency ratio.

A cantilever wing of normal tapered shape will next be considered. It is assumed that there is a similarity in construction along the span for each cross section. The mass is put equal to a constant times the square of the chord; static moments, to the third power; and the moments of inertia, to the fourth power of the chord. Further, the air force is proportional to the chord and the acting moments are proportional to the second power.

Various weight factors of the form $(b/b_r)^n f(x)dx$ are obtained, where $f(x)$ is a weighted wing parameter and x is measured along the span. If the reference section is chosen in such a location that, for a particular $n=m$,

$$\int_0^t \left(\frac{b}{b_r}\right)^m f(x)dx = \int_0^t f(x)dx$$

which is always possible, then

$$\int \left(\frac{b}{b_r}\right)^{m+1} f(x)dx \cong \int f(x)dx$$

In other words, the proper choice of a reference section renders the weight factors of approximately equal magnitudes. If the reference section is taken too close to the tip of the wing, there will be a certain positive correction; if chosen too close inboard, there will be a negative correction. The correct value is thus virtually confined between definite limits. The most representative section will lie close to the three-quarter semispan location.

In the two-dimensional case, the length along the span is considered to be equal to unity and this unity is treated as being large as far as span effects are concerned. If the length is different for the two variables considered, a slight modification of the theory is necessary. Each length is considered to be long enough to permit disregard of aspect-ratio corrections for the air forces.

This sort of consideration is of interest chiefly in the case of ailerons and tail surfaces. The equation giving the equilibrium of the ailerons refers only to the length of the aileron. The included area of the h curve is sometimes a small fraction of the total area under the h curve. This fraction will be called ξ.

The solution of the deflection-aileron case is given in reference 1 by

$$\overline{M}_{a\alpha} = \begin{vmatrix} \overline{R}_{b\beta}+iI_{b\beta} & R_{bh}+iI_{bh} \\ R_{c\beta}+iI_{c\beta} & \overline{R}_{ch}+iI_{ch} \end{vmatrix} = 0$$

and with the effect of ξ:

$$\overline{M}_{a\alpha} = \begin{vmatrix} \overline{R}_{b\beta}+iI_{b\beta} & \xi(R_{bh}+iI_{bh}) \\ R_{c\beta}+iI_{c\beta} & \overline{R}_{ch}+iI_{ch} \end{vmatrix} = 0$$

It is noticed that the factor $\xi<1$ describes a certain uncoupling of the system. The calculation of flutter speed can be performed for any coupling factor ξ. Again it should be remembered that the free-vibration modes are not identical with the flutter modes. A tendency exists for ξ to approach unity since the aileron forces the motion of the wing.

EXPERIMENTAL FLUTTER RESEARCH

GENERAL

The purpose of the experimental research was, first, to check the theory as regards accuracy and, second, to provide a basis for an understanding of problems met with in airplanes.

These tests, about one hundred in all, were conducted in the N. A. C. A. 8-foot high-speed tunnel. (See fig. 10.) In order to protect the propeller, a heavy wire screen was inserted in the test section immediately behind the flutter model. For convenience, models having a flutter speed below 300 miles per hour were tested.

The procedure followed was to increase the tunnel speed slowly until flutter appeared. If the flutter was of a violent type, the load was immediately dropped to save the model. In the tests on ailerons, the lower branch of the flutter curve was similarly obtained. The upper end of the range was obtained by the following method: The aileron was kept in place by restraining wires attached to its rear end and running across the tunnel. By manual operation of the wires from the outside, the arrangement could be conveyed through the dangerous range; on slackening the wires, the operator would receive indication of incipient flutter until the speed had increased above the dangerous range. When the upper stable region had been reached, the wires were completely released and the conventional flutter-test procedure was reversed; that is, the tunnel speed was slowly decreased until the violent flutter appeared. The restraining wires were then immediately tightened, and the speed was noted. The effect of the very fine wire was shown to be negligible in the released condition.

DESCRIPTION OF WING FLUTTER MODELS

All wings tested were cantilever wings and are based on the section given in the following table.

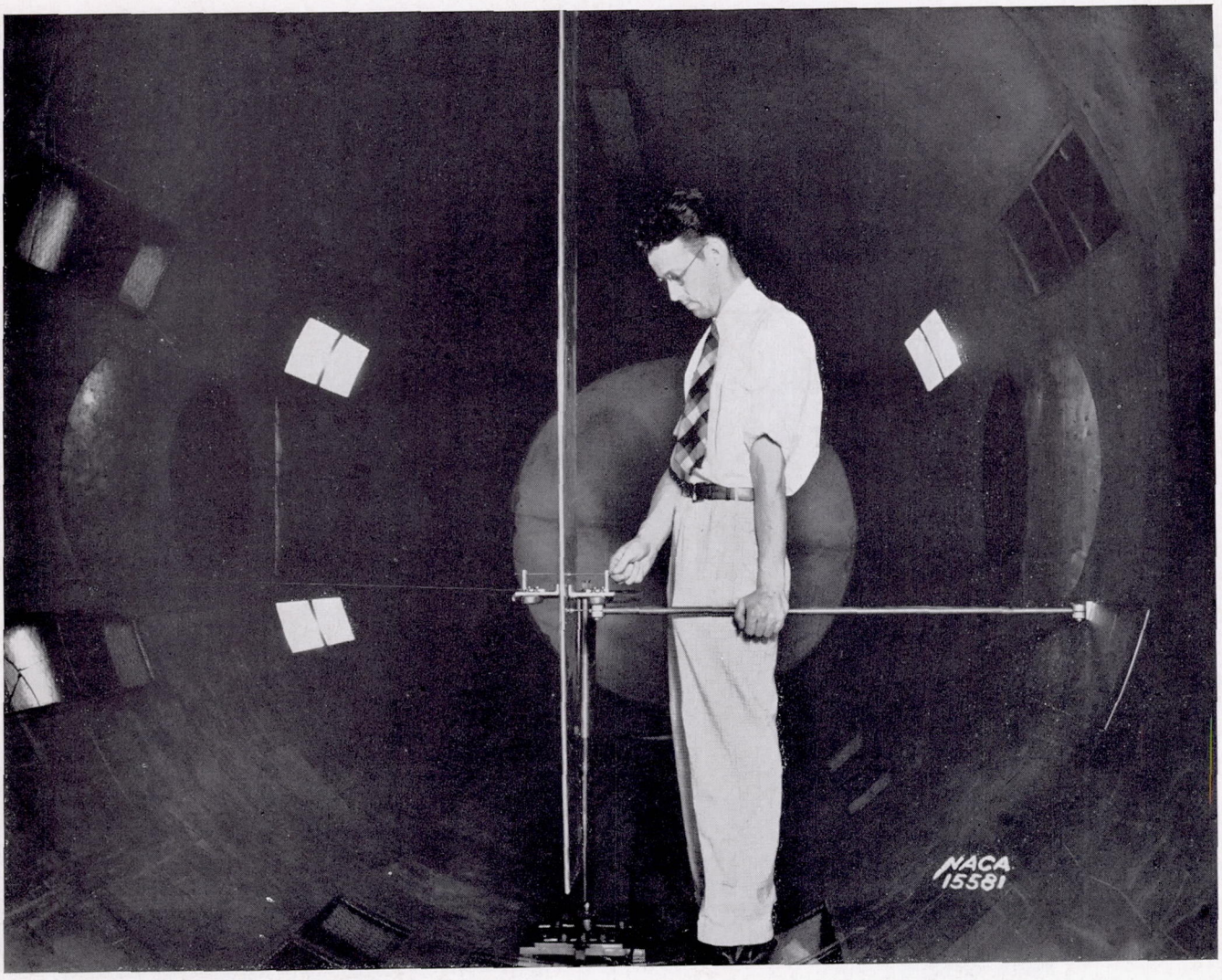


FIGURE 10.—Installation of wing 1 in 8-foot high-speed tunnel. The stop shown was used in only a few initial tests.

AIRFOIL SHAPE USED IN FLUTTER TESTS

Station x (percent chord)	Ordinate y (maximum thickness = 1)
0	0
1.25	.460
2.5	.600
5	.740
7.5	.820
10	.880
15	.940
20	.960
30	1.000
40	.960
50	.900
60	.780
70	.620
80	.440
90	.240
95	.132
100	.020

The frequencies of the various wings are given in the main table of experimental data (table I). All section constants were obtained both by calculation and by direct testing. The basic section has its center of gravity at 42.5 percent from the leading edge. The stiffness axis is at 32 percent but was artificially put at 30 percent in the case 1 tests by chordwise cuts. (See figs. 11 to 13.)

In addition to obtaining the flutter speed of the plain wings, the effects of restraining wires, of mass balancing counterweights in various locations, and of large nacelles both at the wing and some distance away from it were studied. Experimental data are included in table I. In the aileron tests, the effects of mass balancing, hinge location, frequency, and friction were investigated.

Wing 1.—Wing 1 (see fig. 10) was a rectangular cantilever wing model of ½-inch duralumin plate of 12-inch chord by ½-inch thickness by a free length of 6 feet 9 inches perforated with closely drilled ½-inch holes and covered by a $^{6}/_{1000}$-inch sheet of duralumin to give a smooth surface. The constants can be obtained from data in the experimental table.

Wings 2, 3, and 4.—Wings 2, 3, and 4 represent a series of cantilever wings of the same root section (1-foot chord by ½ inch thick), the same span (6 feet 9 inches), but having taper ratios, respectively, of 1:1, 2:1 and 4:1. (See figs. 11, 12, and 13.) The wings are

made of duralumin and are constructed to give similarity in strength and mass distribution. Note that the detail at or near the tips is a scaled-down replica of the detail at the root. The stiffness axis a is put at 30 percent chord or $a=-0.4$ by means of chordwise cuts.

The three types of wing 2 (2A, 2B, and 2C) were so designated because the first one, 2A, finally showed a

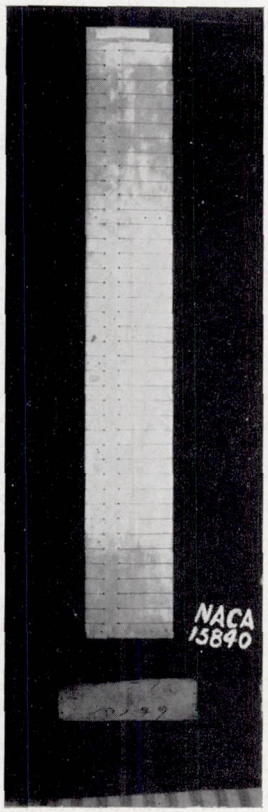


FIGURE 11.—Rectangular cantilever wing 2A. Note chordwise cuts used for purpose of lowering torsional frequency and for placing stiffness axis at 30 percent chord from leading edge.

crack and had to be replaced with 2B, which is almost identical. Wing 2B finally broke at the root, was repaired by shortening it, and was used for some tests under the designation 2C.

Wing 5.—Wing 5 was also a solid duralumin rectangular cantilever wing of 1-foot chord, 4-foot length, and 1-inch thickness at the maximum ordinate; it was used for aileron testing. (See fig. 14) Three ailerons were tested, 14, 24, and 34 inches long with 2, 3, and 4 hinges, respectively. Most of the tests were performed on the 24-inch aileron (aileron A II).

Tests were made for different spring-restraints on the hinge, with a balance counterweight on the outboard end (fig. 15) and with a special arrangement permitting the changing of the hinge axis from the forward edge of the aileron to about 30 percent of the aileron chord behind the center of gravity.

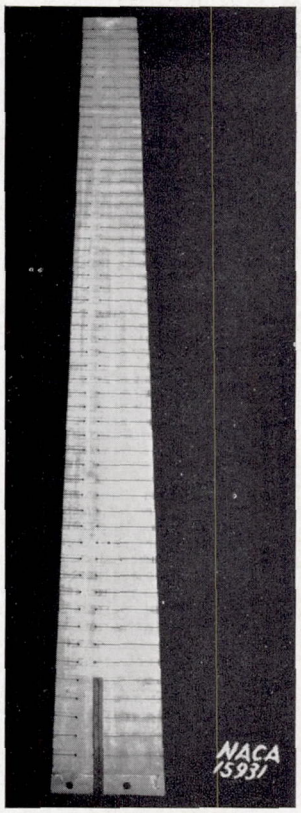


FIGURE 12.—Tapered cantilever wing 3; taper ratio both in chord and thickness is 2:1. Dimensional similarity of cross section and cuts.

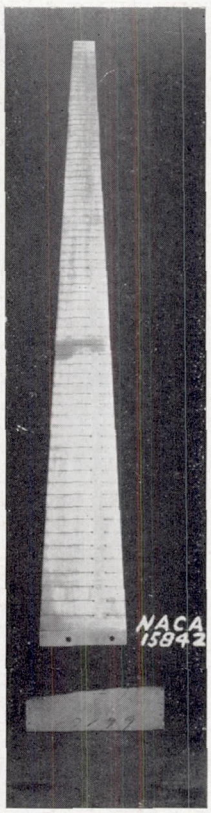


FIGURE 13.—Tapered cantilever wing 4; taper ratio, 4:1.

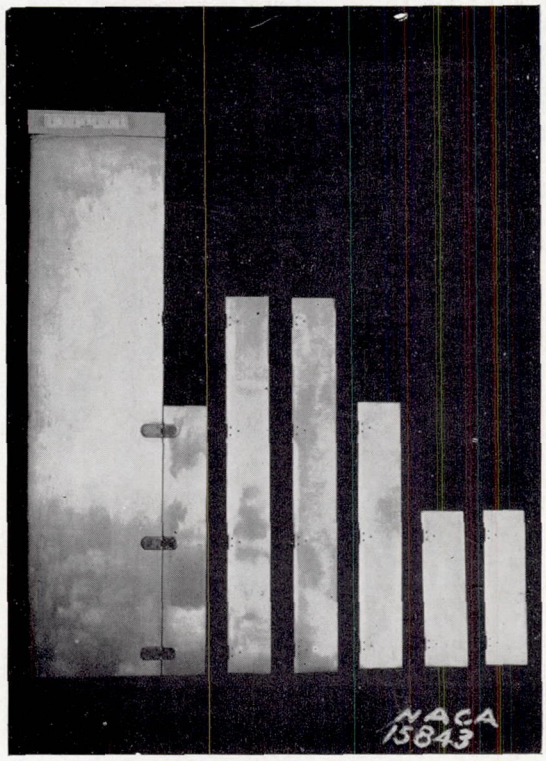


FIGURE 14.—Cantilever wing 5 used for aileron tests.

Wings 6 and 7.—Wings 6 and 7 are model wings of normal density built by covering a balsa structure with 1/16-inch mahogany. Wing 6 has the same external dimensions as wing 2 (fig. 16). Wing 7 has a root chord of 18 inches, a maximum thickness of 1.5 inches, and a taper ratio of 3:2 (fig. 16). All tapered wings were tapered equally in chord and thickness.

DISCUSSION OF EXPERIMENTAL RESULTS

The scheme already discussed of introducing flutter-bending modes completely fits the experimental results into the theoretical picture. Figure 17 shows the theoretical flutter speed for wings 2A, 2B, 3, and 4 with the experimental points plotted. Wing 2A with

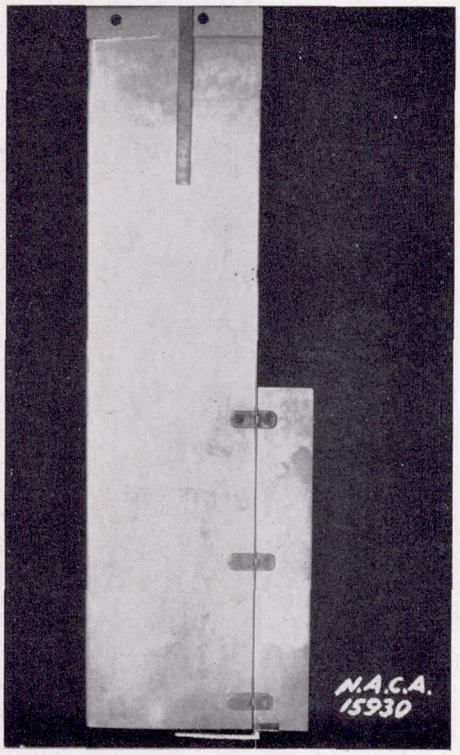


FIGURE 15.—Wing 5 with aileron mass balanced by counterweight at outboard end.

a flutter speed of 202 miles per hour obviously bends in a "first" flutter mode that approaches the second bending mode in appearance and frequency (fig. 18). The flutter frequency calculated on the basis of this bending mode closely checks the measured flutter frequency (fig. 19). Wing 3 checks equally well; its bending frequencies are noted in table I. Wing 4, the most tapered one, obviously collapsed (fig. 20) in the second flutter mode. (See fig. 17.) On this assumption, its experimental flutter speed also fits well in figure 17.

Since the effect of the bending mode was brought so strongly into the picture, an independent study was made on the rectangular wing 2B and on the tapered wing 3 by attaching one point of the torsional axis rigidly to the tunnel walls by restraining wires. The results are shown in figures 21 and 22. Note that the wire attached to the tip had no effect on the flutter speed, which fact again tends to prove the contention that the flutter bending response is closely related to

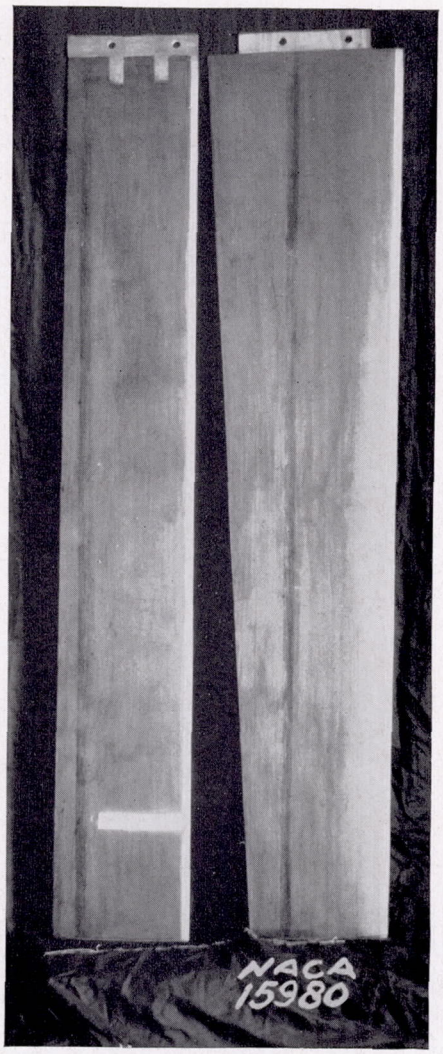


FIGURE 16.—Rectangular wooden wing 6 (left) and tapered wooden wing 7 (right); taper ratio, 3:2.

the second ordinary bending mode. Note also that the observed minimum speeds correspond very nearly to

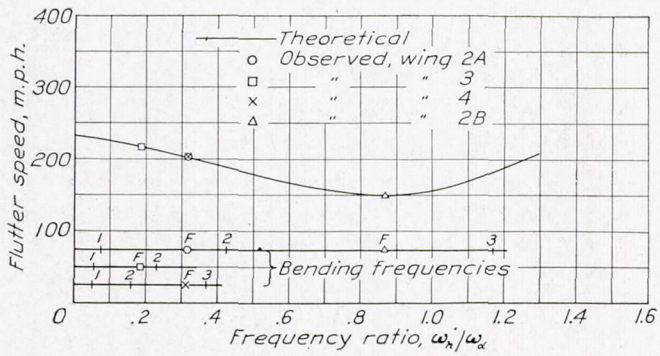


FIGURE 17.—Theoretical flutter speed based on constants pertaining to wings 2A, 2B, 3, and 4. $\kappa=1/90$; $a=-0.4$; $x_\alpha=1/4$; $r_\alpha^2=0.3125$; $b\omega_\alpha=38.8$ miles per hour. Experimental test points are also shown, and flutter modes and frequencies are indicated.

the minimum theoretical speed. (See fig. 17.) Of practical importance is the fact that a stay near the root of a wing gave a higher bending frequency and

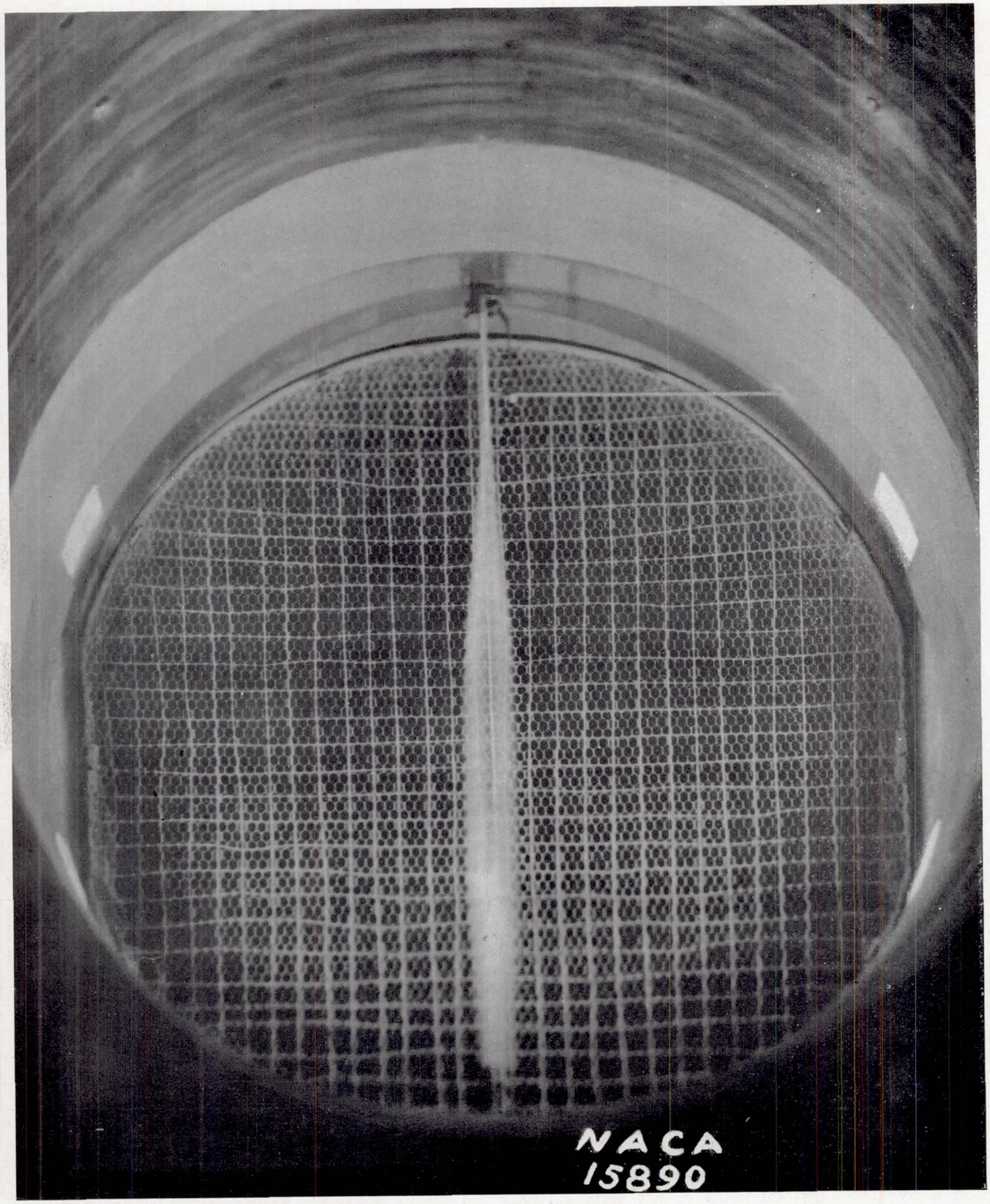


FIGURE 18.—Wing 2A in flutter, demonstrating first flutter mode. Note tendency for node at tip and maximum amplitude near middle.

definitely lowered the critical speed. There existed points, however, near the middle of both wings for

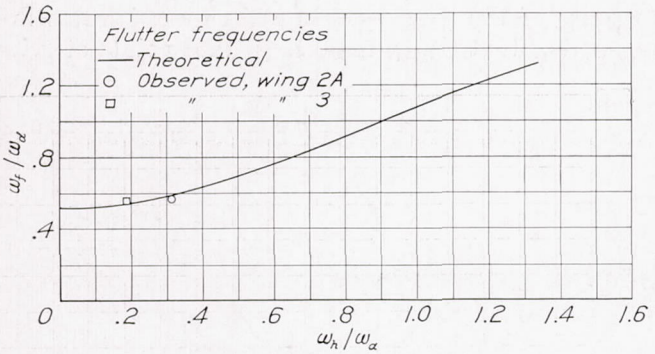


FIGURE 19.—Theoretical flutter frequencies based on constants for wings 2, 3, and 4 with experimentally observed values for wings 2A and 3. $\kappa=\frac{1}{60}$; $a=-0.4$; $x_\alpha=\frac{1}{4}$; $r_\alpha^2=0.3125$. Case 1(h, α).

which the stays caused the flutter speed to attain a large value. The explanation is that, with this point fixed, the average h value becomes very small and the h deflection becomes "ineffective." A relatively high flutter speed results.

The matter of leading-edge counterweights has been investigated, in particular on wing 2C. Figure 23 shows the effect of moving a counterweight along the span. The weight has a rather surprising *negative* effect near the tip, indicating that, in this case, there must be an h node inside the tip and again substantiating the theory of the flutter modes. Farther in along the wing there was an expected increase in the flutter speed. When all three weights were applied at the same time, the flutter speed for wing 2C was increased to 295 miles per hour, which is in good agreement with the calculated value.

A large nacelle at an inboard position (fig. 24) increased the flutter speed from 202 to 216 miles per hour when in the forward position and decreased it to 197 when in the rearward position.

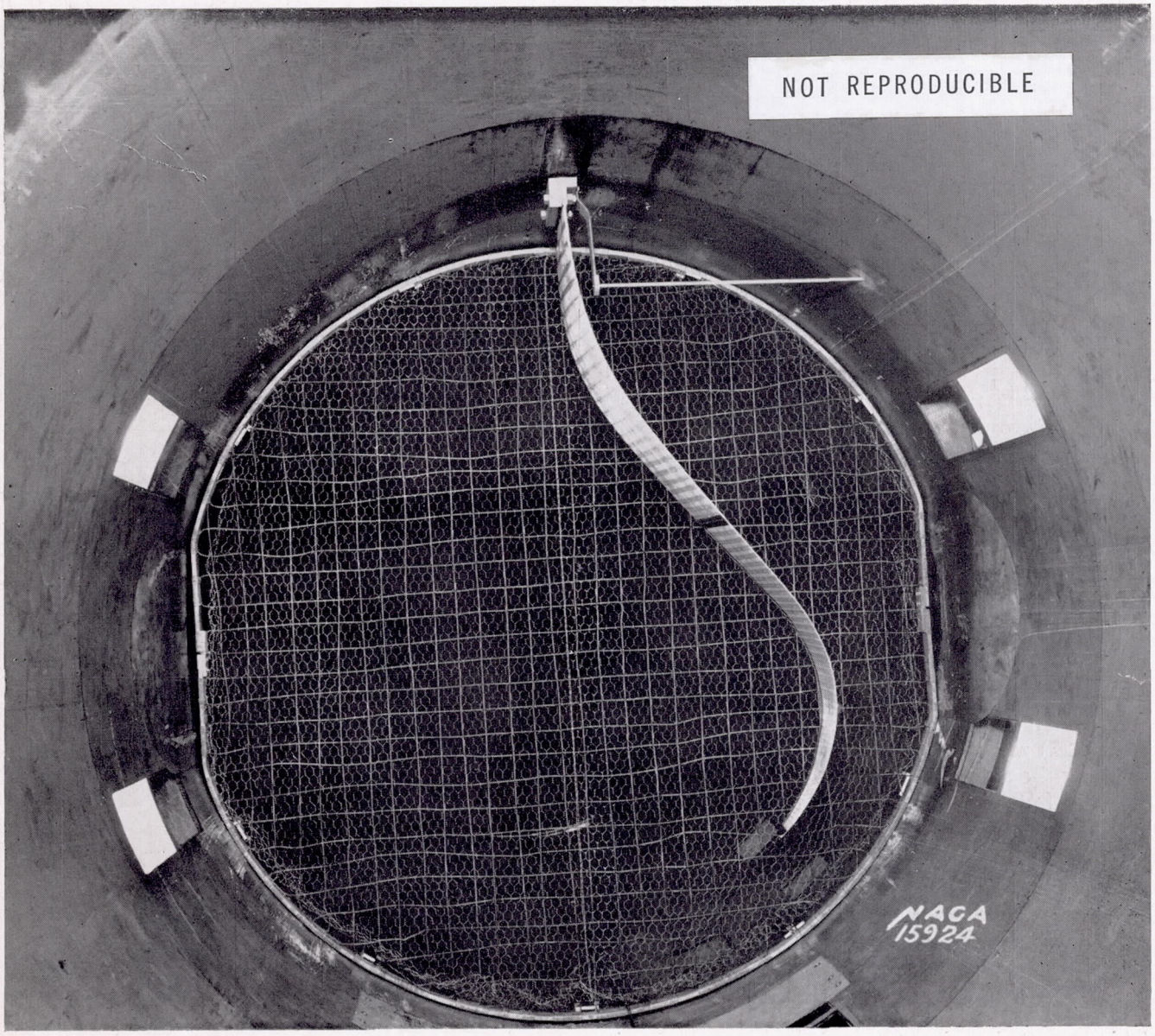


FIGURE 20.—The effect of violent flutter (in second mode) on wing 4.

Large bodies disposed at some distance from the wing, such as floats, were very detrimental as regards the critical speed. (See fig. 25.)

Wing 1 showed a flutter speed that is in agreement with the predicted value within about 1 percent. This agreement is due to the considerable internal damping of this wing. Wing 6, a rectangular wing of the same plan dimensions as wings 1, 2, 3, and 4, but of low density, showed a flutter speed about 3 percent below the theoretical value based on the measured parameters and the lowest ordinary bending mode. This result indicates that, for damped, low-density structures, the flutter mode approaches the first bending mode somewhat more than hitherto indicated.

Wing-aileron flutter has been studied on wing 5. (See fig. 14 and table IA.) The theoretical response is

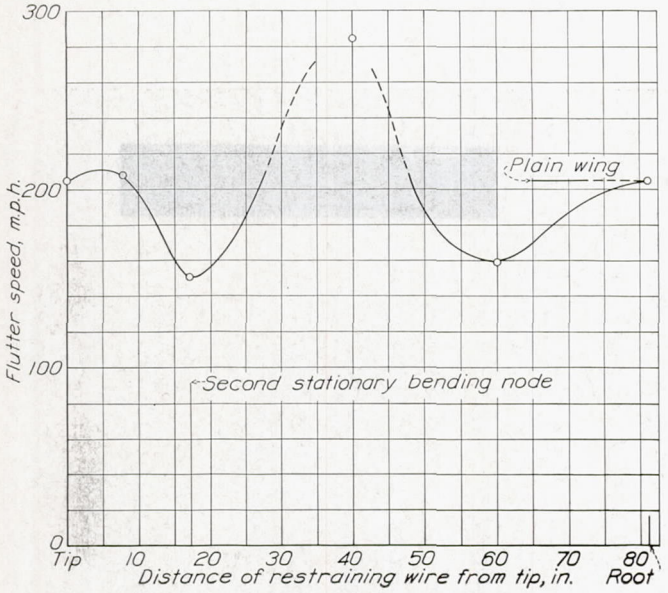


FIGURE 21.—Experimentally observed flutter speed as depending on location of restraining wire along axis of wing 2B.

shown with proper constants in figure 26 for the most representative aileron AII, upon which most of the tests were made. A number of test points have been directly plotted in this figure. In order to obtain internal friction, a lead hinge was used in some tests. It is rather remarkable how well the theory is reaffirmed by the test data. Apparently, if all parameters could be satisfactorily determined, no flutter testing would be necessary. Tests in which the hinge axis (fig. 27) was changed show the beneficial effect of decreasing the aerodynamic moment around the hinge. The lower flutter speed, which is the one of practical importance, is considerably increased as the hinge axis is moved backward. This increase is not only a center-of-gravity effect but is also caused by the decrease in the aerodynamic moment around the hinge. Note that, as the center of gravity is approached, the flutter speed rather suddenly becomes infinite.

AIR DAMPING OF FORCED VIBRATIONS

This report has heretofore been concerned with a study of a border velocity separating stable and unstable velocity regions. Further light on the whole matter of flutter is given by a study of the vibration response of the wing system to impressed forces and moments, that is, generalizing the point of view

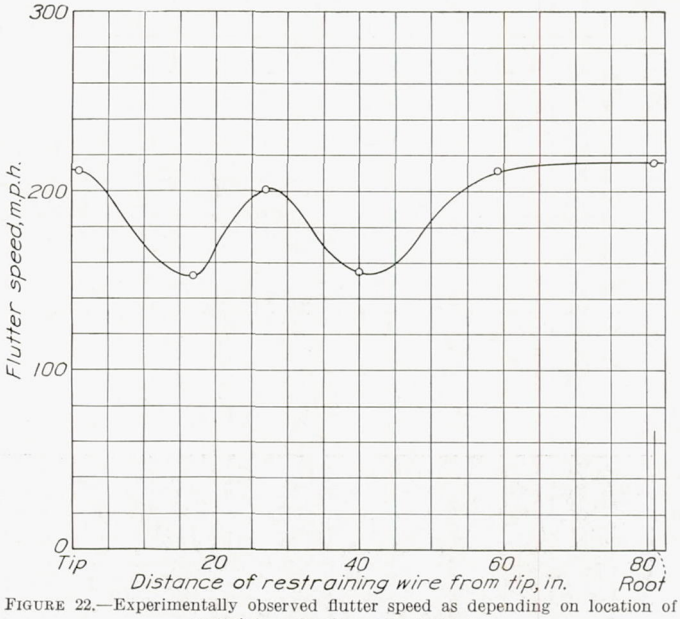


FIGURE 22.—Experimentally observed flutter speed as depending on location of restraining wire along axis of wing 3.

from free vibrations to forced vibrations. Instead of the homogeneous system of equations (A), (B), and (C) (see Introduction), impressed exciting forces and moments introduced on the right-hand side of these equations are considered. In equation (A) a

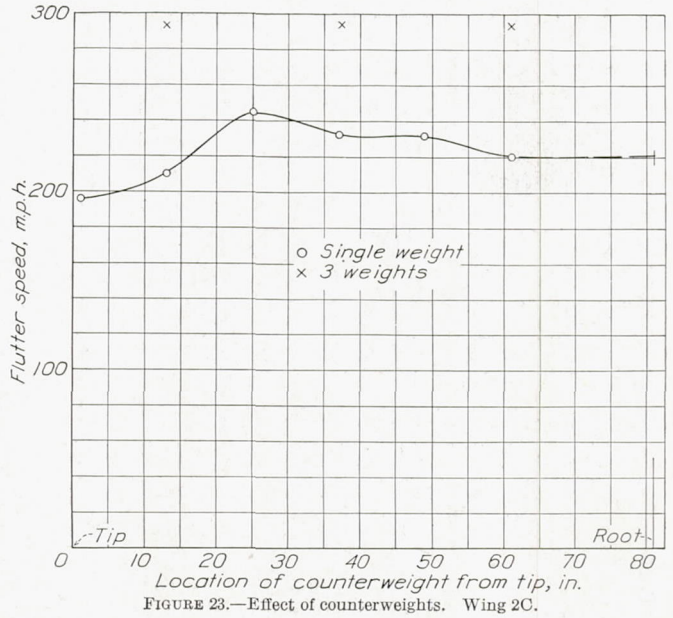


FIGURE 23.—Effect of counterweights. Wing 2C.

term $M_\alpha e^{i(\omega t+\psi_0)}/Mb^2$, in equation (B) a term $M_\beta e^{i(\omega t+\psi_1)}/Mb^2$, and, in equation (C) a term $P_0 e^{i(\omega t+\psi_2)}/Mb$ are introduced. Here M_α and M_β are the magnitudes of the sinusoidal impressed torques in the α and β degrees of freedom, P_0 is the magnitude of the impressed force in the h degree of freedom, ω is the circular frequency of the forced vibrations, and the ψ's are certain phase angles.

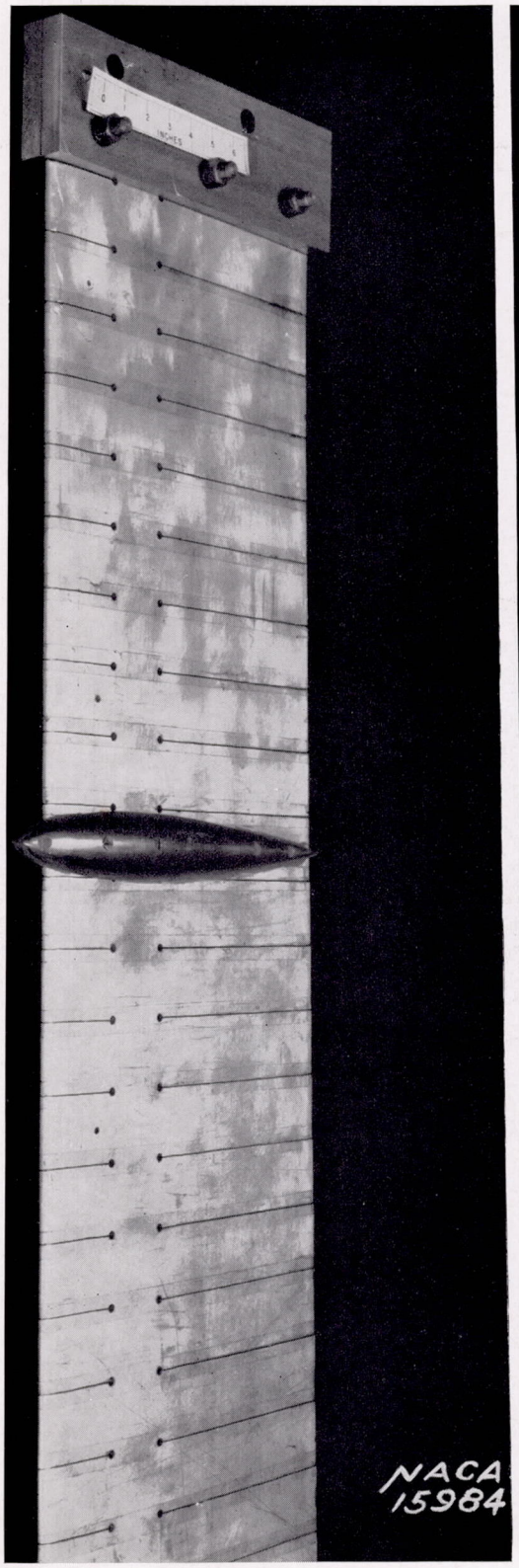


FIGURE 24.—Nacelle on wing 2A.

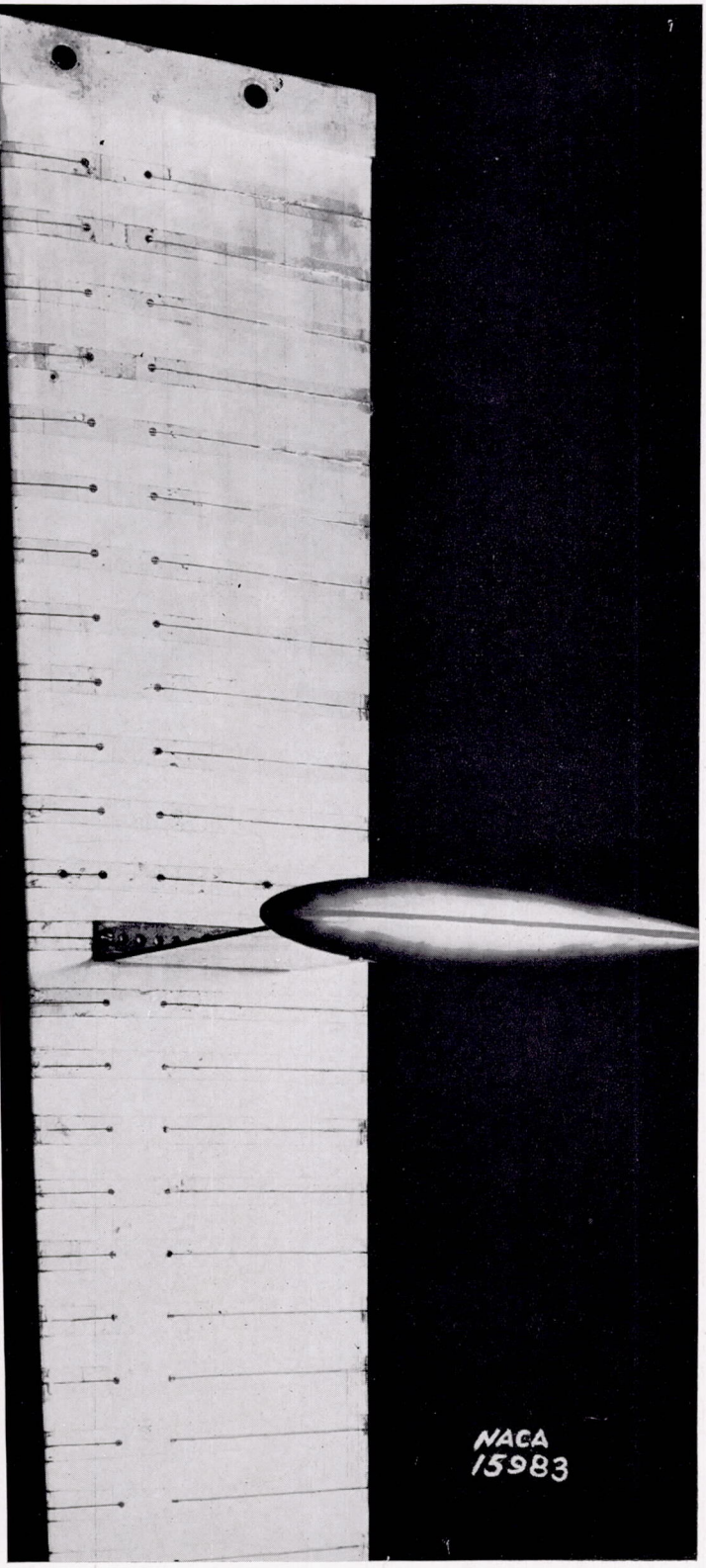


FIGURE 25.—Float attached to wing 3.

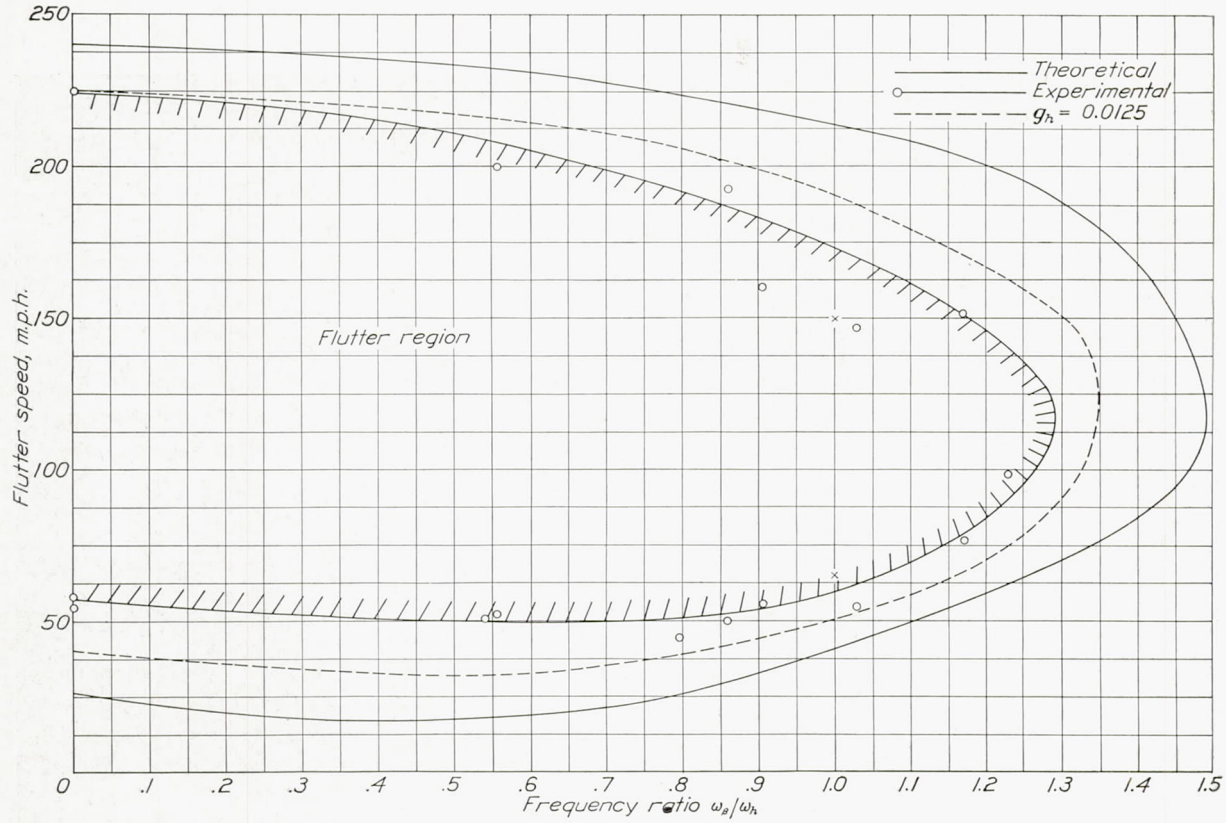


FIGURE 26.—Theoretical flutter speed based on constants pertaining to wing 5 with aileron AII. ($c=\frac{1}{2}$; $x_\beta=0.0076$; $r_\beta{}^2=0.0019$; $\kappa=\frac{1}{105}$; $b\omega_h=30.5$ m. p. h.) Experimental values are shown; flutter region is shaded. Dashed (theoretical) curve corresponds to friction coefficient $g_h=0.0125$.

CASE 1 (h, α)

By substitution of $\alpha=\alpha_0 e^{i(\omega t+\varphi_0)}$, $\frac{h}{b}=\frac{h_0}{b}\ e^{i(\omega t+\varphi_2)}$, in equations (A) and (C) and solving for $\left(\frac{h_0}{b}\right)e^{i\varphi_2}$ and $\alpha_0 e^{i\varphi_0}$ (put $M_\alpha=P_0\, bm$), there results

$$\frac{h_0}{b}\,e^{i\varphi_2}=\frac{P_0 e^{i\psi_2}}{bM\kappa\omega^2}\frac{\begin{vmatrix}\bar{R}_{a\alpha}+i\bar{I}_{a\alpha} & me^{i(\psi_0-\psi_2)}\\ R_{c\alpha}+iI_{c\alpha} & 1\end{vmatrix}}{\Delta_1{}^R+i\Delta_1{}^I}$$

$$\alpha_0 e^{i\varphi_0}=\frac{P_0 e^{i\psi_2}}{bM\kappa\omega^2}\frac{\begin{vmatrix}me^{i(\psi_0-\psi_2)} & R_{ah}+iI_{ah}\\ 1 & \bar{R}_{ch}+i\bar{I}_{ch}\end{vmatrix}}{\Delta_1{}^R+i\Delta_1{}^I}$$

from which both the amplitudes and the phases may be obtained. The R's and the I's are listed in the appendix and $\Delta_1{}^R$ and $\Delta_1{}^I$ represent the real and the imaginary equations listed under the calculation scheme for case 1.

Consider the equation for $h_0 e^{i\varphi_2}$ and denote the determinant in the numerator by N_h, i. e.,

$$N_h=\begin{vmatrix}\bar{R}_{a\alpha}+i\bar{I}_{a\alpha} & me^{i(\psi_0-\psi_2)}\\ R_{c\alpha}+iI_{c\alpha} & 1\end{vmatrix}$$

If the excitation is only in the h degree of freedom $m=0$, i. e., there is no impressed torque about the elastic axis. If a single exciter were placed, for example, 25 percent of the chord in front of the elastic axis, $m=-0.5$.

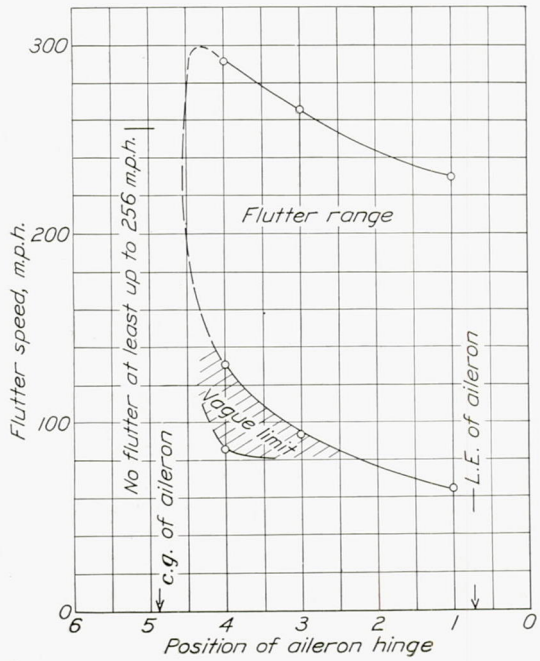


FIGURE 27.—Flutter speed as depending on position of aileron hinge. Observe that no flutter exists when the hinge approaches the center-of-gravity location. Aileron AVIII.

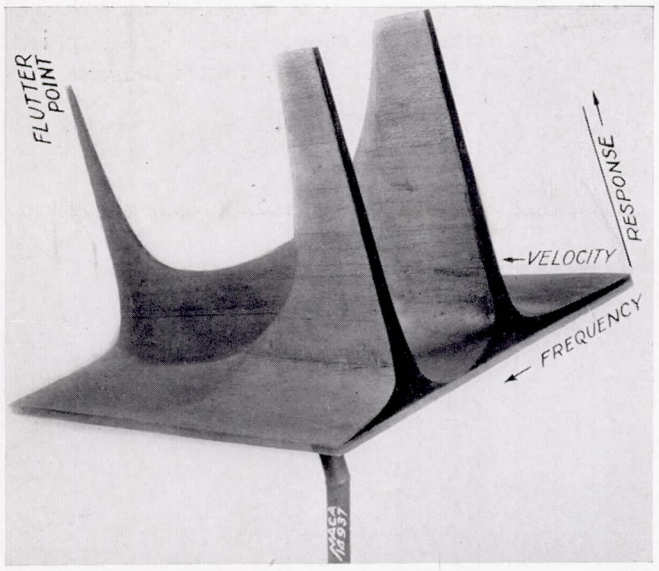


FIGURE 28.—Photograph of model showing forced vibration response in two degrees of freedom as depending on air speed. Note flutter point.

It is convenient to define a certain static deflection h_{st}, which is the deflection due to force P_0,

$$h_{st}=\frac{P_0}{C_h}=\frac{P_0}{M\omega_h^2}$$

Define α_{st} as the static torsional response to an impressed moment $P_0 b$

$$\alpha_{st}=\frac{P_0 b}{C_\alpha}$$

Then

$$\left|\frac{\alpha_0}{\alpha_{st}}\right|=\frac{\omega_\alpha^2}{\omega^2}\left|\frac{N_\alpha}{\Delta}\right|\frac{1}{\kappa}$$

Figure 28 is a photograph of a three-dimensional model of the response ratio h_0/h_{st} as a function of the exciting frequency ratio ω/ω_α and of the speed ratio $v/b\omega_\alpha$ for a case of deflection-torsion for which a critical flutter speed exists. In this example, the exciting force has been assumed to act in the deflection degree of freedom alone ($m=0$). At zero speed there exist two resonant frequencies corresponding to the natural frequencies in the separate degree of freedom. The air damping due to speed is zero and the response is infinite at these frequencies. (With friction g_α and g_h, the responses are approximately $1/g_\alpha$ and $1/g_h$, respectively.) As the speed increases, the air damping increases and the response diminishes until, along one frequency branch (the ω_α branch) the response becomes negligibly small. Along the other frequency branch, however, a minimum response is reached, after which

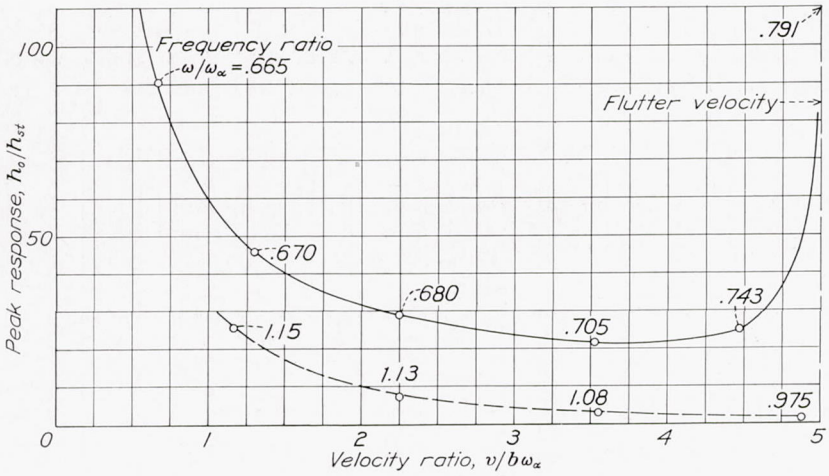


FIGURE 29.—Peak response ridges of figure 28.

Then

$$\left|\frac{h_0}{h_{st}}\right|=\frac{\omega_h^2}{\omega^2}\left|\frac{N_h}{\Delta}\right|\frac{1}{\kappa}$$

where

$$\Delta=\sqrt{(\Delta_1^R)^2+(\Delta_1^I)^2}$$

This result gives the steady-state deflection response h_0 in terms of the static deflection h_{st} due to an impressed force or moment. The results of some numerical calculations will shortly be presented.

The torsional response can be similarly calculated. Let N_α represent the determinant in the numerator of the expression for $\alpha_0 e^{i\rho_0}$:

$$N_\alpha=\begin{vmatrix} me^{i(\psi_0-\psi_2)} & R_{ah}+iI_{ah} \\ 1 & \overline{R}_{ch}+i\overline{I}_{ch} \end{vmatrix}$$

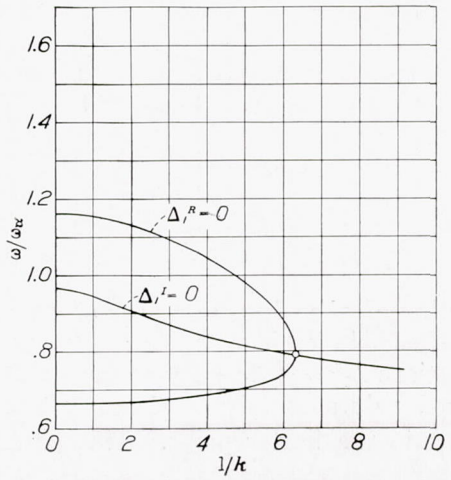


FIGURE 30.—The roots of the real and the imaginary equations (pertaining to case shown in fig. 28) against $1/k$.

the air damping decreases and the response increases (usually rapidly) until the flutter point is reached. The critical flutter frequency lies between the two critical frequencies that exist at zero speed. The two peak response ridges for this case are shown in figure 29. These curves, it may be observed, illustrate the essential characteristics of the three-dimensional figure. The procedure of calculation is as follows:

The equations $\Delta_1{}^R=0$, $\Delta_1{}^I=0$ are solved for ω/ω_α for various fixed values of $1/k$, as already discussed, in order to locate the flutter point. This plot, for the example cited, is shown in figure 30. The value of $\Delta_1{}^I$ is then obtained for various selected points $(1/k,\ \omega/\omega_\alpha)$ along $\Delta_1{}^R=0$. These values may be employed to determine Δ. The numerator is easily evaluated for these same values of $1/k$, ω/ω_α. This process determines the *peak* response with sufficient accuracy for a given value of $1/k$ and conversion to speed is obtained by the relation $v/b\omega_\alpha=(\omega/\omega_\alpha)(1/k)$. Such response curves, calculated with and without the effect of friction, are given in figures 31 and 32.

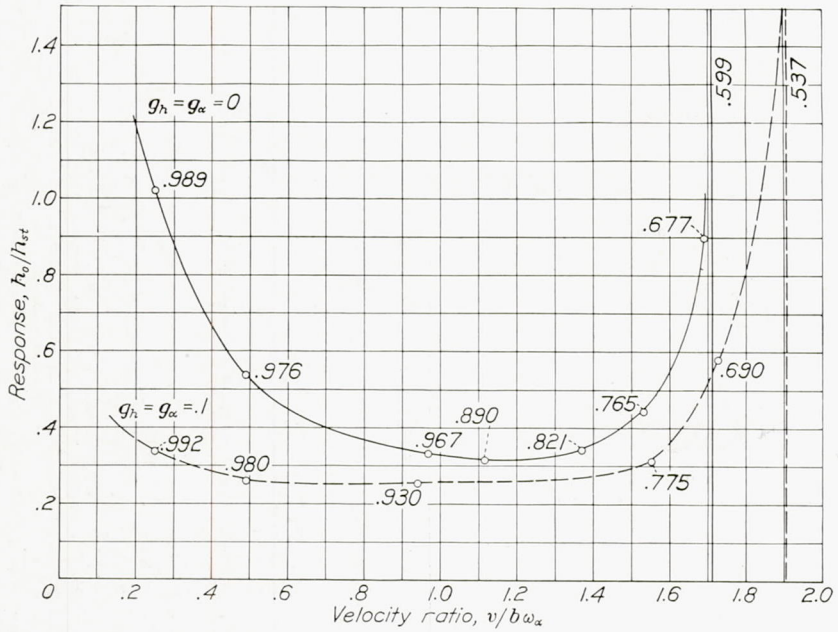


FIGURE 31.—Peak response h_0/h_{st} against velocity $v/b\omega_\alpha$ for the case $\kappa=\frac{1}{10}$; a$=-0.2$; $x_\alpha=0.1$; $m=0$; $(\omega_h/\omega_\alpha)^2=\frac{1}{25}$. The full curve refers to friction coefficients $g_h=g_\alpha=0$; the dashed curve, to $g_h=g_\alpha=0.1$. Case 1 $(h,\ \alpha)$.

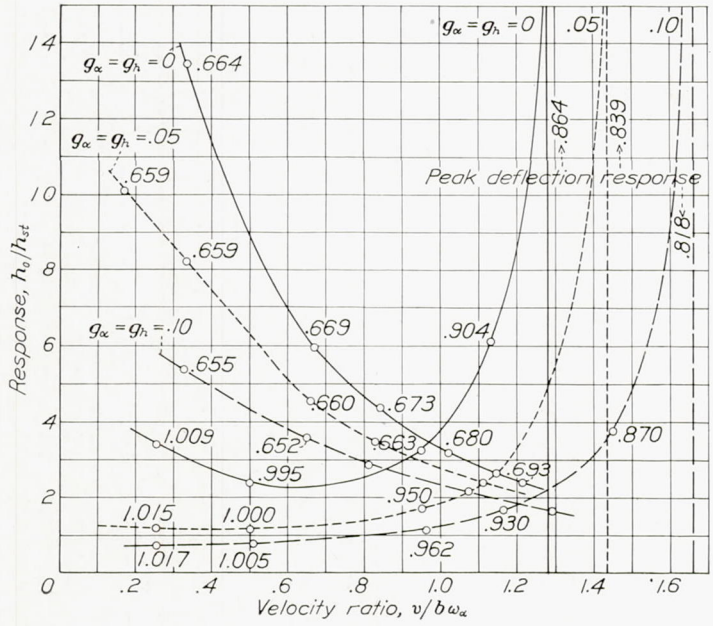


FIGURE 32.—Peak-response ridges for three values of friction coefficients $g_\alpha=g_h=0$, 0.05, and 0.10. $(\kappa=\frac{1}{10};\ a=-0.2;\ x_\alpha=0.1;\ (\omega_h/\omega_\alpha)^2=\frac{1}{25})$. Case 1.

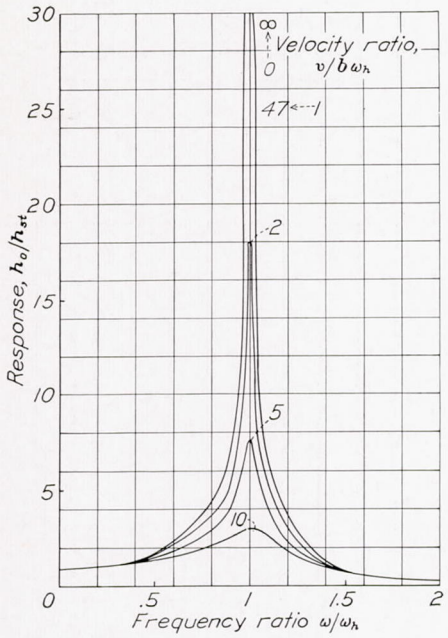


FIGURE 33.—Forced vibration response for deflection degree of freedom ($g_h=0$).

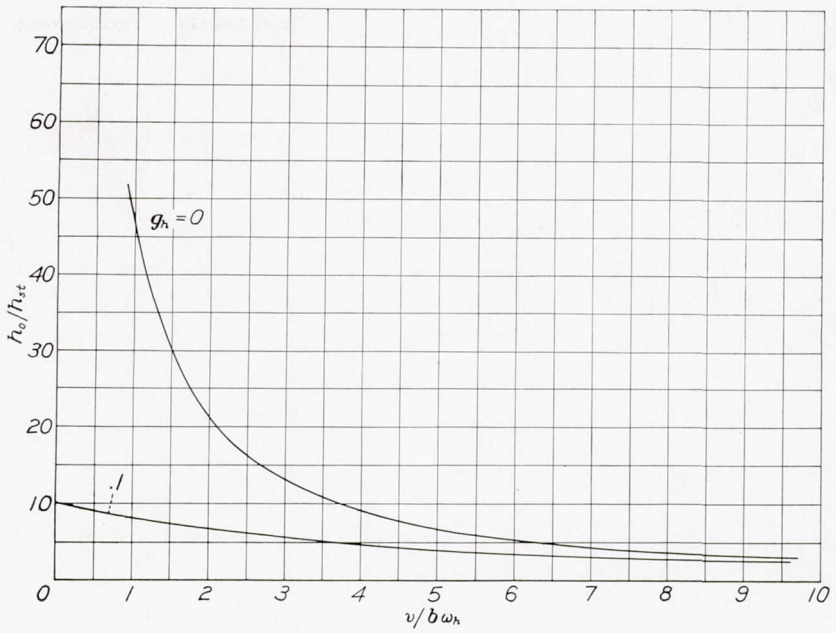


FIGURE 34.—Peak response h_0/h_{st} against velocity ratio $v/b\omega_h$ for two values of the friction coefficient $g_h=0$ and $g_h=0.1$. $\kappa=\frac{1}{50}$.

One degree of freedom (deflection).—Further light on the two-degree-of-freedom case, deflection-torsion, may be obtained by a discussion of the one-degree-of-freedom cases, deflection alone and torsion alone.

When $h=h_0e^{i(\omega t+\varphi_2)}$ is substituted in the deflection equation of motion,

$$h_0e^{i\varphi_2}(\bar{R}_{ch}+i\bar{I}_{ch})\kappa\omega^2=\frac{P_0}{M}e^{i\psi_2}$$

On the introduction of $h_{st}=P_0/C_h$ (static response in deflection to impressed force P_0), it follows that

$$\frac{h_0}{h_{st}}=\frac{1}{\kappa}\left(\frac{\omega_h}{\omega}\right)^2\frac{1}{(R_{ch}^2+I_{ch}^2)^{\frac{1}{2}}}=\frac{\Gamma_h}{[(\Gamma_h-A_h)^2+(g_h\Gamma_h+B_h)^2]^{\frac{1}{2}}}$$

where

$$\Gamma_h=\left(\frac{\omega_h}{\omega}\right)^2$$

$$A_h=1+\kappa\left(1+\frac{2G}{k}\right)$$

$$B_h=\kappa\frac{2F}{k}$$

g_h is the friction coefficient.

It is observed that the speed is determined by $v/b\omega_h=(\omega/\omega_h)(1/k)$.

The resonance response is obtained by putting $\partial/\partial\Gamma_h|h_0/h_{st}|=0$ and solving for Γ_h. There results

$$\Gamma_{res}=\left(\frac{\omega_h}{\omega}\right)^2_{res}=\frac{A_h^2+B_h^2}{A_h-g_hB_h}$$

or

$$\left(\frac{\omega}{\omega_h}\right)_{res}=\left(\frac{A_h-g_hB_h}{A_h^2+B_h^2}\right)^{\frac{1}{2}}$$

The maximum response is then

$$\left(\frac{h_0}{h_{st}}\right)_{res}=\frac{(A_h^2+B_h^2)^{\frac{1}{2}}}{B_h+g_hA_h}$$

Figures 33 and 34 pertain to this case. The results may be summarized as follows: The resonant frequency is practically constant and is approximately $\omega=\omega_h$. The air damping at the maximum response is proportional to $B_h=\kappa\dfrac{2F}{k}$ or, since the frequency is nearly constant, the air damping at the maximum response is proportional to κv. Away from the resonant frequency, however, the response quickly becomes independent of κ. No flutter or self-excitation exists in this case. At zero air speed, the maximum response ratio is simply $1/g_h$.

One degree of freedom (torsion).—When $\alpha=\alpha_0e^{i(\omega t+\varphi_0)}$ is substituted into the α equation of motion

$$\alpha_0e^{i\varphi_0}(\bar{R}_{a\alpha}+i\bar{I}_{a\alpha})\kappa\omega^2=\frac{M_\alpha}{Mb^2}e^{i\psi_0}$$

On the introduction of $\alpha_{st}=M_\alpha/C_\alpha$ (static response in torsion to impressed torque M_α), it follows that

$$\left|\frac{\alpha_0}{\alpha_{st}}\right|=\frac{r_\alpha^2}{\kappa}\left(\frac{\omega_\alpha}{\omega}\right)^2\frac{1}{(R_{a\alpha}^2+I_{a\alpha}^2)^{\frac{1}{2}}}$$

$$=\frac{\Gamma_\alpha}{[(\Gamma_\alpha-A_\alpha)^2+(g_\alpha\Gamma_\alpha+B_\alpha)^2]^{\frac{1}{2}}}$$

where

$$\Gamma_\alpha=\left(\frac{\omega_\alpha}{\omega}\right)^2$$

$$A_\alpha=1+\frac{\kappa}{r_\alpha^2}\left[\frac{1}{8}+a^2-\left(\frac{1}{4}-a^2\right)\frac{2G}{k}+\left(\frac{1}{2}+a\right)\frac{2F}{k^2}\right]$$

$$B_\alpha=\frac{\kappa}{r_\alpha^2}\frac{1}{k}\left[\frac{1}{2}-a-\left(\frac{1}{2}+a\right)\frac{2G}{k}-\left(\frac{1}{4}-a^2\right)2F\right]$$

g_α is the friction coefficient.



FIGURE 35.—Forced vibration response for torsion degree of freedom (axis at $a=0$; $\kappa/r_\alpha^2=1/50$; $g_\alpha=0$).

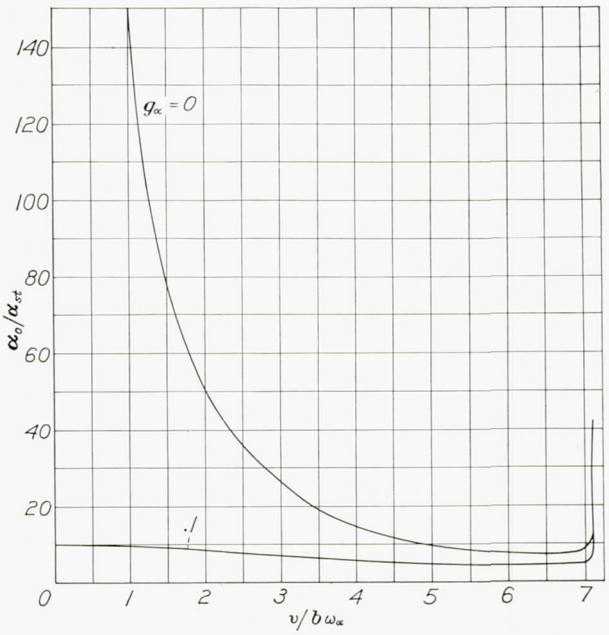


FIGURE 36.—Peak response α_0/α_{st} against velocity ratio $v/b\omega_\alpha$ for two values of the friction coefficient $g_\alpha=0$ and $g_\alpha=0.1$. $a=0$; $\kappa/r_\alpha^2=1/50$.

It is observed that the speed is determined by $v/b\omega_\alpha=(\omega/\omega_\alpha)\ (1/k)$. Put $\partial/\partial\Gamma_\alpha|\alpha_0/\alpha_{st}|=0$. Then

$$\Gamma_{res}=\left(\frac{\omega_\alpha}{\omega}\right)^2_{res}=\frac{A_\alpha^2+B_\alpha^2}{A_\alpha-g_\alpha B_\alpha}$$

or

$$\left(\frac{\omega}{\omega_\alpha}\right)_{res}=\left(\frac{A_\alpha-g_\alpha B_\alpha}{A_\alpha^2+B_\alpha^2}\right)^{\frac{1}{2}}$$

of the torsional axis. The air damping at resonance is essentially proportional to κ/r_α^2 and to the wavelength parameter $1/k$. For the quarter-chord position of the axis, $a=-0.5$, the response α_0/α_{st} is very similar to the deflection response h_0/h_{st} in the preceding case (fig. 33). For any position of the torsional axis back of the quarter-chord point, however, a peculiar result

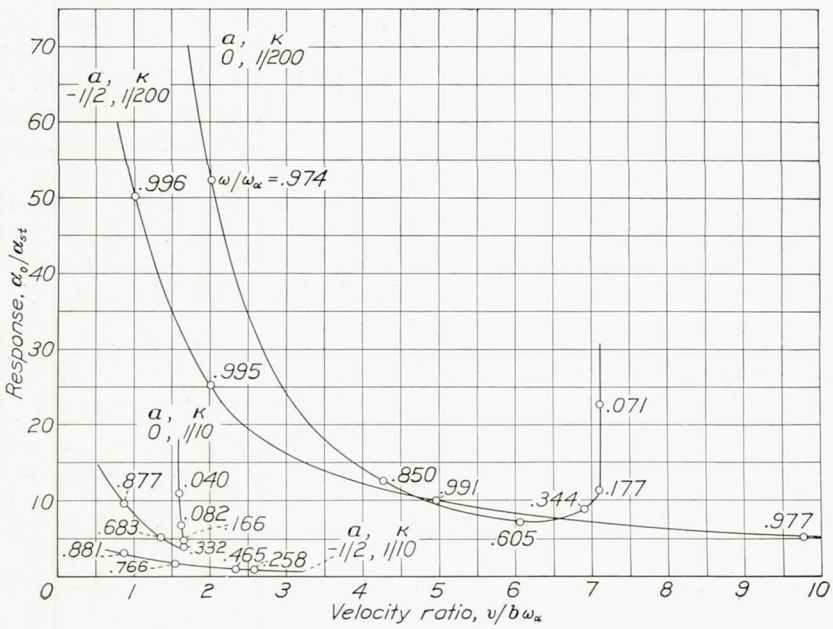


FIGURE 37.—Peak response α_0/α_{st} against velocity ratio $v/b\omega_\alpha$ for two values of a (0 and $-1/2$) and two values of κ ($1/10$ and $1/200$). Case 1 (h, α).

The maximum response is then

$$\left(\frac{\alpha_0}{\alpha_{st}}\right)_{res}=\frac{(A_\alpha^2+B_\alpha^2)^{\frac{1}{2}}}{B_\alpha+g_\alpha A_\alpha}$$

Figures 35, 36, and 37 pertain to this case. The resonant frequency is strongly affected by the position is obtained. The air damping increases with increase in speed and the resonant frequency decreases; but a speed is ultimately reached where the response increases again until, at a vanishingly small resonant frequency, the response is very large. In figure 35, which illustrates a case for the midchord position of the axis,

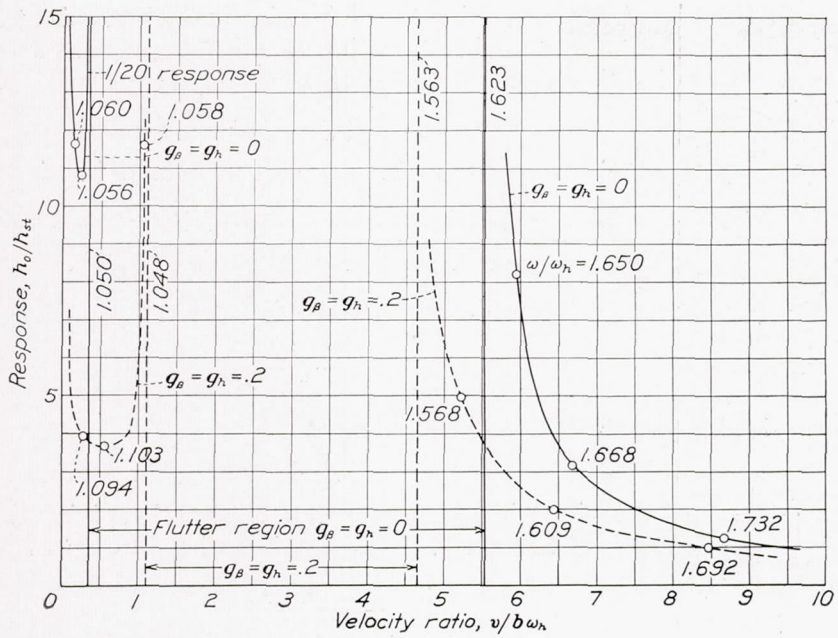


FIGURE 38.—Peak response h_0/h_{st} against velocity ratio $v/b\omega_h$ for a case of flexure-aileron flutter, showing effect of changing friction coefficients $g_h=g_\beta=0$ to $g_h=g_\beta=0.2$. (Other parameters are $c=0.5$; $\kappa=1/10$; $r_\beta^2=1/160$; $x_\beta=1/40$; $(\omega_\beta/\omega_h)^2=1/2$).

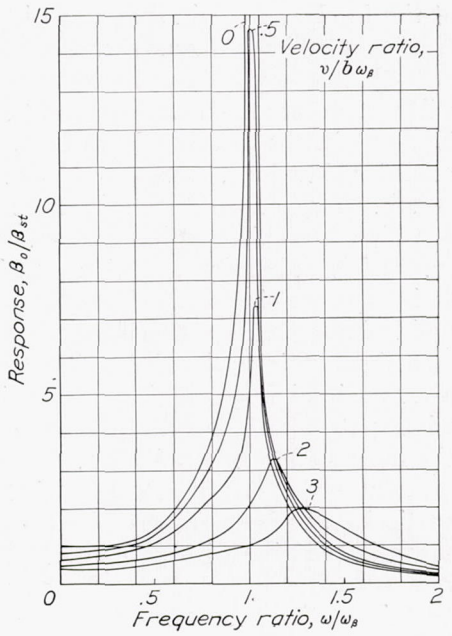


FIGURE 39.—Forced vibration response of aileron alone against frequency and velocity; friction coefficient $g_\beta=0$.

$a=0$, the peak response occurs at $v/b\omega_\alpha=7.10$. This sort of instability has been called divergence. The divergence velocity can be easily calculated as follows:

Let $\omega/\omega_\alpha \to 0$, $1/k \to \infty$ in the expression for α_0/α_{st}.

Then

$$\underset{1/k\to\infty}{\text{Limit}}\left(\frac{\alpha}{\alpha_{st}}\right)_{res}=\frac{1}{1-\frac{\kappa}{r_\alpha^2}2\left(\frac{1}{2}+a\right)\left(\frac{v}{b\omega_\alpha}\right)^2}$$

or

$$\left(\frac{v}{b\omega_\alpha}\right)^2_{div}=\frac{r_\alpha^2}{\kappa}\frac{1/2}{\frac{1}{2}+a}$$

CASE 2 (β, h)

A study of the response characteristics to forced vibrations is also of some interest in the case of flexure-aileron. The details are omitted here. Two figures are presented. An illustration showing the peak response ratio h_0/h_{st} in this case with and without friction is presented in figure 38. A response for one degree of freedom of the aileron alone is shown in figure 39.

REMARKS ON FLUTTER IN AIRPLANES

WING FLUTTER

The wing may flutter as a whole in torsion-flexure. This case is the most easily treated. Experience with models indicates that this flutter speed may be calculated on the basis of the measured constants with an accuracy of a few percent. The actual bending frequency involved in flutter is apparently not exactly the lowest ordinary bending frequency but a slightly higher value.

Probably the most common type of wing flutter is case 2 (flexure-aileron). This type, as well as that involving torsion-flexure, is evidently symmetrical with respect to the fuselage. The ailerons would therefore be in phase and have a frequency considerably in excess of the wing-bending frequency. This condition is favorable. Any slack in the aileron cables, however, permits a motion that may cause a mild type of flutter, which should not be permitted for too long a time.

A nonsymmetrical aileron motion would involve a second bending mode (nonsymmetrical). It is probable that, in most cases, the node would be close to the middle of the aileron and therefore poorly coupled.

There remains to consider a complete case of flutter (torsion-flexure-aileron). Apparently cases do exist in which this type would appear at the lowest speed. The effect of the additional degree of freedom can probably be taken care of by a safety factor applied to the flutter speed obtained for two degrees of freedom. The calculation of the case of three degrees of freedom is perfectly straightforward although more lengthy than the simple cases.

TAIL FLUTTER

In regard to tail flutter, the situation is more complex. The possible combinations are subdivided as follows into three main groups, which will be separately analyzed:

(1) Vertical flexure of tail assembly.
(2) Horizontal flexure of tail assembly.
(3) Torsion of tail assembly.

Vertical flexure.—It is possible, in general, to identify two responses in vertical flexure; one corresponding to the fundamental bending mode of the fuselage and the other, to the bending mode of the horizontal-fin arrangement. The frequency of the fin arrangement is slightly greater than the one obtained with the rear end

of the fuselage fixed in space. It is probable that the fuselage bending mode need not be considered. In any case, the flutter speed calculated for each of the two cases will not differ very much because the density involved is about in the same ratio as the squares of the frequencies involved. Only the vertical fundamental bending frequency of the horizontal fin will therefore be considered. This bending frequency may couple with fin torsion and elevator motion. This motion is necessarily symmetrical and simulates the motion of the main wing system. Since the elevator has no particular restraint to this motion, it is evident that an unbalanced elevator is highly undesirable. As in the case of the wing system, the most frequent cause of flutter is also the flexure-aileron combination.

Horizontal flexure.—Horizontal flexure affects the vertical fin or fins and may be separately considered as a cantilever wing with an aileron. The rudder, which takes the place of the aileron, has no particular restraint to this motion and must therefore be carefully mass balanced.

Torsion.—Torsion is composed of a relatively low-frequency type of flutter involving the fuselage and a higher frequency type involving the fin tips, which may be considered as fin flexure in opposite phase. This type of flutter is not common because the great stiffness of the torque tube prevents its occurrence (β large). The rudder is affected in the same manner as for horizontal flexure.

In summary, it may be said that the expected causes of flutter are the in-phase motion of the horizontal fins as flexure-elevator and the motion of the vertical fin in flexure with rudder motions.

With two rudders disposed at the ends of the horizontal fins, care must be taken that the flexure frequency is sufficiently high. The mass of the rudders at the ends of the horizontal fins also affects the parameters used in the fin-stability calculation; that is, the density of the fins and the radius of gyration are increased. The center-of-gravity location may also be changed.

GROUND TESTS

DETERMINATION OF CENTER-OF-GRAVITY LOCATION

From the theory, it may be observed that the location of the torsional stiffness axis is of fairly secondary importance. The location of the center-of-gravity axis, on the other hand, is of great importance. The application of a very low-frequency (zero) torque will rotate the wing around the torsional stiffness axis a; the application of a very high frequency (infinity) torque will cause the mass center line to remain stationary. As the torsional frequency for wings is several times larger than the lowest bending frequency, it can be shown with all desired accuracy that the axis observed for the torsional frequency is the center-of-gravity line.

Assume the wing to be vibrating around an axis at a distance d behind the stiffness axis. The moment of inertia reduced to the center of gravity is

$$I=M(r_\alpha^2-x_\alpha^2)b^2$$

Moving the axis to d increases the moment of inertia to

$$M(r_\alpha^2-x_\alpha^2)b^2+M(x_\alpha-d)^2b^2=M(r_\alpha^2+d^2-2dx_\alpha)b^2$$

The corresponding torsional stiffness is $C_\alpha+d^2C_h$.

The frequency is consequently

$$\omega^2=\frac{(C_\alpha+d^2C_h)b^2}{M(r_\alpha^2+d^2-2dx_\alpha)b^2}$$

Then

$$2\log\omega=\log(C_\alpha+d^2C_h)b^2-\log Mb^2(r_\alpha^2+d^2-2dx_\alpha)$$

The wing will assume the state of vibration giving the greatest frequency. By derivation, with respect to d,

$$\frac{dC_h}{C_\alpha+d^2C_h}-\frac{d-x_\alpha}{r_\alpha^2+d^2-2dx_\alpha}=0$$

or

$$\frac{dC_h}{d-x_\alpha}=\omega^2M$$

Then

$$d=x_\alpha\frac{1}{1-(\omega_h/\omega)^2}$$

or, with d known,

$$x_\alpha=d[1-(\omega_h/\omega)^2]\cong d \text{ for } \omega_h/\omega\longrightarrow 0$$

That is, the center-of-gravity axis is slightly ahead of the dynamic axis (assuming both axes to be normally behind the stiffness axis). If the torsional frequency is very large, they coincide ($d=x_\alpha$). (If the torsional frequency is very low, $d=0$, giving the stiffness axis.)

In other words, the center-of-gravity location along a finished wing can be determined by establishing the dynamic torsional axis.

DIMENSIONAL CONSIDERATIONS

Proportionally increasing all dimensions of a wing while retaining all details lowers the frequencies in inverse proportion to the size. The reference speed ωb therefore always remains the same, as do all other parameters including the wing density. The actual flutter speed therefore depends on the shape but not on the size. It is important to keep in mind, however, that the reference is to wings or tails similar in all respects. In reality, a lighter contruction is necessarily employed in larger wing sizes, resulting in a weaker structure and a general lowering of the critical flutter speed.

The foregoing considerations are significant in the testing of models. Thus a true model constructed of the same material as the full-scale airplane will have the same flutter speed. For testing purposes, it is very desirable to have a fairly low flutter speed. This end may be achieved by employing models of special

materials related to celluloid, which have a value of $\sqrt{E/\rho}$ nearly five times smaller than that of materials normally used in airplane construction.

The most desirable condition would be to use a material with the same density ρ as the airplane and with the moduli E and G, say, $1/n$ times the original values. Fortunately, the density of the model wing can be very simply corrected by using a suitable thickness of the materials. Thus, if the density of the material used is three times lower than that of the original, the thickness of the skin and all the internal members is increased by a factor of 3.

It should be further noted that the model can be critically checked as to accuracy of reproduction by direct measurements of its mechanical properties. In other words, all the parameters, including the reference quantity ωb, are directly measured on the model itself. The value of ωb is usually close to the predicted value. The important point, however, is that it is not necessary to depend on a predicted theoretical value.

Thus the feasibility of conducting direct flutter tests on models of actual airplanes or of its component parts is indicated. Some work of this nature is now being undertaken. The procedure may be of value in cases that are difficult to treat theoretically and should be of value in accumulating useful experience on special designs.

GENERAL CONCLUSIONS

1. The two-dimensional theory has been verified within the limits of error in the determination of the primary parameters.

2. The most essential three-dimensional effect is the occurrence of distinct flutter bending modes, which differ from the ordinary vibration modes in that they tend to assume a form which approaches the next higher vibration mode and exhibit a correspondingly higher frequency. The flutter speed is consequently lower than that calculated on the basis of the lowest vibration frequency and the flutter frequency itself is higher. For ordinary damped structures, this effect lowers the flutter speed calculated on the basis of the lowest bending mode by only a few percent.

3. A cantilever wing flutters at a speed calculated by using the constants for the most representative section, which is located at approximately three-quarters of the semispan.

4. Aspect ratio and structural damping effects tend to *increase* the flutter speed by a few percent above that calculated for infinite aspect ratio and zero internal damping.

5. The effect of mass balancing to bring the center of gravity forward is essentially as predicted by theory. The effect of nacelles is of lesser importance, but large weights located at some distance away from the wing and attached to it show a very detrimental effect on the flutter speed.

6. Wing-aileron experimental studies show that the characteristic flutter *range* predicted by the theory exists and is in substantial agreement with the predicted values. A decrease in the unbalance and an increase in the frequency ratio are both beneficial. There exists, for each value of the unbalance, a certain critical frequency ratio and, inversely, for each frequency ratio, a certain critical value of the unbalance.

7. The considerable difficulty involved in the determination of the primary structural parameters including the damping is recognized and will constitute one of the chief problems of future flutter research.

LANGLEY MEMORIAL AERONAUTICAL LABORATORY,
NATIONAL ADVISORY COMMITTEE FOR AERONAUTICS,
LANGLEY FIELD, VA., *September 22, 1938.*

APPENDIX

LIST OF NOTATION

α, angle of attack (fig. 40).

β, aileron angle (fig. 40).

h, vertical distance (fig. 40).

$\dot{\alpha}=\frac{d\alpha}{dt}$, $\ddot{\alpha}=\frac{d^2\alpha}{dt^2}$, etc.

α_0, β_0, h_0, φ_1, φ_2, amplitudes and phase angles.

b, half chord, used as reference unit length.

a, coordinate of axis of rotation (torsional axis) (fig. 40). Location of stiffness axis in percentage total chord measured from the leading edge is $100\frac{1+a}{2}$ or $a=\frac{2\ (\text{stiffness axis})}{100}-1$.

c, coordinate of aileron hinge axis (fig. 40). Location of aileron hinge axis in percentage total chord measured from leading edge is $100\frac{1+c}{2}$ or $c=\frac{2\ (\text{aileron hinge})}{100}-1$.

ρ, mass of air per unit of volume.

M, mass of wing per unit span length.

$\kappa=\frac{\pi\rho b^2}{M}$, the ratio of the mass of a cylinder of air of a diameter equal to the chord of the wing to the mass of the wing, both taken for equal length along the span; this ratio may be expressed as $\kappa=0.24(b^2/W)\ (\rho/\rho_0)$ where W is weight in pounds per foot span, b is in feet, and ρ/ρ_0 is ratio of air density to standard air. [The quantity $\sigma=W/4b^2$ (weight per square foot per chord in feet) has been used by British writers. Thus, $\kappa=(0.06/\sigma)\ (\rho/\rho_0)$.]

$x_\alpha=\frac{S_\alpha}{Mb}$, location of center of gravity of wing-aileron system *measured from a* (fig. 40); S_α, static moment of wing-aileron per unit span length referred to a. Location of center of gravity in percentage total chord measured from the leading edge is $100\frac{1+a+x_\alpha}{2}$ or $a+x_\alpha=\frac{2\ (\text{center of gravity})}{100}-1$.

$x_\beta=\frac{S_\beta}{Mb}$, *reduced* location of center of gravity of aileron referred to c (fig. 40). S_β, static moment of aileron per unit span length referred to c.[3]

$r_\alpha=\sqrt{\frac{I_\alpha}{Mb^2}}$, radius of gyration of wing aileron referred to a (fig. 40). I_α, moment of inertia of wing aileron about the elastic axis per unit span length.

$r_\beta=\sqrt{\frac{I_\beta}{Mb^2}}$, *reduced* radius of gyration of aileron referred to c (fig. 40). I_β, moment of inertia of aileron about c per unit span length.

[3] Note that M refers to the total wing mass and not to the mass of the aileron alone.

C_α, torsional stiffness of wing around a per unit span length.

C_β, torsional stiffness of aileron around c per unit span length.

C_h, stiffness of wing in deflection per unit span length.

$\omega_\alpha=\sqrt{\frac{C_\alpha}{I_\alpha}}$, natural angular frequency of torsional vibration around a in vacuum ($\omega_\alpha=2\pi f_\alpha$, where f_α is in cycles per second).

$\omega_\beta=\sqrt{\frac{C_\beta}{I_\beta}}$, natural angular frequency of torsional vibrations of aileron about c.

$\omega_h=\sqrt{\frac{C_h}{M}}$, natural angular frequency of wing in deflection.

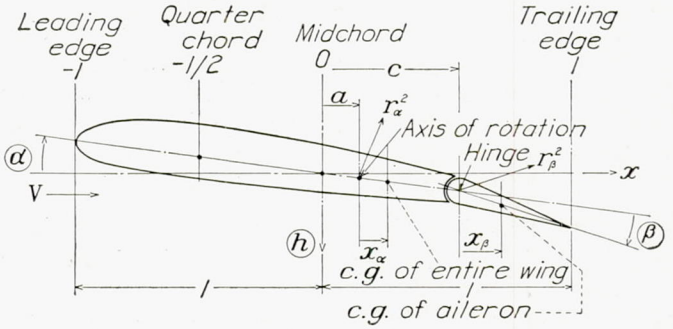


FIGURE 40.—Half chord b is used as the unit length. The positive directions of α, β, and h are indicated by arrows. Note that a is measured from midchord and that x_α is measured from the elastic axis positive to the right. Also note that x_β is a "reduced" parameter and not the actual distance from the hinge to the c. g. of the aileron.

t, time.

v, speed of forward motion.

v_f, flutter or critical speed.

ω, circular frequency of wing vibrations.

$k=\frac{b\omega}{v}$, *reduced* frequency=number of waves in the wake in a distance equal to the semichord$\times 2\pi$.

$1/k$, reduced wave length=length of one wave of the wake in terms of a distance equal to the semichord$\times 2\pi$.

F and G, functions of k in table 2.

$$\begin{cases} R_{a\alpha}=-A_{\alpha 1}+\left(\frac{1}{4}-a^2\right)\frac{2G}{k}-\left(\frac{1}{2}+a\right)\frac{2F}{k^2} \\ R_{a\beta}=-A_{\beta 1}+\frac{1}{k^2}A_{\beta 3}+\left(\frac{1}{2}+a\right)\left(\frac{T_{11}}{2\pi}\frac{2G}{k}-\frac{T_{10}}{\pi}\frac{2F}{k^2}\right) \\ R_{ah}=-A_{h1}+\left(\frac{1}{2}+a\right)\frac{2G}{k} \end{cases}$$

$$\begin{cases} R_{b\alpha}=-B_{\alpha 1}-\dfrac{T_{12}}{2\pi}\left[\left(\dfrac{1}{2}-a\right)\dfrac{2G}{k}-\dfrac{2F}{k^2}\right] \\ R_{b\beta}=-B_{\beta 1}+\dfrac{1}{k^2}B_{\beta 3}-\dfrac{T_{12}}{2\pi}\left(\dfrac{T_{11}}{2\pi}\dfrac{2G}{k}-\dfrac{T_{10}}{\pi}\dfrac{2F}{k^2}\right) \\ R_{bh}=-B_{h1}-\dfrac{T_{12}}{2\pi}\dfrac{2G}{k} \end{cases}$$

$$\begin{cases} R_{c\alpha}=-C_{\alpha 1}-\left(\dfrac{1}{2}-a\right)\dfrac{2G}{k}+\dfrac{2F}{k^2} \\ R_{c\beta}=-C_{\beta 1}-\dfrac{T_{11}}{2\pi}\dfrac{2G}{k}+\dfrac{T_{10}}{\pi}\dfrac{2F}{k^2} \\ R_{ch}=-C_{h1}-\dfrac{2G}{k} \end{cases}$$

$$\begin{cases} I_{a\alpha}=\dfrac{1}{k}\left[-\left(\dfrac{1}{2}+a\right)\dfrac{2G}{k}-\left(\dfrac{1}{4}-a^2\right)2F+A_{\alpha 2}\right] \\ I_{a\beta}=\dfrac{1}{k}\left[-\left(\dfrac{1}{2}+a\right)\left(\dfrac{T_{10}}{\pi}\dfrac{2G}{k}+\dfrac{T_{11}}{2\pi}2F\right)+A_{\beta 2}\right] \\ I_{ah}=\dfrac{1}{k}\left[-\left(\dfrac{1}{2}+a\right)2F\right] \end{cases}$$

$$\begin{cases} I_{b\alpha}=\dfrac{1}{k}\left\{\dfrac{T_{12}}{2\pi}\left[\dfrac{2G}{k}+\left(\dfrac{1}{2}-a\right)2F\right]+B_{\alpha 2}\right\} \\ I_{b\beta}=\dfrac{1}{k}\left[\dfrac{T_{12}}{2\pi}\left(\dfrac{T_{10}}{\pi}\dfrac{2G}{k}+\dfrac{T_{11}}{2\pi}2F\right)+B_{\beta 2}\right] \\ I_{bh}=\dfrac{1}{k}\left(\dfrac{T_{12}}{2\pi}2F\right) \end{cases}$$

$$\begin{cases} I_{c\alpha}=\dfrac{1}{k}\left[\dfrac{2G}{k}+\left(\dfrac{1}{2}-a\right)2F+C_{\alpha 2}\right] \\ I_{c\beta}=\dfrac{1}{k}\left(\dfrac{T_{10}}{\pi}\dfrac{2G}{k}+\dfrac{T_{11}}{2\pi}2F+C_{\beta 2}\right) \\ I_{ch}=\dfrac{1}{k}2F \end{cases}$$

$$\overline{R}_{a\alpha}=R_{a\alpha}+\Omega_\alpha X \qquad \Omega_\alpha X=\frac{r_\alpha^2}{\kappa}\left(\frac{\omega_\alpha}{\omega}\right)^2$$

$$\overline{R}_{b\beta}=R_{b\beta}+\Omega_\beta X \qquad \Omega_\beta X=\frac{r_\beta^2}{\kappa}\left(\frac{\omega_\beta}{\omega}\right)^2$$

$$\overline{R}_{ch}=R_{ch}+\Omega_h X \qquad \Omega_h X=\frac{1}{\kappa}\left(\frac{\omega_h}{\omega}\right)^2$$

$$\overline{I}_{a\alpha}=I_{a\alpha}+g_\alpha\Omega_\alpha X$$

$$\overline{I}_{b\beta}=I_{b\beta}+g_\beta\Omega_\beta X$$

$$\overline{I}_{ch}=I_{ch}+g_h\Omega_h X$$

The quantities $A_{\alpha 1}$, $A_{\beta 1}$, etc. and $\Omega_\alpha X$, $\Omega_\beta X$, etc. are defined under the calculation scheme (pp. 5–7). The T's are listed in table 2. The definitions of the T's are given in reference 1, page 5, should other values than those listed in the table be required.

$v/b\omega_\alpha$, flutter-speed coefficient (cases 1 and 3).

$v/b\omega_h$, flutter-speed coefficient (case 2).

ω_h/ω_α, frequency ratio (case 1).

ω_β/ω_h, frequency ratio (case 2).

$\omega_\beta/\omega_\alpha$, frequency ratio (case 3).

$v_D=b\omega_\alpha\sqrt{\dfrac{r_\alpha^2}{\kappa}\dfrac{1/2}{(1/2)+a}}$, divergence velocity.

g_α, g_β, g_h, structural damping coefficients; πg corresponds approximately to the usual logarithmic decrement.

M_α, M_β, magnitude of sinusoidal impressed torques in the α and β degrees of freedom.

P_0, magnitude of impressed force in the h degree of freedom.

ψ, phase angle.

α_0/α_{st}, β_0/β_{st}, h_0/h_{st}, peak response for the various degrees of freedom.

REFERENCES

1. Theodorsen, Theodore: General Theory of Aerodynamic Instability and the Mechanism of Flutter. T. R. No. 496, N. A. C. A., 1935.
2. Cicala, Placido: Le Azioni aerodinamiche sui profili di ala oscillanti in presenza di corrente uniforme. Mem. R. Accad. Sci. Torino, ser. 2, pt. I, t. 68, 1934–1935, pp. 73–98.
3. Kassner, R., and Fingado, H.: Das ebene Problem der Flügelschwingung. Luftfahrtforschung, Bd. 13, Nr. 11, 20.Nov. 1936, S. 374–387.
4. Küssner, H. G.: Zusammenfassender Bericht über den instationären Auftrieb von Flügeln. Luftfahrtforschung, Bd. 13, Nr. 12, 20.Dec. 1936, S. 410–424.
5. Garrick, I. E.: Propulsion of a Flapping and Oscillating Airfoil. T. R. No. 567, N. A. C. A., 1936.
6. Voigt, H.: Wind-Tunnel Investigations on Flexural-Torsional Wing Flutter. T. M. No. 877, N. A. C. A. 1938.
7. von Schlippe, B.: The Question of Spontaneous Wing Oscillations. T. M. No. 806, N. A. C. A., 1936.

TABLE 1

k	$1/k$	F	$-G$	$-2G/k$	$2F/k^2$
∞	0.000	0.5000	0	0	0
10	.100	.5006	.0124	.00248	.010012
6	.16667	.5017	.0206	.00686	.02787
4	.250	.5037	.0305	.01525	.06296
3	.33333	.5063	.0400	.02667	.1125
2	.500	.5129	.0577	.0577	.2565
1.5	.66667	.5210	.0736	.0948	.4631
1.2	.83333	.5300	.0877	.1462	.7361
1.0	1.000	.5394	.1003	.2006	1.0788
.80	1.250	.5541	.1165	.2912	1.7316
.66	1.51516	.5699	.1308	.3964	2.6166
.60	1.66667	.5788	.1378	.4593	3.2156
.56	1.78572	.5857	.1428	.5100	3.7353
.50	2.000	.5979	.1507	.6028	4.7832
.44	2.27273	.6130	.1592	.7236	6.3326
.40	2.500	.6250	.1650	.8250	7.8125
.34	2.94118	.6469	.1738	1.022	11.192
.30	3.33333	.6650	.1793	1.195	14.778
.24	4.16667	.6989	.1862	1.552	24.267
.20	5.000	.7276	.1886	1.886	36.380
.16	6.250	.7628	.1876	2.345	59.592
.12	8.33333	.8063	.1801	3.002	111.99
.10	10.000	.8320	.1723	3.446	166.4
.08	12.500	.8604	.1604	4.010	268.9
.06	16.66667	.8920	.1426	4.753	495.6
.05	20.000	.9090	.1305	5.220	727.2
.04	25.000	.9267	.1160	5.800	1158.3
.025	40.000	.9545	.0872	6.976	3054.4
.01	100.000	.9824	.0482	9.640	19648
0	∞	1.000	0	∞	∞

TABLE 2

Values of T

$c\longrightarrow$	−1	−0.5	0	0.1	0.2	0.3
T_1/π	−1.00000	−0.54008	−0.21221	−0.16539	−0.12490	−0.09064
T_3/π^2	−1.25000	−.38882	−.08191	−.05434	−.03429	−.02031
$T_4/\pi(=-C_{\beta 2})$	−1.00000	−.80450	−.50000	−.43644	−.37353	−.31192
T_7/π	−1.12500	−.37922	−.06250	−.03540	−.01672	−.00489
T_{10}/π	1.00000	.94233	.81831	.78483	.74779	.70666
$T_{11}/2\pi$	1.50000	1.01125	.56831	.48813	.41146	.33870
$T_{12}/2\pi$	.50000	.20675	.06831	.05168	.03793	.02679
p/π	0	−.06891	−.10610	−.10452	−.09980	−.09105
$A_{\beta 3}=\frac{T_4+T_{10}}{\pi}$	0	.13783	.31831	.34789	.37426	.39474
$B_{\alpha 2}=\frac{1}{\pi}\left(p-T_1-\frac{T_4}{2}\right)$	1.50000	.87342	.35611	.27909	.21187	.15555
$B_{\beta 2}=-\frac{T_4T_{11}}{2\pi^2}$	1.50000	.81355	.28416	.21304	.15369	.10565
$B_{\beta 3}=\frac{T_5-T_4T_{10}}{\pi^2}$	0	.05376	.05783	.05275	.04643	.03922

$c\longrightarrow$	0.4	0.5	0.6	0.7	0.8	0.9	1.0
T_1/π	−0.06238	−0.04008	−0.02322	−0.01145	−0.00420	−0.00076	0
T_3/π^2	−.01107	−.00539	−.00223	−.00071	−.00014	−.00001	0
$T_4/\pi(=-C_{\beta 2})$	−.25231	−.19550	−.14238	−.09406	−.05204	−.01868	0
T_7/π	−.00161	.00421	.00428	.00302	.00144	.00032	0
T_{10}/π	.66075	.60900	.54982	.48050	.39582	.28231	0
$T_{11}/2\pi$	.27029	.20675	.14874	.09712	.05314	.01889	0
$T_{12}/2\pi$	.01798	.01125	.00636	.00306	.00110	.00020	0
p/π	−.08169	−.06891	−.05433	−.03864	−.02292	−.00879	0
$A_{\beta 3}=\frac{T_4+T_{10}}{\pi}$	.40844	.41350	.40744	.38644	.34378	.26843	0
$B_{\alpha 2}=\frac{1}{\pi}\left(p-T_1-\frac{T_4}{2}\right)$	.10685	.06892	.04008	.01984	.00830	.00131	0
$B_{\beta 2}=-\frac{T_4T_{11}}{2\pi^2}$	.06820	.04042	.02118	.00914	.00277	.00035	0
$B_{\beta 3}=\frac{T_5-T_4T_{10}}{\pi^2}$	.03156	.02384	.01651	.00999	.00476	.00127	0

The expressions for the T's are listed in reference 1, page 5.

TABLE 3

Values of $R_{a\alpha}''$

$$R_{a\alpha}=-A_{\alpha 1}+R_{a\alpha}''$$

$1/k$ \ a	−0.5	−0.45	−0.4	−0.3	−0.2	−0.1	0
0	0	0	0	0	0	0	0
.100	0	−.00061840	−.00122	−.00240	−.00352	−.00460	−.00563
.16667	0	−.0017193	−.00341	−.00567	−.00980	−.01079	−.01566
.250	0	−.0038724	−.00767	−.01503	−.02209	−.02884	−.03539
.33333	0	−.0068918	−.01365	−.02677	−.03935	−.05140	−.06292
.500	0	−.015566	−.03084	−.06053	−.08907	−.11645	−.14268
.66667	0	−.027658	−.05484	−.10779	−.15884	−.20799	−.25525
.83333	0	−.043749	−.08677	−.17061	−.25153	−.32953	−.40460
1.000	0	−.063468	−.12593	−.24786	−.36577	−.47966	−.58955
1.250	0	−.10041	−.19937	−.39291	−.58063	−.76253	−.93860
1.51516	0	−.14966	−.29734	−.58674	−.86822	−1.14178	−1.40740
1.66667	0	−.18260	−.36290	−.71661	−1.06113	−1.39647	−1.72263
1.78572	0	−.21098	−.41943	−.82866	−1.22769	−1.61652	−1.99515
2.000	0	−.26779	−.53257	−1.05309	−1.56125	−2.05795	−2.54230
2.27273	0	−.35100	−.69838	−1.38230	−2.05174	−2.70670	−3.34720
2.500	0	−.42981	−.85555	−1.69450	−2.51700	−3.32300	−4.11250
2.94118	0	−.60814	−1.21120	−2.40192	−3.57222	−4.72208	−5.85150
3.33333	0	−.79566	−1.58535	−3.14680	−4.68435	−6.19800	−7.68775
4.16667	0	−1.2871	−2.56638	−5.10072	−7.60602	−10.07728	−12.52150
5.000	0	−1.9086	−3.80774	−7.57776	−11.31006	−15.00464	−18.66150
6.250	0	−3.0910	−6.17025	−12.29360	−18.37005	−24.39960	−30.38225
8.33333	0	−5.7421	−11.46918	−22.87832	−34.22742	−45.51648	−56.74550
10.000	0	−8.4837	−16.95014	−33.83136	−50.64366	−67.38704	−84.06150
12.500	0	−13.635	−27.25090	−54.42160	−81.51210	−108.52240	−135.45250
16.66667	0	−25.006	−49.98777	−99.88048	−149.67813	−199.38072	−248.98825
20.000	0	−36.608	−73.18980	−146.27520	−219.25620	−292.13280	−364.90500

TABLE 3—Continued

Values of $I_{a\alpha}''$

$I_{a\alpha}=1/k\ I_{a\alpha}''$

$1/k$ \ a	−0.5	−0.45	−0.4	−0.3	−0.2	−0.1	0
0	1.00000	0.90250	0.81000	0.64000	0.49000	0.36000	0.25000
.100	1.00000	.90256	.81014	.64031	.49049	.36070	.25094
.16667	1.00000	.90268	.81038	.64083	.49135	.36192	.25258
.250	1.00000	.90291	.81086	.64187	.49303	.36432	.25578
.33333	1.00000	.90323	.81154	.64331	.49535	.36764	.26019
.500	1.00000	.90415	.81345	.64741	.50189	.37689	.27240
.66667	1.00000	.90524	.81570	.65224	.50962	.38784	.28690
.83333	1.00000	.90696	.81922	.65962	.52126	.40404	.30810
1.000	1.00000	.90879	.82297	.66751	.53363	.42133	.33060
1.250	1.00000	.91192	.82938	.68093	.55464	.45051	.36855
1.51516	1.00000	.91568	.83706	.69691	.57956	.48501	.40325
1.66667	1.00000	.91797	.84175	.70664	.59469	.50590	.44025
1.78572	1.00000	.91986	.84557	.71457	.60701	.52286	.46215
2.000	1.00000	.92334	.85266	.72923	.62972	.55413	.50245
2.27273	1.00000	.92794	.86202	.74856	.65962	.59520	.55530
2.500	1.00000	.93187	.87000	.76500	.68500	.63000	.60000
2.94118	1.00000	.93964	.88576	.79739	.73490	.69829	.68755
3.33333	1.00000	.94657	.89980	.82620	.77920	.75960	.76500
4.16667	1.00000	.96120	.92949	.88675	.87206	.88533	.92655
5.000	1.00000	.97518	.95763	.94437	.96021	1.00515	1.07920
6.250	1.00000	.99478	.99720	1.02490	1.08312	1.17186	1.29110
8.33333	1.00000	1.0235	1.05507	1.24238	1.26195	1.41378	1.59785
10.000	1.00000	1.0433	1.09484	1.32296	1.38436	1.57904	1.80700
12.500	1.00000	1.0688	1.14613	1.42667	1 54163	1.79101	2.07480
16.66667	1.00000	1.1029	1.21474	1.56516	1.75126	2.07304	2.43050
20.000	1.00000	1.1246	1.25838	1.65312	1.88422	2.25168	2.65550

TABLE 4

Values of $R_{b\beta}''$

$R\beta=-B_{\beta 1}+R_{b\beta}''$

$1/k$ \ c	0	0.1	0.2	0.3	0.4	0.5	0.6	0.7	0.8	0.9	1.0
0	0	0	0	0	0	0	0	0	0	0	0
.100	.00123	.00100	.00078	.00060	.00045	.00032	.00021	.00011	.00005	.00001	0
.16667	.00342	.00267	.00219	.00168	.00124	.00087	.00057	.00032	.00014	.00004	0
.250	.00768	.00623	.00493	.00378	.00279	.00196	.00126	.00071	.00032	.00008	0
.33333	.01367	.01109	.00877	.00673	.00498	.00349	.00225	.00119	.00056	.00015	0
.500	.03085	.02505	.01978	.01519	.01122	.00787	.00507	.00290	.00126	.00033	0
.66667	.05494	.04461	.03525	.02706	.01999	.01402	.00905	.00515	.00225	.00059	0
.83333	.08647	.07018	.05540	.04250	.03137	.02236	.01419	.00806	.00352	.00092	0
1.000	.12517	.10158	.08015	.06146	.04535	.03177	.02048	.01164	.00510	.00133	0
1.250	.19729	.16000	.12621	.09670	.07130	.04990	.03214	.01825	.00798	.00208	0
1.51516	.29270	.23723	.18699	.14317	.10547	.07373	.04744	.02690	.01175	.00307	0
1.66667	.35614	.28854	.22733	.17398	.12810	.08952	.05755	.03262	.01425	.00371	0
1.78572	.41062	.33258	.26195	.20040	.14750	.10302	.06620	.03750	.01637	.00426	0
2.000	.51910	.42022	.33078	.25290	.18595	.12980	.08335	.04717	.02058	.00535	0
2.27273	.67692	.54753	.43071	.32902	.24177	.16857	.10813	.06113	.02664	.00691	0
2.500	.82550	.66738	.52463	.40050	.29407	.20488	.13131	.07417	.03230	.00838	0
2.94118	1.15907	.93605	.73500	.56040	.41094	.28588	.18296	.10318	.04486	.01162	0
3.33333	1.50670	1.21566	.95364	.72637	.53204	.36968	.23630	.13308	.05779	.01495	0
4.16667	2.40775	1.93923	1.51852	1.15435	.84375	.58495	.37303	.20958	.09080	.02342	0
5.000	3.53385	2.84190	2.22193	1.68628	1.23036	.85134	.54187	.30380	.13137	.03380	0
6.250	5.65191	4.00926	3.54031	2.68138	1.95216	1.34764	.85572	.47853	.20644	.05296	0
8.33333	10.34067	8.28124	6.44720	4.87081	3.53670	2.43454	1.54135	.85928	.36960	.09447	0
10.000	15.14353	12.11112	9.41589	7.10321	5.14958	3.53887	2.23667	1.24464	.53443	.13633	0

TABLE 4—Continued

Values of $I_{b\beta}''$

$I_{b\beta}=1/k\ I_{b\beta}''$

$1/k$ \ c	0	0.1	0.2	0.3	0.4	0.5	0.6	0.7	0.8	0.9	1.0
0	0.32298	0.23827	0.16930	0.11472	0.07306	0.04275	0.02213	0.00944	0.00283	0.00035	0
.100	.32289	.23820	.16925	.11468	.07304	.04273	.02212	.00944	.00283	.00035	0
.16667	.32273	.23808	.16916	.11462	.07300	.04269	.02211	.00943	.00283	.00035	0
.250	.32242	.23784	.16899	.11450	.07292	.04260	.02209	.00942	.00282	.00035	0
.33333	.32198	.23751	.16874	.11433	.07280	.04243	.02205	.00940	.00282	.00035	0
.500	.32075	.23658	.16806	.11386	.07250	.04241	.02195	.00937	.00280	.00035	0
.66667	.31931	.23548	.16727	.11331	.07213	.04220	.02184	.00931	.00279	.00034	0
.83333	.31714	.23385	.16609	.11249	.07161	.04183	.02168	.00925	.00277	.00034	0
1.000	.31483	.23212	.16484	.11163	.07106	.04156	.02150	.00917	.00274	.00034	0
1.250	.31090	.22919	.16273	.11019	.07013	.04101	.02121	.00904	.00271	.00034	0
1.51516	.30625	.22572	.16024	.10849	.06903	.04036	.02087	.00890	.00267	.00033	0
1.66667	.30343	.22362	.15873	.10746	.06837	.03997	.02067	.00881	.00264	.00033	0
1.78572	.30112	.22190	.15752	.10662	.06783	.03966	.02050	.00874	.00262	.00033	0
2.000	.29688	.21876	.15526	.10509	.06685	.03908	.02021	.00861	.00257	.00033	0
2.27273	.29130	.21462	.15231	.10307	.06556	.03832	.01981	.00845	.00252	.00032	0
2.500	.28657	.21112	.14980	.10137	.06448	.03768	.01948	.00831	.00249	.00031	0
2.94118	.27726	.20423	.14491	.09803	.06235	.03643	.01883	.00803	.00240	.00030	0
3.33333	.26899	.19813	.14056	.09509	.06046	.03533	.01826	.00778	.00232	.00029	0
4.16667	.25166	.18536	.13152	.08894	.05655	.03305	.01708	.00728	.00217	.00027	0
5.000	.23522	.17325	.12292	.08315	.05286	.03089	.01596	.00681	.00203	.00025	0
6.250	.21229	.15642	.11100	.07510	.04775	.02791	.01442	.00615	.00183	.00023	0
8.33333	.17895	.13197	.09372	.06345	.04038	.02362	.01220	.00521	.00155	.00019	0
10.000	.15613	.11525	.08194	.05551	.03535	.02069	.01070	.00457	.00135	.00017	0

TABLE I.—EXPERIMENTAL RESULTS OF FLUTTER INVESTIGATION

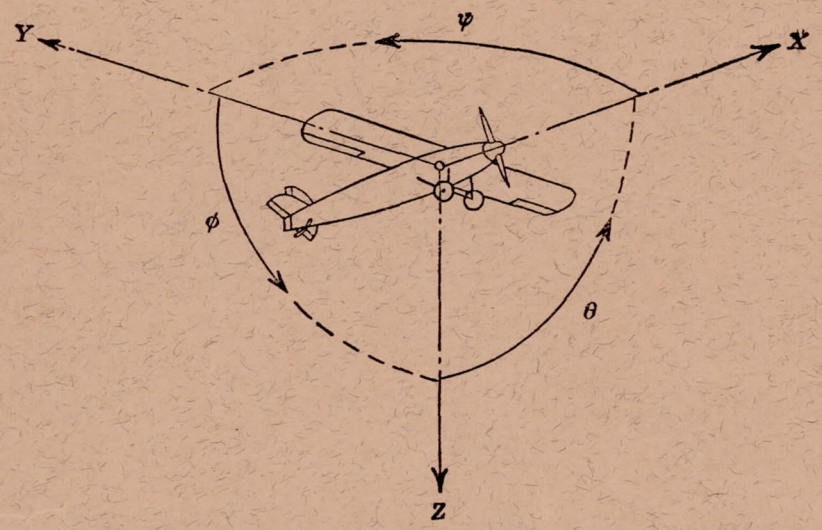
Figure number	Wing model	Wing dimensions	First bending (cycles/sec.)	Second bending (cycles/sec.)	Third bending (cycles/sec.)	Fourth bending (cycles/sec.)	First torsion (cycles/sec.)	Second torsion (cycles/sec.)	c. g. location (percent chord from L. E.) Calculated	c. g. location (percent chord from L. E.) Observed	Stiffness axis (percent chord from L. E.)	r_α^2 (radius of gyration)^2 (cf. notation)	Wing weight (lb.)	Test conditions and remarks	Run	Air density, ρ	Flutter frequency (cycles/sec.)	Flutter velocity (m. p. h.)	Theoretical results
10	1	Rectangular: 12-in. chord; 6-ft. 9-in. span	1.09	6.8	19.7		15.0		41.2	41.2	30.0	0.3125	7.32	Tests on wing 1 were preliminary. A stop was used.	20–2	2.283×10^{-3}		97.1	
														Later tests employed a screen instead	20–3	2.278		99.2	100
														Damping test	20–4				
														Run 20–3 repeated	20–5	2.274		98.5	
														Weight, 0.028 lb. on L. E. 18 in. from tip.	20–8	2.265		114.4	
11	2A		1.29	7.7	21.0		18.1		41.2	42.3	30.0	0.3125	36.50	Stop used; all other tests screen used (tip flutter).	20–10	2.256	15.0	188.0	Figs. 17 and 19
														Model support fractured	20–11			203.0	
														Model repaired	20–15	2.154	10.2	202.0	
														Restraining wires 17 in. from tip, 3.6 in. from L. E.	20–16	2.216		151.0	
							16.7							Nacelle 6.10 lb. placed 2 ft. from top, 2.70 in. ahead of c. g.	20–17	2.116	9.45	216.0	
							17.0							Nacelle placed 2 ft. from top, 1.34 in. back of c. g.	20–18	2.170		197.0	
														Run 20–16 repeated	20–19	2.225		154.0	
							14.8							Counterweight 3.07 lb. at L. E. 13 in. from tip.	20–20	2.173		197.0	
														Run 20–20 repeated	20–21	2.174		202.0	
11	2B	Same as 2A	1.31	7.7	20.8		17.8		42.5		30.0		35.95	Plain; no weight attached	20–23	2.159	10.2	205.9	Figs. 17 and 19
														Disk 12.77 lb. 12-in. diam. on bottom; c. g. of disk on c. g. of airfoil.	20–24	2.204	8.35	154.2	
														Disk 12.45 lb. 17-in. diam. in same position as 20–24.	20–25	2.228	7.35	121.5	
														Disk as in 20–25 placed 1 in. ahead of c. g.	20–26	2.232	7.48	116.2	
														Disk as in 20–25 placed 1 in. back of c. g.	20–27	2.214	7.25	131.9	
														Run 20–23 repeated	20–28	2.149		205.0	
														Airfoil tip restrained by wires	20–29	2.154		205.1	
														Run 20–25 repeated	20–30	2.232		120.7	
														Run 20–23 repeated	20–31	2.146		199.3	
														Same as 20–31, movies taken	20–32	2.144		198.7	
														Plain; restraining wires 8 in. from tip	20–33	2.122	10.8	208.0	Fig. 21
														Plain; restraining wires 60 in. from tip	20–34	2.171	13.1	159.5	
														Restraining wires 40 in. from tip; model broke near tip.	20–35	2.053	8.24	284.7	

TABLE I.—EXPERIMENTAL RESULTS OF FLUTTER INVESTIGATION—Continued

Figure number	Wing model	Wing dimensions	First bending (cycles/sec.)	Second bending (cycles/sec.)	Third bending (cycles/sec.)	Fourth bending (cycles/sec.)	First torsion (cycles/sec.)	Second torsion (cycles/sec.)	c. g. location (percent chord from L. E.)		Stiffness axis (percent chord from L. E.)	r_a^2 (radius of gyration)^2 (cf. notation)	Wing weight (lb.)	Test conditions and remarks	Run	Air density, ρ	Flutter frequency (cycles/sec.)	Flutter velocity (m. p. h.)	Theoretical results
									Calculated	Observed									
11	2C	Rectangular; 12-in. chord; 6-ft. 4-in. span	1.40	8.2	22.5		18.8		42.5		30.0			Model 2B repaired	20–73	2.133×10^{-3}		220.4	Fig. 23
			1.22	7.2	20.8		16.2							With 3.05-lb. counterweight 1 in. from tip at L. E.	20–74	2.169		196.8	
			1.29	8.2	22.4		15.8							Counterweight 13 in. from tip at L. E.	20–75	2.152		210.5	
			1.34	8.0	22.2		16.0							Counterweight 25 in. from tip at L. E.	20–76	2.101		244.6	
			1.38	7.6	22.5		16.8							Counterweight 37 in. from tip at L. E.	20–77	2.119		235.7	
			1.39	7.8	22.0		17.4							Counterweight 49 in. from tip at L. E.	20–78	2.122		232.2	
			1.39	8.0	21.2		18.2							Counterweight 61 in. from tip at L. E.	20–79	2.136		219.8	
			1.24	7.7	19.8		13.8							With weights simultaneously at 13 in., 37 in., and 61 in. from tip.	20–81	2.056		294.3	
12	3	Taper ratio, 2:1	1.65	6.8	16.5	30.7	29.1		42.5	42.0	30.0		20.48	Plain tapered wing	20–22	2.160	16.4	216.0	
														Run 20–22 repeated	20–68	2.150		214.9	
			1.64	5.2	13.1	28.4	8.9	37.8						Nacelle 6.10 lb.; c. g. 3.10 in. back of c. g. of airfoil.	20–69	2.232		109.2	
							9.1							Nacelle placed 1.10 in. back of c. g. Fig. 25.	20–70	2.245		91.0	
							8.8							Nacelle placed 2.80 in. ahead of c. g.	20–71	2.240	8.50	90.4	
														Run 20–68 repeated	20–72	2.149	14.0	213.3	
13	4	Taper ratio, 4:1	2.07	6.0	13.3	24.0	36.2		41.2	41.5			16.88	Violent flutter suddenly. Wing bent out of shape. Fig. 20.	20–67	2.174		203.9	Fig. 17
12	3	Taper ratio, 2:1	1.65	6.8	16.5	30.7	29.1		42.5	42.0			20.48	Restraining wires 59 in. from tip at stiffness axis.	20–89	2.187		211.1	Fig. 22
														Same except wires 2 in. ahead of stiffness axis.	20–90	2.200		204.4	
														Same except wires 4 in. back of stiffness axis.	20–91				
														Restraining wires 40 in. from tip at stiffness axis.	20–93	2.234		155.8	
														Restraining wires 17 in. from tip at stiffness axis.	20–94	2.229		152.9	
														Restraining wires 1 in. from tip at stiffness axis.	20–95	2.182		211.4	
														Restraining wires 27 in. from tip at stiffness axis.	20–96	2.202		200.8	
16	6		2.30	12.8	31.2		19.2		42.5	45.2			3.45	Rectangular wooden model; 81-in. span.	20–82	2.268		73.8	
16	7		4.92	25.0	67.2		35.8		42.5	43.9			6.01	Tapered wooden model; completely destroyed by violent flutter.	20–92	2.199		205.6	

TABLE 1A.—WING-AILERON FLUTTER TESTS

Wing model	Aileron (see fig. 14)	Wing weight (lb.)	Aileron weight (lb.)	First bending (cycles/sec.)	Aileron frequency (cycles/sec.)	r_β^2 (cf. notation)	Test conditions and remarks	Run	Air density, ρ	Lower critical velocity (m. p. h.)	Air density, ρ	Upper critical velocity (m. p. h.)
5	AII	44.84	0.950	10.68	0	0.0019	Aileron with 3 free hinges	20–36	2.273×10^{-3}	53.9		
	AV		.618		0			20–37	2.278	50.7		
	AII		.950		5.75		Aileron with springs	20–38	2.273	50.4		
	AV		.618		7.91			20–39	2.271	42.4		
	AII		.950		12.5			20–40	2.269	76.8		
	AII				8.50		Theoretical results for aileron AII shown in fig. 26	20–41	2.306	44.8		
	AII				11.0			20–42	2.301	55.4		
	AII				11.0			20–43			2.240×10^{-3}	147.0
	AII				12.5			20–44			2.229	151.6
	AII				13.1			20–45	2.259	98.4		
	AII				9.67			20–46	2.283	57.4	2.236	159.3
	AII				9.17			20–47	2.268	50.0	2.162	193.0
	AII				5.75			20–48	2.245	52.6	2.165	199.9
	AII				0		Hinges free	20–49	2.242	58.3	2.138	225.1
	AII				13.3			20–50	2.242	60.3	2.200	125.7
	AII				10.8			20–51	2.240	65.0	2.199	149.9
	AII				0		3 free hinges with aileron counterweight, 0.557 lb., Fig. 15.	20–52		No flutter		
	AII				0		Counterweight, 0.452 lb	20–53		No flutter		
	AII				0		Counterweight, 0.346 lb	20–54	2.249	75.2	2.243	206.1
	AII				0		Counterweight, 0.398 lb	20–55	2.243	99.5	2.173	197.8
	AII				3.00		do	20–56	2.243	99.9	2.193	167.3
	AII				6.92		do	20–57	2.262	62.8	2.218	147.1
	AI		.567		0		2 free hinges	20–58	2.262	65.3	2.163	218.7
	AVII		.300		0		3 free hinges	20–59	2.259	57.8	2.221	105.7
	AIII		1.43		0		4 free hinges	20–60	2.250	60.2	2.161	205.3
	AIII				0		4 free hinges with lead for damping	20–61	2.251	52.2	2.199	145.3
	AIII				0		do	20–63	2.261	78.0	2.171	199.5
	AIII				0		do	20–64	2.255	97.8	2.150	223.2
	AIII				4.67		do	20–65	2.259	67.3	2.178	166.8
	AIII				6.00		do	20–66	2.260	63.8	2.210	161.6
	AVIII		2.01		0		Hinge-pin position varied as shown in fig. 27	20–83	2.285	64.4	2.178	230.5
	AVIII				0		do	20–84	2.281	93.6	2.143	266.0
	AVIII				0		do	20–86		No flutter		
	AVIII				0		do	20–87	2.250	85.5	2.098	290.8
	AVIII				7.00		do	20–88	2.259	41.1	2.130	264.1



Positive directions of axes and angles (forces and moments) are shown by arrows

Axis		Force (parallel to axis) symbol	Moment about axis			Angle		Velocities	
Designation	Symbol		Designation	Symbol	Positive direction	Designation	Symbol	Linear (component along axis)	Angular
Longitudinal	X	X	Rolling	L	$Y \longrightarrow Z$	Roll	ϕ	u	p
Lateral	Y	Y	Pitching	M	$Z \longrightarrow X$	Pitch	θ	v	q
Normal	Z	Z	Yawing	N	$X \longrightarrow Y$	Yaw	ψ	w	r

Absolute coefficients of moment

$C_l = \frac{L}{qbS}$ (rolling) $\quad C_m = \frac{M}{qcS}$ (pitching) $\quad C_n = \frac{N}{qbS}$ (yawing)

Angle of set of control surface (relative to neutral position), δ. (Indicate surface by proper subscript.)

4. PROPELLER SYMBOLS

D, Diameter

p, Geometric pitch

p/D, Pitch ratio

V', Inflow velocity

V_s, Slipstream velocity

T, Thrust, absolute coefficient $C_T = \frac{T}{\rho n^2 D^4}$

Q, Torque, absolute coefficient $C_Q = \frac{Q}{\rho n^2 D^5}$

P, Power, absolute coefficient $C_P = \frac{P}{\rho n^3 D^5}$

C_s, Speed-power coefficient $= \sqrt[5]{\frac{\rho V^5}{P n^2}}$

η, Efficiency

n, Revolutions per second, r.p.s.

Φ, Effective helix angle $= \tan^{-1}\left(\frac{V}{2\pi r n}\right)$

5. NUMERICAL RELATIONS

1 hp.=76.04 kg-m/s=550 ft-lb./sec.
1 metric horsepower=1.0132 hp.
1 m.p.h.=0.4470 m.p.s.
1 m.p.s.=2.2369 m.p.h.

1 lb.=0.4536 kg.
1 kg=2.2046 lb.
1 mi.=1,609.35 m=5,280 ft.
1 m=3.2808 ft.

RECEIVED
DEC 19 1969
INPUT SECTION
CLEARINGHOUSE